

Unterschrift des Betreuers



TECHNISCHE
UNIVERSITÄT
WIEN

DIPLOMARBEIT

Hydrothermal Polymerization: Towards Highly Crystalline Polyimides

ausgeführt am Institut für Materialchemie der Technischen Universität Wien

unter der Betreuung von Univ.Ass. Dipl.-Chem. Dipl.-Ing. Dr.rer.nat. Miriam M. Unterlass, MSc
und Em.O.Univ.Prof. Dipl.-Ing. Dr.rer.nat. Ulrich Schubert

durch

Bettina Baumgartner, BSc

1026080

Meidlgasse 27/4/4

A-1110 Wien

Wien, am 16.12.2015

für meine Mama

Acknowledgements

First and foremost I offer my sincerest gratitude to my supervisor, Dr. Miriam M. Unterlass, who has supported me throughout my thesis with her patience and knowledge whilst allowing me the room to work in my own way. I am thankful for her encouragement and effort. One simply could not wish for a better supervisor.

My sincere thank also goes to Prof. Ulrich Schubert, who provided me an opportunity to join his team, and who gave access to the laboratory and research facilities.

I want to thank the whole research group for the awesome atmosphere, especially my short-time office colleagues Tobia, Sebastian and Alonso for great evenings after work.

I am indebted to Michael J. Bojdys for a very fruitful collaboration on crystalline polyimides and for crystal structure refinement.

Special thanks goes to Werner Artner and Philipp Hans for assistance with XRD measurements, as well as Philipp Skrinjar for LC/MS measurements and Michael Puchberger for NMR measurements.

I want to thank Sophia, Heribert and Thomas for sharing the interest and their dedicative practical work.

Very big and sincere thanks to Max B., Lucki, Hänz, Meister Eder, Lisi, Max K., Alina, Sofia, Anna and Zacha, without them, my years of study would not have been the same.

I want to thank Jakob for so much more than fruitful discussions. Thank you, for your perpetual support and believing in me.

Last but not the least, I would like to thank my family: my mother and my brother for supporting me spiritually throughout writing this thesis and in my life in general. They always encouraged me to make my way.

Abstract

Aromatic Polyimides (PIs) belong to the class of high performance polymers (HPPs). Due to their important properties, *e.g.* thermal stability, chemical resistance and outstanding mechanical performance, PIs find numerous applications, for instance as insulating materials in electric devices or as membrane materials. Unfortunately, these high-performance properties of PIs go hand in hand with one major drawback: Due to the insolubility and infusibility of PIs, conventional crystallization techniques cannot be applied and hence PIs are hard to crystallize. However, PI's features can be even enhanced by crystallinity. Despite PIs technological relevance, only few attempts have been made to find new methods to synthesize crystalline PIs. We recently reported a novel synthetic approach to PIs: *Hydrothermal Polymerization* (HTP). This synthetic route is mimicking a naturally occurring ore formation process. In the earth's crust, highly crystalline materials, *e.g.* zeolites or natural gemstones, are formed at high temperatures and pressures (> 100 °C and > 1 bar) by condensation reactions. Intriguingly, hydrothermal synthesis is also applicable for the synthesis of crystalline PIs. Moreover, in contrast to classical PI synthesis, which employs high-boiling, toxic solvents and harsh reaction conditions, HTP is carried out in solely water at elevated temperatures and pressures. While classical PI syntheses involve *poly*(amic acid) intermediates, HTP passes *via* monomer salt species that inevitably form when diamine and dianhydride monomers are brought in contact in water.

The aim of this work was to gather deeper insights into HTP and its mechanisms as well as to determine the applicability to different PI systems of this novel route. Therefore, a comprehensive picture of HTP is presented that was developed from thoroughly characterizing multiple PIs synthesized at numerous different reaction conditions. Several polymerization pathways were identified that occur during the HTP experiment. These pathways were correlated with the physicochemical characteristics of starting compounds, monomer salt intermediates, and the reaction medium water (*e.g.* dielectric constant, ionic product). Based on these findings, experiments that allowed for increasing the crystallinity of the PI products even further were designed. The thus obtained PIs were of such high crystallinity that their crystal structure could be refined from powder XRD data. This master thesis presents a major step towards a global understanding of HTP, a synthetic route towards highly crystalline PIs in solely water.

Kurzfassung

Polyimide (PIs) zählen zu den Hochleistungspolymeren (HPPs von *engl.* high-performance polymers) und sind hinsichtlich ihrer z.B. mechanischen, elektrischen und optischen Eigenschaften herkömmlichen Kunststoffen und anderen Werkstoffen überlegen. Sie finden daher Anwendung in z.B. Isolierungsmaterialien von elektronischen Bauteilen oder in Membranmaterialien. Unglücklicherweise gehen diese herausragenden Eigenschaften mit folgendem Nachteil Hand in Hand: HPPs sind typischerweise unlöslich und zersetzen sich vor ihrem Schmelzpunkt, daher ist eine herkömmliche Rekristallisation (aus Schmelze oder Lösung) zur Erhöhung der Kristallinität nicht möglich. Allerdings, können die Eigenschaften von PIs deutlich durch Kristallinität verbessert werden. Trotz der hohen technologischen Relevanz von PIs wird derzeit wenig Aufwand betrieben um Methoden zu ihrer Kristallisation zu entwickeln. Wir konnten kürzlich einen neuen Syntheseweg zur Herstellung von kristallinen PIs vorstellen: die *hydrothermale Polymerisation* (HTP). Diese Darstellungsmethode ist an einen geologischen Mineralbildungsprozess angelehnt. In der Erdkruste fördern Hochtemperatur- Hochdruckbedingungen ($> 100\text{ °C}$ und $> 1\text{ bar}$) die Bildung hochkristalliner Materialien, wie z.B. Zeolithe oder natürliche Edelsteine. Wir konnten zeigen, dass sich hydrothermale Bedingungen nicht nur für die Kondensation und Kristallisation anorganischer Materialien eignen, sondern auch für die Synthese rein organischer Polymere. Im Gegensatz zu konventionellen PI Synthesen, die hochsiedende Lösungsmittel und giftige Katalysatoren benötigen, wird HTP in lediglich heißem Wasser durchgeführt. Klassische Synthesen beinhalten *Poly*(Amidsäure)-Zwischenprodukte, während in HTP-Reaktionen Monomersalzspezies (die unumgänglich durch in Kontakt bringen von Diamin- und Dianhydridmonomeren in Wasser entstehen) als Zwischenprodukt vorliegen.

In dieser Diplomarbeit wird ein umfassendes Bild der HTP präsentiert, welches durch eine Vielzahl an Experimenten mit unterschiedlichen PI-Systemen unter verschiedensten Bedingungen gezeichnet werden konnte. Es wurden mehrere Polymerisationswege, die während des HTP-Experiments stattfinden, identifiziert. Diese Polymerisationswege konnten mit den physikochemischen Eigenschaften der Edukte, der Monomersalz-Zwischenprodukte sowie dem Reaktionsmedium Wasser (z.B. Dielektrizitätskonstante, Ionenprodukt) in Beziehung gesetzt werden. Mit Hilfe dieser Korrelationen wurden HTP-Experimente konzipiert, die eine weitere Erhöhung der Kristallinität der Produkte ermöglichten. Dadurch konnten die Kristallstrukturen der verwendeten PIs aus Pulverdiffraktogrammdaten verfeinert werden. Diese Arbeit trägt zu einem globalen Verständnis der HTP bei, einer Syntheseroute für hochkristalline Polyimide in lediglich heißem Wasser.

Parts of this Work have been subject to Publication

A. Journal Articles

B. Baumgartner, M. J. Bojdys, and M. M. Unterlass, "Geomimetics for green polymer synthesis: Highly ordered polyimides via hydrothermal techniques," *Polym. Chem.*, **2014**, *5*, 12, 3771-3776.

B. Baumgartner, M. Puchberger, and M. M. Unterlass, "Towards a general understanding of hydrothermal polymerization of polyimides," *Polym. Chem.*, **2015**, *6*, 31, 5773-5781.

B. Baumgartner, M. Puchberger, and M. M. Unterlass, "Design Strategies in Hydrothermal Polymerization of Polyimides," *Macromol. Chem. Phys.*, DOI:macp.201500287-R1, **2015**, *in press*.

B. Patents

M. M. Unterlass; B. Baumgartner "Verfahren zur Herstellung von kristallinen Polyimiden", AT Patent A 304/2015, submitted: 13.05.2015.

C. Poster Presentations and Conference Talks

B. Baumgartner, M. M. Unterlass: "Geomimetic Polymer Synthesis: Highly Crystalline Polyimides via Hydrothermal Polymerization, Talk at *Vienna Young Scientist Symposium*, Vienna, Austria, 25.-26.6.2015.

B. Baumgartner, M. M. Unterlass: "Geomimetic Polymer Synthesis: Hydrothermal Polymerization of Polyimides." Poster at *Gordon Research Conference Polymer Physics 2014*, Mount Holyoake College, South Hadley, MA, USA, 13.7.-18.7.2014.

B. Baumgartner, M. M. Unterlass: "Highly Crystalline Polyimides by Hydrothermal Polymerization, Poster at *Functional Nanomaterials Symposium (FuNMat) 2015*, Prague, Czech Republic, 30.7.2015.

B. Baumgartner, M. M. Unterlass: "Geomimetic Polymer Synthesis: Highly Crystalline Polyimides by Hydrothermal Polymerization, Poster at *Austrian Chemistry Days*, Innsbruck, Austria, 20.-22.9.2015.

List of abbreviations and symbols

BTA	benzophenone-3,3',4,4'-tetracarboxylic acid
COF	covalent organic framework
DMF	dimethylformamide
DMSO	dimethylsulfoxide
FWHM	full width at half maximum
hHT	higher hydrothermal
HPP	high-performance polymer
HT	hydrothermal
HTP	hydrothermal polymerization
IPP	4,4'-(4,4'-isopropylidenediphonoxy)bis(phthalic anhydride)
IR	infrared
K	equilibrium constant
L	leaving group
LC	liquid crystals
lHT	lower HT
MOF	metal organic framework
M	molar mass
MOF	metal organic framework
n	molar amount of substance
NMP	N-methyl-2-pyrrolidone
NMR	nuclear magnetic resonance
ODA	4,4'-oxydianiline
PAA	<i>poly</i> (amic acid)
PDA	<i>p</i> -phenylene diamine
PDI	polydispersity index
PE	polyethylene
PI	polyimide
PMA	pyromellitic acid
PMDA	pyromellitic dianhydride
PPPI	<i>poly</i> (<i>p</i> -phenylene pyromellitimide)
PP	polypropylene
PTFE	polytetrafluoroethylene
SEM	scanning electron microscopy
SSP	solid-state polymerization
T_g	glass transition temperature
t_h	heating time
t_R	reaction time
T_R	reaction temperature
TGA	thermogravimetric analysis
X_i	degree of polymerization
XRD	X-ray diffraction
χ	molar fraction

NMR Abbreviations

δ	chemical shift
s	singlet
d	doublet
t	triplet
q	quartet
m	multiplet

Contents

Acknowledgements	iv
Abstract	v
Parts of this Work have been subject to Publication	vii
List of abbreviations and symbols	viii
1 Introduction	1
2 Theoretical Background	4
2.1 Crystallinity in Polymers	4
2.2 Theory of Polycondensations	6
2.2.1 Equilibrium Constant in Polycondensations Reactions ¹	7
2.2.2 Extent of Reaction and Degree of Polymerization ¹	8
2.2.3 Extent of Reaction and Distributions of the Degree of Polymerization ¹	10
2.3 Target Polymer Class: Aromatic Polyimides	12
2.3.1 Properties and Applications of Polyimides	12
2.3.2 Synthetic Routes for Polyimides	13
2.3.3 Crystalline Polyimides	14
3 Basics of Hydrothermal Synthesis	15
3.1 Physicochemical Properties of Water in the HT Regime	18
4 Hydrothermal Polymerization of Polyimides	20
4.1 Proof of Concept: <i>poly(p</i> -phenylene pyromellitimide)	20
4.1.1 The Monomer Salt	21
4.1.2 HTP of <i>poly</i> (PDA-PMA)	21
4.2 Benzophenonetetracarboxylic Acid-Based Polyimides: Systems with Increased Flex- ibility	27
4.2.1 Benzophenonetetracarboxylic Acid-based Monomer Salts	28
4.2.2 HTP of Benzophenone Tetracarboxylic acid-based PIs	29
4.3 Global Picture: General Ongoings in Hydrothermal Polymerization	31
4.3.1 Consequences of the Physicochemical Properties of the Monomer Salt for HTP	31
4.3.2 Influence of Reaction Temperature T_R in Lower HT regime	35
4.3.3 Effect of Heating Rate t_h in Higher HT Regime	38
4.3.4 Solid-State Polymerization in HT Regime	41

4.3.5	Morphology in HTP: Effect of sHTR, lHTP and SSP Pathways	43
4.3.6	Outstanding Crystallinity <i>via</i> HTP: A Hypothesis	44
4.3.7	Experimental Design of Crystalline PIs and their Crystal Structure	47
5	Conclusion	50
6	Experimental Section	52
6.1	General Methods	52
6.2	Chemicals	53
6.3	Monomer Salt Synthesis	53
6.4	HTP experiments	54
6.5	Classical PI Synthesis	58
6.6	Solid-State Polymerization	58
7	Appendix	59
7.1	Solubility tests of monomer salts	59
7.2	NMR analysis of monomer salts	59
7.3	FT-IR-ATR Analysis of Monomer Salts	63
7.4	Aspect of PIs	64
7.5	Solubility of PIs	64
7.6	NMR Analysis of Dimers	65
7.7	FT-IR-ATR Analysis of PIs	66
7.8	Powder X-ray Diffraction of PIs	70
7.9	Crystal Structure Data	73
7.10	Thermogravimetric Analysis of Monomer Salts and PIs	74
7.11	Characterization of supernatant in PDA-based PIs	75
	References	77

1 Introduction

The development of mankind goes along with the invention and utilization of novel materials. Their importance is reflected in the names of periods in human history, *e.g.* stone age, iron age *etc.*, according to the mainly used materials in each era. Today, in the 21st century, novel technologies long for highly sophisticated materials, consequently, new materials are developed every day to meet the needs of advanced technologies.

Novel materials can be classified according to different criteria *e.g.* by origin (natural or synthetic materials), mechanical properties (hardness, YOUNG's modulus *etc.*), or types of chemical bonds involved in 'holding the material together' on a molecular level. The chemical bond can be differentiated into strong bonding (metallic bond, covalent bond, ionic bond) and weak bonding (VAN DER WAALS bond, hydrogen bond). In general, there are five main types of materials:² *(i)* metals, *(ii)* semiconductors, *(iii)* ceramics, *(iv)* organic matter including polymers and biological materials, and *(v)* composites. The material's physico-mechanical properties such as rigidity, crystallinity, or tensile strength are highly influenced by the nature of the chemical bond. For example, ductility is defined as deformation produced by gliding of atomic planes, which is equivalent to the displacement of dislocations. The latter is facilitated by the absence of preferential direction in metallic bonds and therefore, metals deform but do not break upon strain. In contrast, covalently and/or ionically bonded materials exhibit highly directional bonds, where displacement of dislocations generally leads to a definitive rupture of the bonds between the atoms. Thus, materials with covalent and/or ionic bonds are considered to be brittle, while metals are ductile. In analogy to displacements of dislocations in metals, in polymeric materials, flexible molecular chains are rearranged.

Hence, the properties of the five main types of materials mentioned above vary considerably between each other, and thus define their possible applications. The property - profiles (*e.g.* strength - density chart and a YOUNG's modulus - strength chart) of different material classes are shown in **Fig. 1**. Metals reach high strength and YOUNG's moduli while having high densities. Composites fill the 'gaps' between metals and polymers, which exhibit lower densities and mechanical stability. Metals are the best mechanically performing materials and thus are applied as materials for building or transportation. Cars or airplanes have to withstand high forces they experience during acceleration and deceleration, and also to protect the occupants in case of an accident. The drawback of metals is the high density and therefore the high specific weight of these materials.

Metals are heavy and would lead to means of transportation that are uneconomic because of higher fuel consumption due to a higher weight. At the same time, to ensure take-off, the weight of airplanes should not be too high. In order to ensure mechanical stability at light weight, transportation materials use strong but light alloys, composite materials and polymers to meet these criteria. These materials can be understood as a compromise that enables both mechanical stability and light weight.

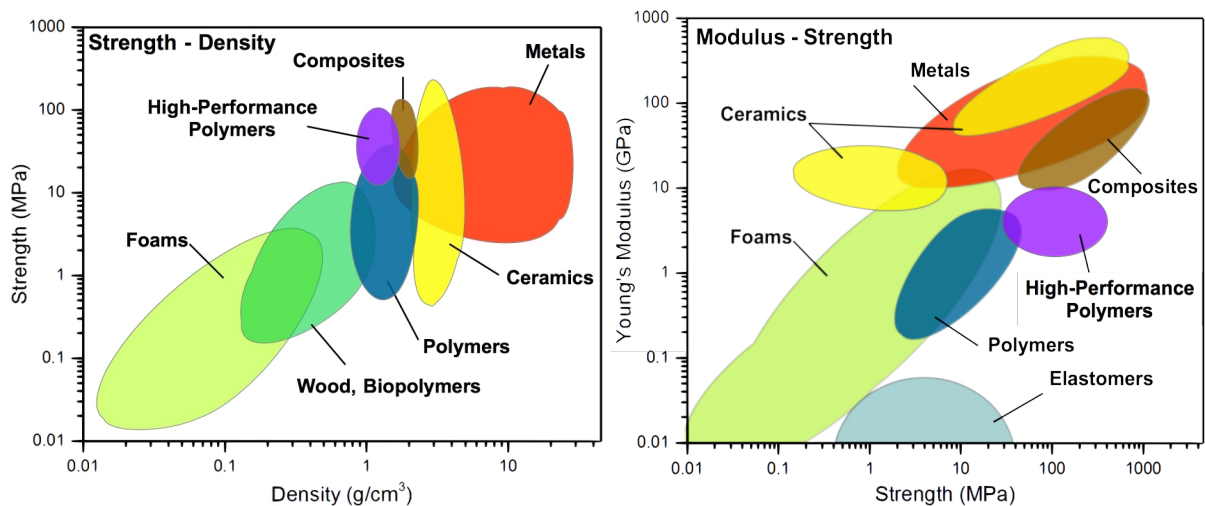


Figure 1: Strength - density chart (left) and Y_{oung} 's modulus - strength chart (right) of different materials. Data was adapted from ASHBY.³ HPPs are highlighted in violet.

Today, the requirement of light weight for materials is formulated in almost every product development. For this reason, polymers have replaced metals in many fields of application. Organic polymers are C, H, N, O - based compounds, which implies low densities ($\approx 0.7 - 2.0 \text{ g cm}^{-3}$; **Fig. 1** left),⁴ and are macromolecular, *i.e.* of high molecular weight. Commodity plastics (*e.g.* polyethylene, polystyrene *etc.*) reach tensile strengths of $\approx 70 \text{ MPa}$ and YOUNG's moduli of $\approx 3 \text{ GPa}$. They are used in high volume and for numerous applications, where mechanical properties are not very critical such as packaging, clothing or bottles. Their advantage of easy processing (*e.g.* by injection molding, extrusion, *etc.*) that is related to high molecular weight and entanglement, go hand in hand with inferior mechanical characteristics. In contrast, high-performance polymers (HPPs) provide outstanding mechanical (tensile strength of up to 200 MPa and YOUNG's moduli of 6 GPa), chemical, and thermal (up to 600 °C) stability, which makes them the lightweight materials of choice under working conditions where 'soft' polymers fail (see **Fig. 1** for property - profiles of HPPs in violet).⁵ Conditions that are highly demanding for polymeric materials include high temperatures and mechanical strain. The presence of aromatic and/or heterocyclic rings in the macromolecular backbone generates such HPP properties,

which are related to molecular stiffness, and thus higher energetic demands for thermal or mechanical degradation. The downside of these stiff polymeric chains is harsh reaction conditions (toxic solvents and catalysts, high reaction temperatures, long reaction times) are required to form and process high-performance polymers.⁶ With the growing awareness for environment and health as well as governmental regulations becoming stricter in this respect, there is an increasing need for less harmful synthetic procedures.

We have recently shown that fully aromatic PIs can be synthesized *via Hydrothermal polymerization* (HTP).⁷ Hydrothermal conditions refer to the use of water at elevated temperatures and pressures (> 100 °C, > 1 bar). The possibility of synthesizing PIs in solely hot water is most surprising, because polyimides are formed *via* polycondensation reactions by eliminating water. Hence, performing polycondensations in water seems to be contradicting LE CHATELIER's principle.⁸ Intriguingly, HTP is not just circumventing LE CHATELIER's principle, but leads to much reduced polymerization times compared to conventional polycondensations. Additionally, toxic solvents are replaced by water, which is considered as 'green synthesis' techniques.⁹ Moreover, HTP yields highly crystalline PIs, whose crystallinity exceeds the crystallinity of conventionally prepared analogues to a considerable degree.

The motivation for this work was the understanding of HTP of polyimides as well as finding the limits of this pathway. In the first part of this master thesis, the state-of-the-art of polycondensations and hydrothermal synthesis will be reviewed. The results are divided in three sections: *(i)* proof of the HTP concept by polymerization of *poly(p-phenylene pyromellitimide)*, *(ii)* the results of other, more flexible PIs systems deviating from the first system regarding crystallinity. The understanding of these new and deviating results lead to *(iii)* the development of a comprehensive mechanistic picture of HTP of all studied polymers and their polymerization. HTP was correlated to the physicochemical features of starting compounds and reaction medium water and different polymerization mechanisms occurring during the HTP experiment were identified.

2 Theoretical Background

This chapter provides the theoretical background, which covers the main topics within this thesis. The first part evolves around crystallinity in polymers as a desirable feature (**section 2.1**). In the second part the basics as well as the theory of polycondensation reactions are discussed (**section 2.2**). In **section 2.3**, a short introduction into the synthesis, characteristics and applications of polyimides will be given. Furthermore, the various applications for crystalline polyimides are pointed out within this section.

2.1 Crystallinity in Polymers

Owing to their versatile spectrum of applications, polymers are omnipresent in our daily life. Their properties are deeply influenced by chain composition or chain length, but also by the relative arrangement of different chains to each other *i.e.* crystallinity or amorphicity. In general, amorphous solid polymer materials are transparent, which is an important feature for many applications *e.g.* lenses, food packaging and many more. Amorphous or non-crystalline materials can be obtained by quenching molten or dissolved polymers *i.e.* fast cooling or precipitation into non-solvents. In both approaches, there is no time for the molecules to arrange into an ordered array and the material is amorphous.

In contrast, by using moderate to low cooling rates, ordered domains can form and lead to semicrystalline or even crystalline materials. The features of ordered polymers differ from amorphous polymers not just in terms of transparency, but in many more properties: Mechanical stability is increased by crystallinity. In order to break the polymeric material, one has to overcome the barrier of the crystal lattice energy in addition to the rupture of the polymer chain itself. For instance, mechanical characteristics of aramid fibres can be improved by increasing the overall degree of molecular orientation.¹⁰ Intermolecular interactions (hydrogen bonds, π - π stacking) within the crystal structure lead to mechanically more stable materials. Another highly orientation-dependent feature is electrical conductivity: Directional properties enable the electric conduction in polymeric materials. Thiophene-based polymers for organic photovoltaic devices show indeed high degrees of crystallinity.¹¹ In this case, a low number of defects and therefore a highly ordered material leads to maximal conductivity. Moreover, crystalline perylene-based polyimides are applied in OLEDs as electrode material.¹² Furthermore, crystallinity gives rise to many optical properties *e.g.* for organic electroluminescent devices or

photosensors.¹³

Thus, crystallinity in polymers opens a broad field of remarkable applications and is therefore a highly desired feature. However, the concepts of crystalline polymeric materials deviate from the common definition of crystallinity in materials such as salts or metals. In polymeric crystals, molecular chains have to arrange instead of just atoms, ions or low - molecular weight compounds.

The most common concept to describe ordered states in polymers apply only to flexible chain polymers, such as PE or PP. These polymers have flexible backbones, which enables arrangement into both crystalline domains and into amorphous coils (see **Fig. 2** top).¹⁴ In contrast, monomers with stiff moieties, *e.g.* aromatic rings, cannot arrange in coil-like structures, due to their inflexibility. Hence, the flexible chain approach is not applicable for these so-called rigid-rod polymers (**Fig. 2** bottom). High-performance polymers such as polybenzimidazoles, polyamides or *poly*(arylene ether)s are representatives of this class. The target polymer class polyimides is also a HPP and is considered to be a rigid-rod polymers.¹⁵ Especially, fully aromatic PIs show only little mobility within the polymeric chain which leads to their outstanding properties.

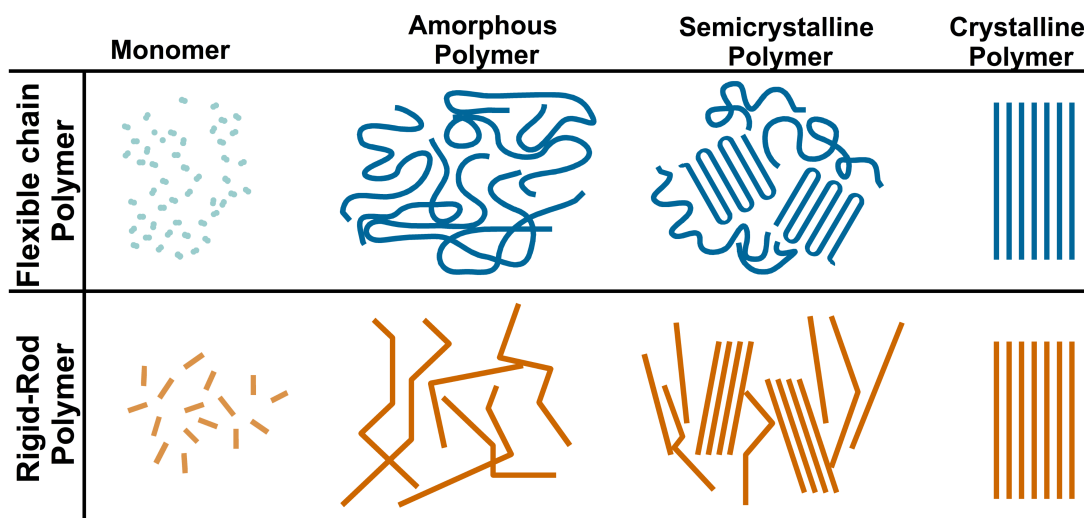


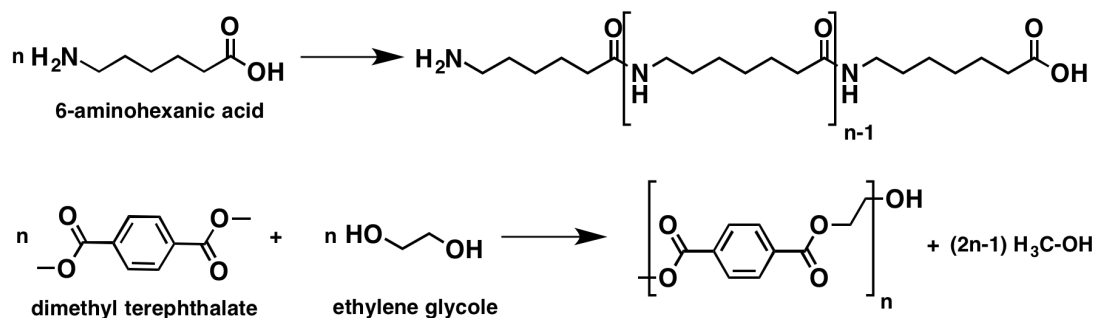
Figure 2: Concepts of crystallinity for flexible chain polymers (top) and rigid-rod polymers (bottom) in amorphous, semicrystalline and crystalline states with corresponding chain arrangements.

The HPPs of interest, polyimides, are obtained *via* polycondensations. The following section will provide the theoretical background of these reactions.

2.2 Theory of Polycondensations

In polymer chemistry two general polymerization types are distinguished: chain-growth polymerizations and step-growth polymerizations. The first proceeds by the addition of unsaturated monomers to the active site of a growing polymer chain, which is located at the chain end. The reaction is always started by an initiation step. The coupling of active polymer or oligomer chains leads to the termination of chains. In contrast, step-growth polymerizations form in a first step short oligomers *i.e.* dimers, trimers and so forth. These short oligomers condense with either each other or with yet unreacted monomers and form longer chains. Usually, these reactions are acid or base catalysed. Here, chain coupling does not lead to termination, but termination occurs *via e.g.* cyclization or back-biting.

Polycondensation reactions are considered step-growth polymerizations and lead to polymers and a leaving group L, which is a molecule with low molecular weight, that is cleaved off, *e.g.* H₂O or HCl. The simplest polycondensation reaction is between bifunctional monomers with different functional groups either on the same molecule AB or on two different molecules AA and BB *i.e.* AB condensations or AA/BB condensations (see **Scheme 1**). An example for an AB condensation is Nylon 6 which can be synthesized by condensation of *e.g.* 6-aminohexanoic acid.¹ The reaction of dimethyl terephthalate (AA) and ethylene glycol (BB) to *poly*(ethylene terephthalate) as well as the target polymer class polyimides are examples of AA/BB polycondensations.



Scheme 1: Different types of polycondensations: AB polycondensation of 6-aminohexanoic acid to Nylon 6 (top) and AA/BB polycondensation of dimethyl terephthalate and ethylene glycol to *poly*(ethylene terephthalate)(bottom).

CAROTHERS and FLORY developed the theoretical basics of polycondensation reactions.^{14,16,17} Fundamental understanding of the importance of stoichiometry and functionality of monomers was introduced by CAROTHERS.^{16,17} FLORY gathered insights into the statistical character of

¹Alternatively, Nylon 6 can be synthesized by ring opening polymerization of ϵ -caprolactam, which is not a condensation.

polycondensations and assumed the equal reactivity of functional groups on molecules with variable chain length.¹⁴ These understandings gave rise to the theoretically derived relationship between the degree of polymerization and the monomer conversion.

2.2.1 Equilibrium Constant in Polycondensations Reactions¹

Mostly, polycondensations are equilibrium reactions, where a group A and a group B are at equilibrium with a group AB and a byproduct L (leaving group). AB polycondensations are intrinsically of ideal stoichiometry, since bifunctional monomers possess $n_A = n_B$ ($A, B =$ functional groups). However, AA/BB polycondensations are distinguished between being stoichiometric ($n_A = n_B$) or non-stoichiometric ($n_A \neq n_B$). **Equations 1** and **2** define the equilibrium constant K for a stoichiometric reaction (**Eq. 2**, with $\chi_A = \chi_B = 1 - \chi_{AB}$) and a non-stoichiometric reaction (**Eq. 1**, with $\chi_A \neq \chi_B$).

$$K = \frac{[AB][L]}{[A][B]} = \frac{\chi_{AB}\chi_L}{\chi_A\chi_B} \quad (1) \quad K = \frac{[AB][L]}{[A][B]} = \frac{\chi_{AB}\chi_L}{(1 - \chi_{AB})} \quad (2)$$

K equilibrium constant
 χ molar fraction

In the chemistry of small molecules, the equilibrium can be shifted to the desired product AB by using greater amounts of A or B. This cannot be realized in AB condensations, since the functional groups persist as end groups in the same monomer molecule. In AA/BB condensations, this approach would be realizable, but it would lead to lower yields and smaller degrees of polymerization (as discussed in **section 2.2.3**). A perfect 1:1 stoichiometry leads to high degrees of polymerization in AA/BB condensations, though, the reaction is still controlled by the equilibrium constant. To achieve high yields of AB, the molar fraction of the leaving group L has to be reduced severely. Therefore, higher reaction temperatures facilitate the polycondensation because the removal of the leaving groups is eased. The separation of the leaving group is usually performed by removal with DEAN-STARK traps.

Furthermore, under certain circumstances the thermodynamic activity deviates from the concentration (activity coefficient $f \neq 1$). This occurs especially if the reactants are ionized. Thereby, the activity coefficient changes and a prediction using **Eq. 2** is not valid any more. This is an important fact, because, as discussed later, the reaction of interest, the hydrothermal polymerization, is performed in water and with ionic monomer salt species as starting compounds.

The equilibrium constants of polyimidizations, are remarkably high ($K > 10^3$) compared to

other polycondensations.^{18,19} This is due to the formation of the strong imide bond, which has a C=N double bond character (compare bond length of imide bond: $r(\text{C-N})_{\text{imide}} = 141 \text{ pm}$, $r(\text{C-N}) = 147 \text{ pm}$, $r(\text{C=N}) = 130 \text{ pm}$).²⁰ Hence, polycondensations of polyimides are considered irreversible.

2.2.2 Extent of Reaction and Degree of Polymerization¹

Polycondensations in equilibrium without side reactions are characterized by the *degree of polymerization* \bar{X}_n , *i.e.* the number of monomer units in a macromolecule, given by:

$$\bar{X}_n = \frac{n_{M,0}}{n_R} = \frac{n_{A,0}}{n_A} = \frac{1}{1 - p_A} \quad (3) \quad p_A = \frac{n_{A,0} - n_A}{n_{A,0}} \quad (4)$$

\bar{X}_n	degree of polymerization
$n_{M,0}$	initial amount of monomer
n_R	amount of substance of all reactants at time t
$n_{A,0}$	initial amount of monomer A
n_A	amount of substance of monomer A at time t
p_A	extent of reaction for monomer A

For AB polycondensations, $n_{M,0}$ corresponds to the initial amount of monomer molecules, since every monomer molecule contains a group A and B ($n_{M,0} = n_{A,0} = n_{B,0}$). The amount of substance of all reactants at time t is n_R , which corresponds to the amount of unconsumed monomer n_A . The extent of reaction for monomer A (p_A) is defined by the consumption of functional groups of A. Inserting **equation (4)** into **equation (3)** yields CAROTHERS' equation, which describes \bar{X}_n as function of the extent of reaction (see **Fig. 3**, black line, for graphical representation). The application is limited to AB condensations and stoichiometric AA/BB condensations and is not applicable for intramolecular ring closing reactions.

As shown in **Fig. 3**, the degree of polymerization is very low at conversions $< 90 \%$. For ideal stoichiometry, $r_0 = 1$, at 50 % conversion \bar{X}_n is 2 (emphasized as dot in **Fig. 3**) *i.e.* dimers are formed. High \bar{X}_n are achieved at very high conversions, *e.g.* $p_A = 95 \%$ leads to $\bar{X}_n = 20$ (emphasized as dot in **Fig. 3**); $p_A = 99,5 \%$ leads to $\bar{X}_n = 200$. Theoretically, $p_A = 100 \%$ leads to infinite chain length ($\bar{X}_n = \infty$).

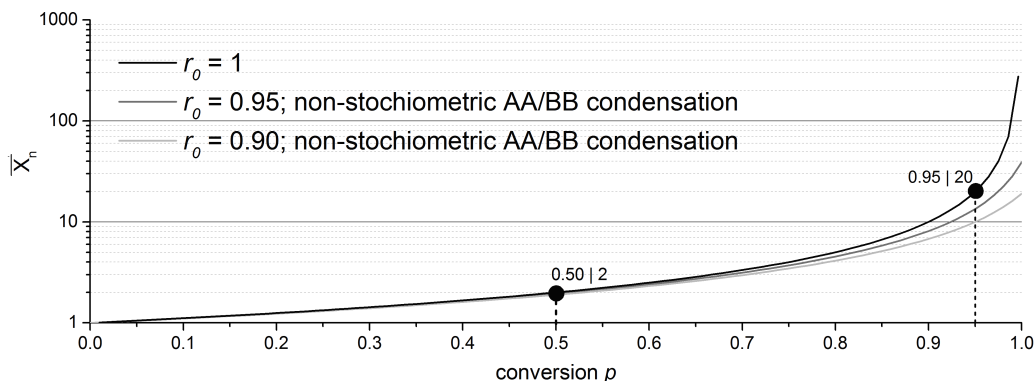


Figure 3: Carothers' law: Degree of polymerization as function of the extent of reaction. Black line corresponds to stoichiometric condensations ($r_0 = 1$); light and dark gray lines describe non-stoichiometric condensations with $n_{AA} : n_{BB} = 1:0.95$ and $1:0.90$ stoichiometry, $r_0 = \frac{n_{A,0}}{n_{B,0}}$.

CAROTHERS' law can be extended to non-stoichiometric AA/BB condensations. To that end, **equation (3)** has to be adapted, because either monomer A or B are in excess. Since every monomer has two identical functional groups AA or BB, the initial amount of monomer molecules is the arithmetic average of both: $n_{M,0} = (n_{A,0} + n_{B,0})/2$. The amount of substance of all reactants n_R results from the difference of $n_{M,0}$ and $n_{M,el}$. The latter corresponds to the elimination of monomer A (A is in excess) by coupling to other molecules; $n_{M,el} = n_{A,0} - n_A$. Hence, n_A is the remaining amount of monomer A, that was in excess.

$$\bar{X}_n = \frac{n_{M,0}}{n_R} = \frac{n_{M,0}}{n_{M,0} - n_{M,el}} = \frac{(n_{A,0} + n_{B,0})/2}{[(n_{A,0} + n_{B,0})/2] - (n_{A,0} - n_A)} = \frac{1 + r_0}{1 + r_0 - 2r_0p_A} \quad (5)$$

$n_{M,0}$	initial amount of monomer
n_R	amount of substance of all reactants at time t
$n_{A,0}$	initial amount of monomer A
$n_{B,0}$	initial amount of substance of monomer
$n_{M,el}$	amount of substance of monomer eliminated by coupling to other molecules
n_A	unreacted amount of substance of monomer A (A is in excess)
r_0	molar ratio of monomer A and B

The insertion of factor $r_0 = \frac{n_{A,0}}{n_{B,0}}$ into **Eq. (3)** gives **Eq. (5)**. $r_0 = 1$ is conform to stoichiometric condensations and **Eq. (5)** takes the form **Eq. (3)**. Assuming full conversion ($p_A = 1$) **Eq. (5)** simplifies as follows:

$$\bar{X}_n = \frac{1 + r_0}{1 - r_0} \quad (6)$$

Thus, the maximal degree of polymerization is determined by r_0 , *i.e.* the initial amount of groups A and B. Contrary to stoichiometric condensations, \bar{X}_n yields for $p_A = 1$ and $r_0 = 0.99$ only 199 (instead of ∞). For $r_0 = 0.90$ or 0.95 , respectively, \bar{X}_n is 19 or 39 (compare gray curves in **Fig. 3**) and so forth. Hence, high conversions and perfect stoichiometry of the starting compounds are

essential for high degrees of polymerization. In the case of HTP, ideal stoichiometry is achieved by preparing monomer salts that ensure 1:1 stoichiometry.

2.2.3 Extent of Reaction and Distributions of the Degree of Polymerization¹

The simplest case of polycondensations is considering that the reactivity of all functional groups regardless the chain length are equal. This assumption leads to the formation of a mixture of molecules with different degrees of polymerization since no X_n is favored for reactions. The distribution of $\overline{X_n}$ can be described by statistics.

The probability p of the combination of two functional groups A and B is given by the extent of reaction $p_A = p$. Thus, the probability of a combination of molecules with $X_n = i$ and $(i - 1)$ linkages is p^{i-1} . The probability P_i of the occurrence of one polymeric molecule with $X_i = i$ is given by the probability p^{i-1} for $(i - 1)$ linkages and the probability $(1 - p)$ for unreacted endgroups of A (**Eq. 7**):

$$P_i = p^{i-1}(1 - p) \quad (7) \quad n_i = n_R P_i = n_R p^{i-1}(1 - p) \quad (8)$$

P_i	probability for polymers with $X = i$
p	probability of combining A and B
p_A	extent of reaction for monomer A
n_i	amount of substance of polymers with $X = i$
n_R	amount of substance of all reactants at time t

The amount of substance n_i of all molecules of the reactant i with degree of polymerization X_i is proportional to the probability P_i and the amount of substance for all reactants with different degrees of polymerization n_R (**Eq. 8**). The molar fraction χ_i for molecules with X_i is described by the following equation:

$$\chi_i = \frac{n_i}{n_R} = p^{i-1}(1 - p) \quad (9)$$

Fig. 4 shows a SCHULZ-FLORY distribution for mole fractions χ_i of molecules with a degree of polymerization X_i for different extents of reaction p . For given p and increasing X_i , the mole fraction declines continuously. The distribution flattens for higher extent of reaction $p = p_A = p_B$. According to **equation (9)**, the amount of monomer decreases moderately: For an extent of reaction of 50 % ($p = 0.5$) the amount of substance of the monomers ($i = 1$) is $\chi_{monomer} = 0.5$ and for $p = 0.8$ $\chi_{monomer}$ is still 0.2. **Eq. (9)** is valid for AB condensations as well as for stoichiometric AA/BB reactions.

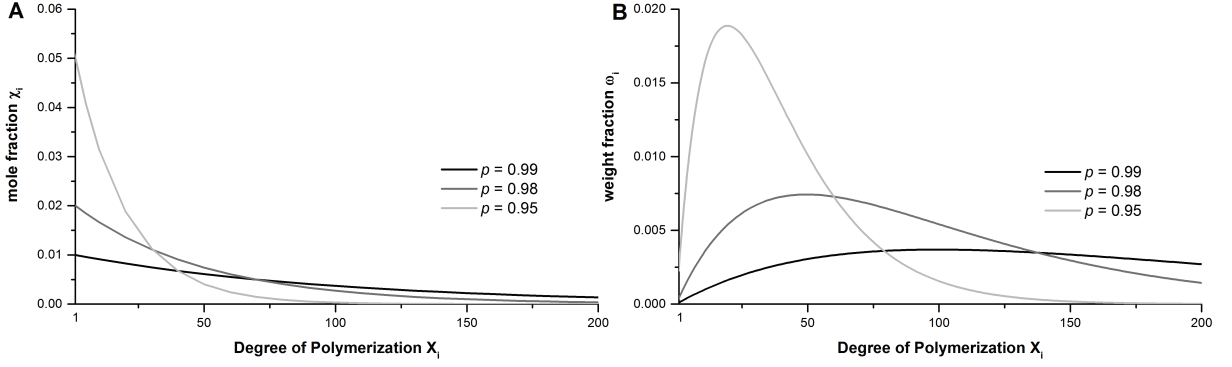


Figure 4: Distribution of mole fractions χ_i (**A**) and mass fractions w_i (**B**) of molecules with X_i for different extents of reaction p . The distribution of the mass fraction was calculated for p -phenylene diamine and pyromellitic dianhydride ($M_U = 254 \text{ g}\cdot\text{mol}^{-1}$, $M_L = 18 \text{ g}\cdot\text{mol}^{-1}$).

For the mass fractions distribution of polycondensations one has to take the molar mass M_L of the leaving group into account. The following derivation for an AB condensation is also valid for AA/BB condensations. The mass fraction w_i for a reactant molecule with X_i is expressed as amount of substance of i -molecules n_i or all reactants n_R , respectively, and the molar masses $M_i = M_L + M_U X_i$ or $(\overline{M}_R)_n = M_L + M_U (\overline{X}_R)_n$, respectively (compare **equation (10)**).

$$w_i = \frac{m_i}{m_R} = \frac{n_i M_i}{\sum_i n_i M_i} = \frac{n_i M_i}{n_i (\overline{M}_R)_n} = \frac{n_i (M_L + M_U X_i)}{n_R [M_L + M_U (\overline{X}_R)_n]} \quad (10)$$

w_i	molar fraction for polymers with $X = i$
m_i	mass of polymer with $X = i$
m_R	mass of all reactants
M_i	molar mass of a polymer with $X = i$
M_L	molar mass of leaving group L
M_U	molar mass of repeating unit
\overline{M}_R	average molar mass of reactants; $(\overline{M}_R)_n = M_L + M_U (\overline{X}_R)_n$
M_i	molar mass of polymer with X_i ; $M_i = M_L + M_U X_i$

Inserting **equation (3)** and **(8)** into **equation (10)** shows the dependency of the mass fraction distribution on the molar masses of reactants and leaving group.

$$w_i = \left(\frac{M_L + M_U X_i}{M_U + M_L(1-p)} \right) p^{i-1} (1-p)^2 \quad (11) \quad w_i = X_i p^{i-1} (1-p)^2 \quad (12)$$

Fig. 4B shows the mass fraction distribution of one of the target polycondensations of this thesis: *poly*(PDA-PMA) from p -phenylene diamine (PDA) and pyromellitic dianhydride (PMDA) for different p . All curves pass through a maximum at *ca.* $(\overline{M}_R)_n$ and broaden with increasing p . For polycondensations with big leaving groups ($M_L > 50 \text{ g}\cdot\text{mol}^{-1}$) the difference between calculated and the actual mass fraction has to be considered. The molar mass of the leaving group water ($M_L = 18 \text{ g}\cdot\text{mol}^{-1}$) in our example can be neglected and **equation (11)** simplifies

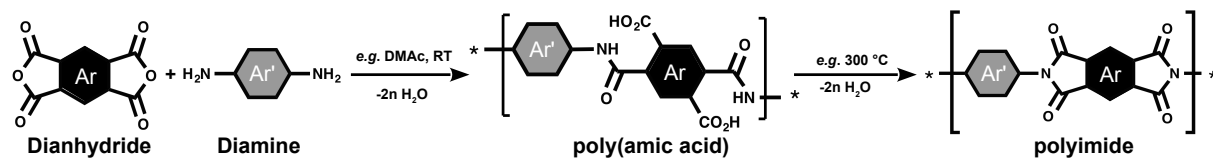
to equation (12).

In summary, the important parameters that influence the degree of polymerization of polycondensation products were discussed in this chapter. The following subsection will give a short introduction into features and synthesis of our target polymer class: polyimides.

2.3 Target Polymer Class: Aromatic Polyimides

Polyimides form by cyclo-polycondensations, which require monomers with ≥ 2 functional groups. These reactions lead to linear polymers with intramolecular rings *i.e.* 5- or 6-membered imide rings. In a first step linear oligomers form *via* polyaddition and result in *poly(amic acids)*. In the case of aromatic PIs, the aromatic diamine and dianhydride monomers form such a *poly(amic acid)*, as depicted in **scheme 2**. The heterocyclic ring formation and cleavage of the leaving group takes place in a second annealing step (**scheme 2**).

In the following subsections, properties and applications as well as the synthetic approach towards PIs will be introduced. Moreover, particular attention is given to crystallinity in PIs.



Scheme 2: Classical synthesis of PIs: Aromatic diamine and dianhydride react to *poly(amic acids)*, which are condensed to PIs in a second thermal annealing step.

2.3.1 Properties and Applications of Polyimides

As mentioned in the previous section, fully aromatic Polyimides (*aka* Aramides) are high-performance polymers (HPPs) with outstanding properties, such as high mechanical and thermal stability or high chemical resistance. Since, they are purely organic (typically composed of C, H, N, O, S, F), light weight results as additional feature. Due to their rigid-rod backbone owing to the hetero-cyclic rings and aromatic moieties, PIs reach glass transition temperatures of $T_g \gtrsim 200$ °C.⁵ Molecular rigidity also imparts high mechanical stability: Commercially available PIs such as KAPTON[®] reach YOUNG's moduli of 1.5 to 3.0 GPa and tensile strengths of 70 to 200 MPa.²¹ In fact, the most rigid member of the PI family is *poly(p-phenyl pyromellitimide)*,

with a predicted YOUNG's modulus of over 500 GPa, which is the highest value for a polymer ever reported.²² Furthermore, PIs exhibit a high chemical and heat resistance (up to 650 °C). These features impart their use as dielectrics in printed circuit boards,²³ components in scientific instrumentation, *e.g.* as window material in X-Ray diffractometers,²⁴ or applications as materials in aircrafts or spacecrafts.²⁵ Moreover, PIs are interesting candidates for conditions that are highly demanding for polymeric materials including corrosive environments at increased temperatures as found in gas separation membranes or fuel cells.^{26,27}

All these outstanding properties go hand in hand with PI's major drawback: harsh conditions are required to form and process these polymers. The main characteristics of the synthetic approach towards PIs are given in the following subsection.

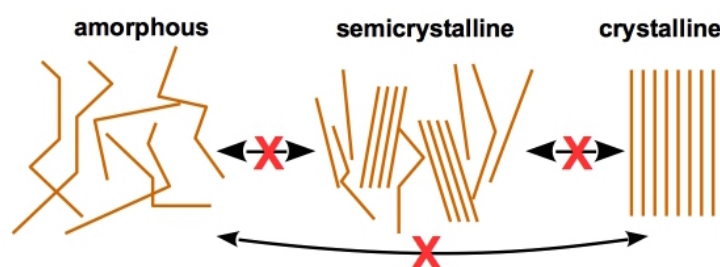
2.3.2 Synthetic Routes for Polyimides

Conventionally, PIs are produced in a two-step synthesis. These syntheses employ high-boiling solvents (*e.g.* cresols, NMP or DMF), toxic catalysts (*e.g.* isoquinoline) and harsh reaction conditions (up to several hundred °C).²⁸ Usually, PIs are obtained *via* detours: the diamines and dianhydrides are transformed into polymeric intermediates, *poly*(amic acids), PAAs (see **scheme 2**, page 12). The *para*-position of the tetracarboxylic acid is mainly linked.¹ PAAs are typically used in low solids content solutions ($\sim 10 - 15$ wt%) in order to keep conversions low (< 50 %) to avoid further substitutions and cross-linking, which would lead to insoluble and non-meltable PAAs and/or PIs. The obtained solutions are processable as cast or lacquer. In a second thermal annealing step, the *poly*(amic acid) is reacted to the final PI by applying high temperatures (> 200 °C).

Despite PIs importance as HPPs, only little progress has been made in the last decades towards alternative polymerization techniques. The few reported non-classical approaches are: *(i)* phase-separation of PAA oligomers in apolar solvents such as liquid paraffins at around 300 °C,²⁹ *(ii)* polymerization of dianhydrides and diisocyanates *via* decarboxylation,³⁰ *(iii)* heterophase polymerization of dianhydride and diamine in ionic liquids,³¹ and *(iv)* the rearrangement of polyisoimides.³² In recent years, our research group could add two novel techniques: solid-state polymerization,^{33,34} and hydrothermal polymerization,^{7,35-37} which are both discussed in **section 4** (page 20 *ff.*).

2.3.3 Crystalline Polyimides

Polyimide products obtained by conventional synthetic routes are semicrystalline at best.³⁸ Despite PIs technological relevance, only few attempts have been made to find new methods to synthesize crystalline PIs. In principle, there are the following crystallization mechanisms in order to achieve crystalline polymers: (i) Crystallization from melt, (ii) crystallization from solution and (iii) crystallization by stretching/shearing. All these mechanisms rely on the possibility to process, *i.e.* melt, dissolve or deform, the polymer. On the upside, PIs have outstanding properties as mentioned previously, but on the downside, the insolubility and infusibility of PIs preclude the application of conventional crystallization techniques (*cf.* **scheme 3**). Thus, the final order in PIs is set during polymerization. Therefore, procedures that allow to crystallize



Scheme 3: Aromatic polyimides are infusible and insoluble; different phases cannot be converted. The final order is set during polymerization.

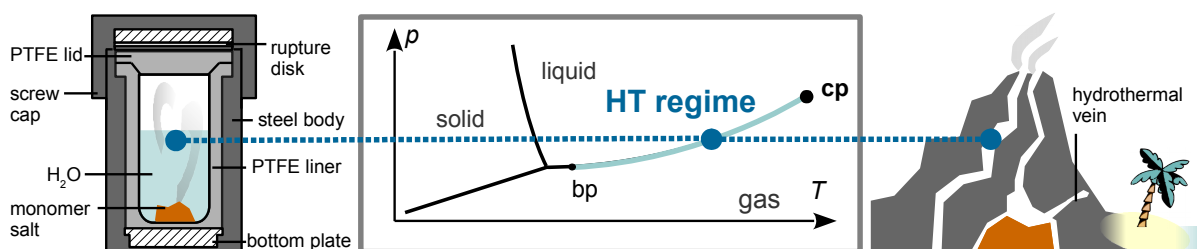
and polymerize *simultaneously* are the only option towards crystalline PIs.

One approach for growing *poly*(4,4'-oxydiphenylene- pyromellitimide) single crystals was found by MARTIN and co-workers by heating low-concentration *poly*(amic acids) solutions for several hours at 160 °C.³⁹ Another unconventional method is the crystallization during polymerization in the melt state between two glass slides at 300 °C.^{40,41} The previously mentioned phase-separation technique with PAA oligomers in apolar solvents at high temperatures also leads to crystalline PIs.²⁹ YUAN and co-workers have reported microwave-assisted PI syntheses at temperatures > 300 °C in the monomer melt, obtaining crystalline PIs.⁴² Most recently the first PI covalent organic framework (COF) was synthesized by heating the monomers for 5-7 days in NMP in the presence of additional solvents and catalysts to 200 - 250 °C.⁴³

However, all new methods still rely on high-boiling toxic solvents and/or harsh reaction conditions. Thus, finding novel approaches for synthesizing crystalline HPPs is a challenging endeavour. We have recently developed *Hydrothermal Polymerization* (HTP) as means to synthesize crystalline, fully aromatic PIs in nothing but hot water.^{7,35-37} The fundamentals of hydrothermal synthesis in general are presented in the following section (**section 3**).

3 Basics of Hydrothermal Synthesis

Hydrothermal synthesis is an important crystallization technique taking place in aqueous solutions at elevated temperatures and pressures, which is typically used for inorganic compounds. In nature, especially minerals *e.g.* silicates, oxides or carbonates, are formed in the HT regime.⁴⁴ Hydrothermal crystallization is a naturally occurring geological ore formation process, which takes place in so-called hydrothermal veins in the earth's crust (**scheme 4**, right side). As a result of limited space within these veins and elevated temperatures an autogenous water vapor pressure arises and one works ideally on the liquid-vapor-line in the phase diagram of water (>1 bar, > 100 °C, see **scheme 4**, center).ⁱⁱ On the lab scale, these conditions are mimicked in closed steel vessels, so-called *autoclaves* (see **scheme 4**, left side).



Scheme 4: Hydrothermal Synthesis: Left: Scheme of a non-stirred autoclave with PTFE liner used to generate HT conditions. Center: Phase diagram of H₂O showing the HT region situated at $T > 100$ °C and $p > 1$ bar, but below the critical point (cp 374 °C, 220 bar). If the pressure in an autoclave arises autogenously, one works ideally on the liquid vapor line (light blue). Right: Earth's crust with hydrothermal veins. Scheme adapted from BAUMGARTNER.³⁶

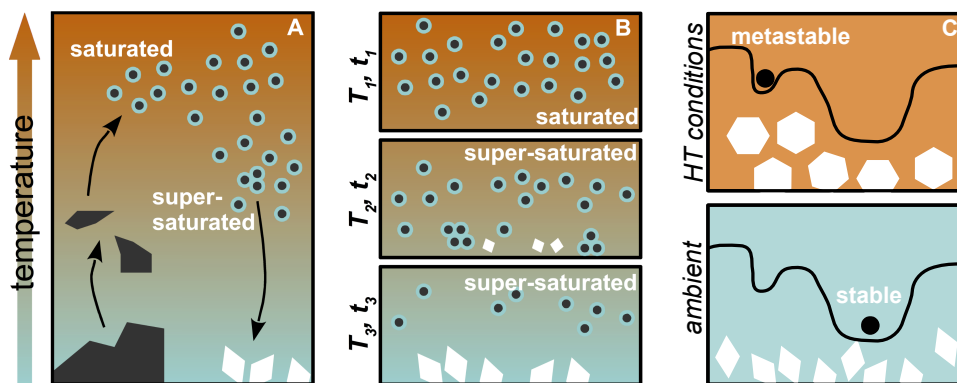
Numerous substances otherwise difficult to dissolve at ambient conditions, go into solution in the hydrothermal regime and in combination with transport processes (*e.g.* convective motion) they can undergo chemical transport reactions. Therefore, HT reactions are sometimes considered to be a special case of the latter,⁴⁵ where water serves as transport phase.ⁱⁱⁱ In HT chemistry, several crystallization methods are distinguished:⁴⁶

- *Temperature-difference method:* Supersaturated solutions are achieved by temperature gradients (emphasized as color gradient in **scheme 5A**). The substances dissolve in hotter regions and form a saturated solution, that is transported to low-temperature zones by convective motion, becomes supersaturated and crystal growth occurs there.

ⁱⁱNote that actual pressure differs from the autogenous pressure as the system is not pure water and can hence not be described by water's phase diagram.

ⁱⁱⁱNote that other definitions insist on the transport phase having to be gaseous. While under HT conditions a coexistence of H₂O_(g) and H₂O_(l) exists, transport processes in the HT regime cannot be assigned to H₂O_(g) due to the closeness of the system.

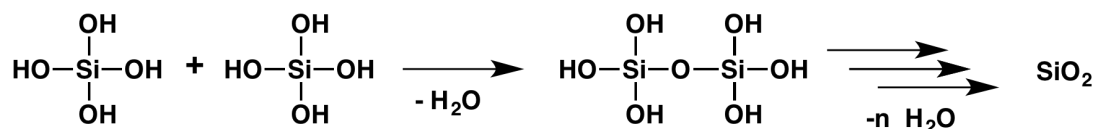
- *Temperature-reduction method*: By slow regular cooling of hot saturated solutions, supersaturation can be achieved without temperature gradients (see **scheme 5B** with $t_1 < t_2 < t_3$).
- *Metastable-phase technique*: This method is based on the thermodynamical instability of different phases under HT conditions. A certain metastable phase is formed under HT conditions as a local energetic minimum. (**scheme 5C**).



Scheme 5: Different methods of HT crystallization. **A:** temperature-difference method, **B:** temperature-reduction method, **C:** metastable-phase technique.

The industrial breakthrough of HT synthesis was paved by NACKEN in 1950 by the introduction of HT synthesis of quartz crystals.⁴⁷ Although, in 1845, probably the first clue for HT reactions was found by SCHAFHÄUTL when he obtained quartz micro-crystals formed from *ortho*-silicic acid.⁴⁸ Today, numerous inorganic compounds in different fields are of hydrothermal origin, *e.g.* single crystals of various elements (*e.g.* Au,⁴⁹ diamonds,⁵⁰ *etc.*), or zeolites,⁵¹ catalyst materials as in metal organic frameworks,⁵² or synthetic gemstones.⁵³

Interestingly, inorganic materials formed in the HT regime are often highly crystalline and many of them form by polycondensation: silicates form, for instance, by condensation of silicic acid species (**scheme 6**).



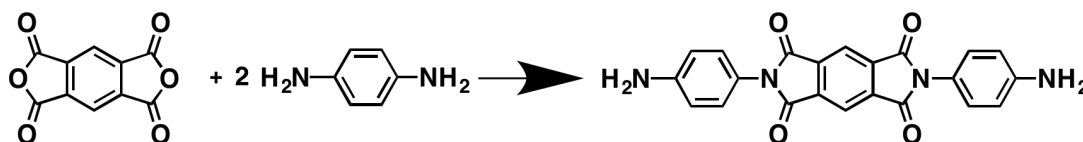
Scheme 6: Condensation of *ortho*-silicic acid to silica.

For example, the naturally occurring zeolite *Chabazite* ($\text{Ca}_2[\text{Al}_4\text{Si}_8\text{O}_{24}]\cdot 12 \text{H}_2\text{O}$) is synthesized under basic conditions for 4 days at 160 °C.⁵⁴

In organic synthesis, HT conditions have been proven highly fruitful for obtaining carbons or carbonaceous materials and the technique is then called hydrothermal carbonization (HTC).⁵⁵ Typically, these materials are amorphous if synthesized at ~ 300 °C. Well-crystallized carbon

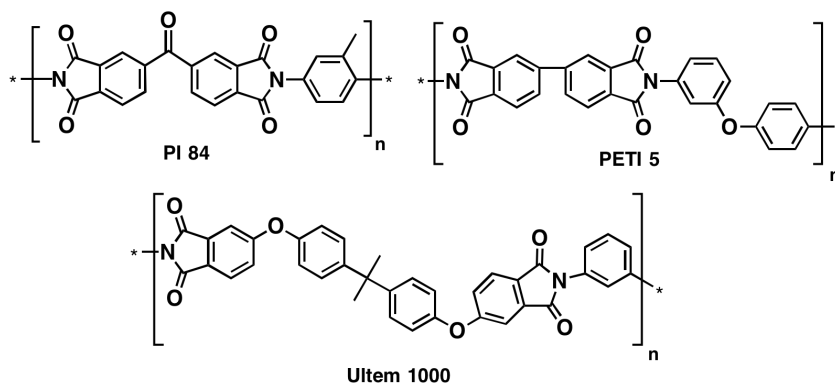
nanotubes can be obtained at higher temperatures ($> 700\text{ }^{\circ}\text{C}$) under HT conditions.⁵⁶ TAKAHASHI *et al.* performed metal catalyzed HT reductions of CO_2 to formic acid at $300\text{ }^{\circ}\text{C}$.⁵⁷

The first steps towards HT synthesis in imide chemistry were made by MORTON and co-workers in 1994 by synthesizing diaminobisimides in water under pressure.^{58,59} They performed HT syntheses of various diaminobisimides systems (for example PDA-PMDA as shown in **scheme 7**) at 150 to $250\text{ }^{\circ}\text{C}$ and 10 to 36 bar, by choosing the required 1:2 stoichiometry.



Scheme 7: Reaction equation of HT syntheses of pyromellitic dianhydride (PMDA) and *p*-phenylene diamine (PDA) to corresponding diaminobisimide.

Diaminobisimides are interesting candidates for solar cell materials or as dyes.^{60,61} Furthermore, diaminobisimides show potential advantages over currently used diamines, especially in terms of oxidative and thermal stability and toxicity. Furthermore, in 2007 FRAGA-DUBREUIL *et al.* reported the successful synthesis of several phthalimide derivatives in water at high pressures and temperatures ($> 300\text{ }^{\circ}\text{C}$, $> 80\text{ bar}$).⁶²



Scheme 8: PIs synthesized by Brunel and Hodgkin under HT conditions.

HT PI syntheses have been reported previously by BRUNEL *et al.*,⁶³ and HODGKIN and co-workers. In 2003 the group of HODGKIN synthesized PIs at $180 - 200\text{ }^{\circ}\text{C}$ in water with additional pre-pressure and compared the outcome with commercial available analogs (PI 84: *poly*(2-methyl-*p*-phenylene benzophenone imide); Ultem 1000[®]: *poly*[3,4'-oxydianiline 4,4'-(4,4'-isopropylidenebis(4-phenyleneoxy))bis(phthalic imide)] (*poly*(3,4'-ODA-IPP)); PETI 5: *poly*(3,4'-oxydianiline 4,4'-biphenyl imide)) (compare **scheme 8**).⁶⁴ Ultem 1000[®] and PETI-5 synthesized hydrothermally showed the same properties in terms of T_g , M_n and M_w compared to the commercially

available PIs. Only PI 84 lead to PIs with lower molecular weights. PI 84 and Ultem 1000[®] reached degrees of polymerization of $\approx 90 - 100$, which corresponds to \overline{M}_W of *ca.* 37500 g·mol⁻¹ or 56500 g·mol⁻¹, respectively.

BRUNEL *et al.* obtained PIs from 4,4'-ODA and 4,4'-(4,4'-isopropylidendiphonoxy)bis(phthalic anhydride) (IPP) by heating by microwave irradiation to > 200 °C and ~ 25 bar.⁶³ The resulting PI (*poly*(4,4'-ODA-IPP)) reached PDIs of 1.4 - 1.6 and $\overline{X}_n \approx 50$ ($\overline{M}_W \approx 29500$ g·mol⁻¹). DAO *et al.* synthesized statistical co-polyimides. UNTERLASS *et al.* reported the hydrothermal synthesis of several fully aromatic PIs with moderate molecular weights (up to $\overline{M}_W \approx 48000$ g·mol⁻¹ and $\overline{X}_n \approx 70$).⁷ However, the final PIs in all reports are non-crystalline.

In general, hydrothermal syntheses are performed at similar conditions, *i.e.* at > 150 °C and autogeneous water pressures. The reaction medium water shows a strikingly different physicochemical behaviour in this regime than at ambient, as discussed in the following section.

3.1 Physicochemical Properties of Water in the HT Regime

HT reactions are carried out at > 100 °C and > 1 bar.⁴⁶ Interestingly, water behaves very differently under HT conditions than water at ambient conditions. Therefore, it is worth to take a closer look at the features of H₂O in the HT regime.

The physicochemical properties of water change as function of temperature and pressure. Changing properties are, amongst others, viscosity,⁶⁵ density,⁶⁵ dielectric constant,⁶⁶ and ionic product,⁶⁷ as depicted in **Fig. 5**.

In the temperature range of 0 °C to 250 °C and autogeneous water vapor pressure (1 to 40 bar) the density of water decreases from 1 g cm⁻³ to 0.80 g·cm⁻³ (**Fig. 5A**). Within this range the viscosity of water drops rapidly from $1800 \cdot 10^{-6}$ Pa·s to $129 \cdot 10^{-6}$ Pa·s (**Fig. 5B**). The static dielectric constant ϵ is a measure of the polarity of the medium water and therefore an important constant. At ambient conditions ϵ is ~ 80 A·s·V⁻¹·m⁻¹ and decreases with temperature to 30 A·s·V⁻¹·m⁻¹ at 250 °C (which roughly corresponds to the dielectric constant of methanol at ambient,⁶⁸ **Fig. 5C**). Consequently, water is considerably more apolar at higher temperatures. The ionic product K_W describes the autodissociation of H₂O into OH⁻ and H₃O⁺ ions. The ionic product increases with temperature: $K_W \sim 10^{-14}$ mol²·kg⁻² at room temperature and becomes 10^{-11} mol²·kg⁻² at 200 °C (**Fig. 5D**).

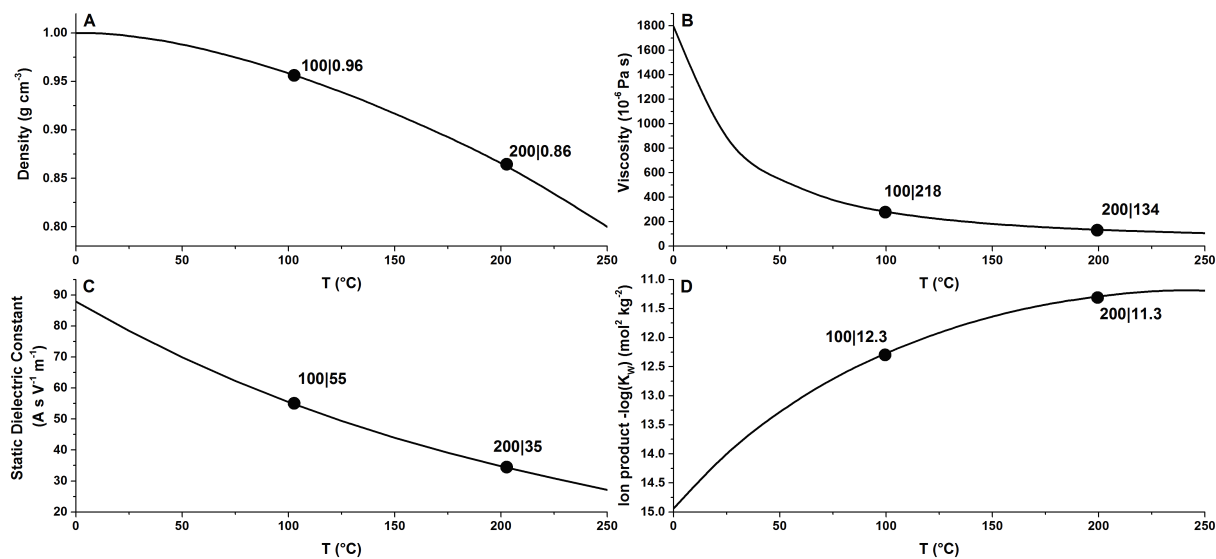


Figure 5: Properties of pure water at autogeneous pressure as function of temperature. Their values at 100 and 200 °C are depicted in each diagram. **A**: Density; **B**: Viscosity; **C**: Static Dielectric Constant; **D**: Ionic product. Plotted using data reported by SENGERS, UEMATS and FRANCK.^{65–67}

As shown later, these changes in properties within the HT regime are beneficial for HTP, in particular in terms of polarity and basicity/acidity of water: Growing polymeric chains become more and more apolar and therefore a more apolar solvent improves the polymerization. Moreover, polycondensations are acid- or base-catalyzed, thus higher amounts of OH^- and H_3O^+ ions are as well beneficial.

In the following chapter the results of this thesis are discussed. **Section 4.1** presents the first steps towards crystalline PIs *via* HTP at the example of *poly(p*-phenylene pyromellitimide). In **section 4.2** the results of benzophenone tetracarboxylic acid-based PI systems are discussed. In **section 4.3**, a comprehensive mechanistic hypothesis of HTP is provided.

4 Hydrothermal Polymerization of Polyimides

Hydrothermal synthesis is inspired by natural ore formation and a powerful technique for crystallizing different materials (see **section 3**). Intriguingly, the formation of many minerals occurs by polycondensation reactions, *e.g.* silicates form by condensation of silicic acid species. Only little progress has been made to apply HT synthesis to fully organic polycondensations.^{63,64} We could recently show that hydrothermal processes can be applied to polycondensation reactions of polyimides with outstanding crystallinity. By generating HT conditions (>100 °C, >1 bar) in autoclaves we were able to synthesize crystalline PIs, that exceed the crystallinity of conventionally prepared analogues, while avoiding harsh reaction conditions.

Within my thesis I studied various PI-systems. The first investigations and the proof of concept were made on *poly(p-phenylene pyromellitimide)* (*poly*(PDA-PMA)). From studying this system, we were able to develop a hypothesis of morphology formation, and could refine the crystal structure of this polyimide from powder XRD (**section 4.1**).³⁵ Furthermore, we could show that HTP is also applicable for other PI systems. HTP of less stiff benzophenone tetracarboxylic acid-based monomers first lead to less crystalline products (**section 4.2**). Numerous experiments at different parameters (T , t , p , c) lead to a comprehensive picture of HTP including polymerization pathways that occur in the HTP experiment, and the correlation of characteristics of starting compounds and reaction medium water. The crystallinity of BTA-based PIs could be further improved based on this findings, enabling the refinement of the crystal structure from powder XRD (**section 4.3**).^{36,37}

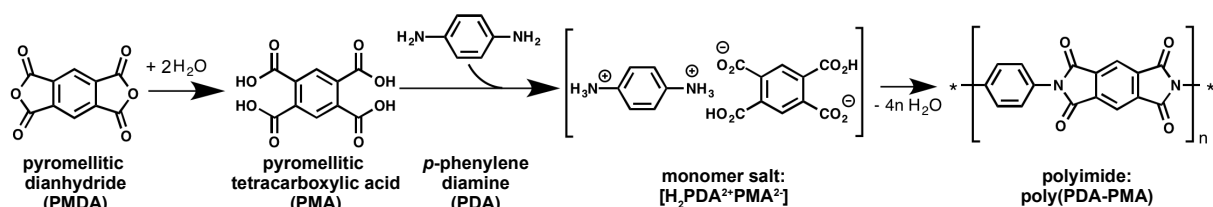
4.1 Proof of Concept: *poly(p-phenylene pyromellitimide)*

In this section, the outcome of the first HTP reactions is discussed. The proof of concept was demonstrated with *poly*(PDA-PMA). It is the most rigid member of the HPP family,²² and therefore the best candidate in terms of achieving high crystallinity according to YAGHI's principles of reticular chemistry by using stiff molecular tectonics.⁶⁹

Poly(PDA-PMA) is obtained from *p*-phenylene diamine (PDA) and pyromellitic acid (PMA) (**scheme 9**). Both monomers form a monomer salt if brought in contact in protic solvents. The monomer salt undergoes HT polycondensation to highly crystalline *poly*(PDA-PMA) as discussed in the following sections.

4.1.1 The Monomer Salt

The preparation of monomer salts prior to the polycondensation is an established method for controlling the monomers stoichiometry, *i.e.* generating ideal stoichiometry within one single precursor.⁷⁰ Therefore, we choose to start directly from the monomer salt to ensure ideal stoichiometry, which is needed to obtain high conversion and degrees of polymerization according to CAROTHERS' law (see **section 2.2.2**).¹⁷ Accordingly, we prepared the monomer salt for PI synthesis: In a first step, pyromellitic dianhydride (PMDA) is hydrolysed to PMA, when subjected to the reaction medium water. The diamminium dicarboxylate dicarboxylic acid salt $[H_2PDA^{2+}PMA^{2-}]$ is formed by an acid-base reaction with *p*-phenylene diamine (PDA) (**scheme 9**) as a consequence of the pK_A difference between amine and carboxylic acid functions and mediated by the protic solvent water. The formation of monomer salts is unavoidable in the HT regime.⁷



Scheme 9: Formation of *poly*(PDA-PMA): PMDA is hydrolyzed to PMA that undergoes an acid-base reaction with PDA to the monomer salt. HTP of monomer salt leads to *poly*(PDA-PMA).

The monomer salt $[H_2PDA^{2+}PMA^{2-}]$ is soluble in several protic and aprotic polar solvents (solubility experiments **section 7.1**), thereby allowing for solution NMR analysis (see **section 7.2** for spectra). ¹H NMR and PXRD proved the equimolar ratio of PDA to PMA, and the diamminium-dicarboxylate-dicarboxylic acid salt structure could be confirmed as $[H_2PDA^{2+}PMA^{2-}]$.

4.1.2 HTP of poly(PDA-PMA)

The purified monomer salt is re-suspended in water, transferred to a PTFE-lined autoclave, which is placed in a preheated oven for the reaction time t_R and reaction temperature T_R (typically 200 °C, 16.7 bar, 1 h, see **section 6.4** for experiments). After t_R the autoclave is quickly cooled back to room temperature by quenching in cold water.

In general, we observe the formation of three phases in the reaction vessel (see **Fig. 6**, page 22) after HTP: The *a*-phase (major phase, 92 - 98 wt%) appears as orange-yellowish powder at the bottom of the glass liner, the minor brown *b*-phase (2 - 8 wt%) is less dense and on the top of

the *a*-phase. The reddish color of the translucent aqueous *c*-phase is a result of the oxidation of PDA (see **section 7.11** for further explanation).

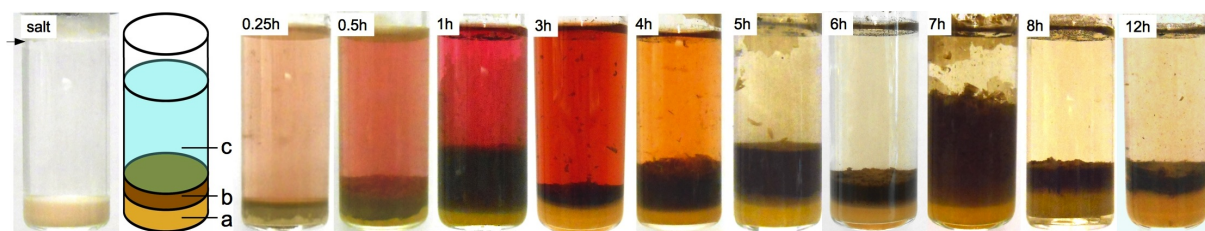


Figure 6: Aspect of monomer salt dispersion prior to HTP, and *poly*(PDA-PMA) dispersions. From left to right: $[\text{H}_2\text{PDA}^{2+}\text{PMA}^{2-}]$ dispersed in distilled water prior to HTP; Schematic of a glass liner after HTP with nomenclature of the product phases; Photographs of liners after 0.25, 0.5, 1, 2, 4, 5, 7, 8, 12 h of reaction. Figure was reproduced from BAUMGARTNER.³⁵

The *a*- and *b*-phases were isolated, dried and characterized by FT-IR-ATR. All HTP products show the classical cyclic imide modes ($\tilde{\nu}_{\text{as}}(\text{C}=\text{O}) \approx 1775 \text{ cm}^{-1}$, $\tilde{\nu}_{\text{s}}(\text{C}=\text{O}) \approx 1720 \text{ cm}^{-1}$ and $\tilde{\nu}_{\text{s}}(\text{C}-\text{N}) \approx 1365 \text{ cm}^{-1}$) in the FT-IR-ATR spectra (**Fig. 7**). We conclude full consumption of the monomer salt for reactions at $t_R > 1 \text{ h}$, since the typical monomer salt modes ($\tilde{\nu}_{\text{as}}(\text{Ar}-\text{NH}_3^+) \approx 2830 \text{ cm}^{-1}$, $\tilde{\nu}_{\text{s}}(\text{Ar}-\text{NH}_3^+) \approx 2580 \text{ cm}^{-1}$, $\tilde{\nu}(\text{C}=\text{O}, \text{Ar}-\text{COOH}) \approx 1690 \text{ cm}^{-1}$, $\nu_{\text{as}}(\text{C}=\text{O}, \text{Ar}-\text{COO}^-) \approx 1605 \text{ cm}^{-1}$ and $\nu_{\text{s}}(\text{C}=\text{O}, \text{Ar}-\text{COO}^-) \approx 1570 \text{ cm}^{-1}$ emphasized by gray dotted lines in **Fig. 7**) are not visible in the FT-IR-ATR spectra of *poly*(PDA-PMA). In FT-IR-ATR spectra of *poly*(PDA-PMA) synthesized at $t_R < 1 \text{ h}$, modes of unreacted monomer salt can be observed (see **section 7.7** for spectra). Moreover, *a*- and *b*-phase are chemically identical according to IR analysis. We do not observe modes related to *poly*(amic acids) which would appear as strong modes at $\tilde{\nu}(-\text{NH}-) \approx 3100 \text{ to } 3300 \text{ cm}^{-1}$ corresponding to amid N-H vibrations.

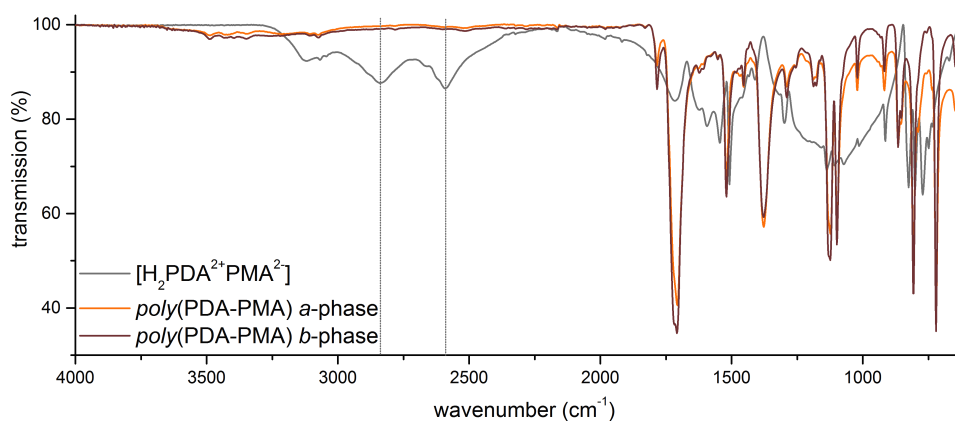


Figure 7: FT-IR-ATR spectra of *a*- and *b*-phase of *poly*(PDA-PMA) and monomer salt; Orange for *poly*(PDA-PMA) *a*-phase, red for *poly*(PDA-PMA) *b*-phase and gray for $[\text{H}_2\text{PDA}^{2+}\text{PMA}^{2-}]$. Characteristic ammonium modes ($\tilde{\nu}_{\text{as}}(\text{Ar}-\text{NH}_3^+) \approx 2830 \text{ cm}^{-1}$, $\tilde{\nu}_{\text{s}}(\text{Ar}-\text{NH}_3^+) \approx 2580 \text{ cm}^{-1}$) are emphasized by gray dotted lines. No ammonium modes are visible in spectra of *p*(PDA-PMA) but imide modes ($\tilde{\nu}_{\text{as}}(\text{C}=\text{O}) \approx 1775 \text{ cm}^{-1}$, $\tilde{\nu}_{\text{s}}(\text{C}=\text{O}) \approx 1720 \text{ cm}^{-1}$ and $\tilde{\nu}_{\text{s}}(\text{C}-\text{N}) \approx 1365 \text{ cm}^{-1}$). Figure was reproduced from BAUMGARTNER.³⁵

Due to the insolubility (see **section 7.5** for solubility tests) and the high thermal stability ($T_d \approx 600$ °C; see **section 7.10** for TGA) of both $p(\text{PDA-PMA})$ phases, we conclude a high degree of condensation.

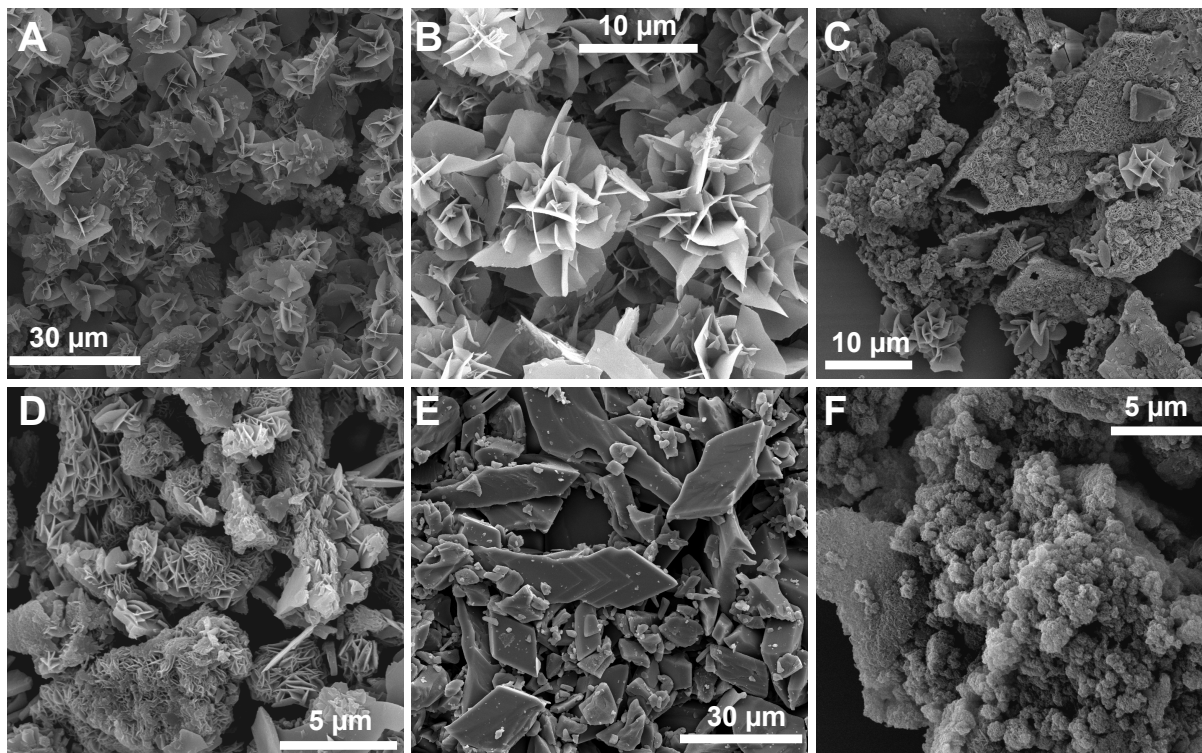
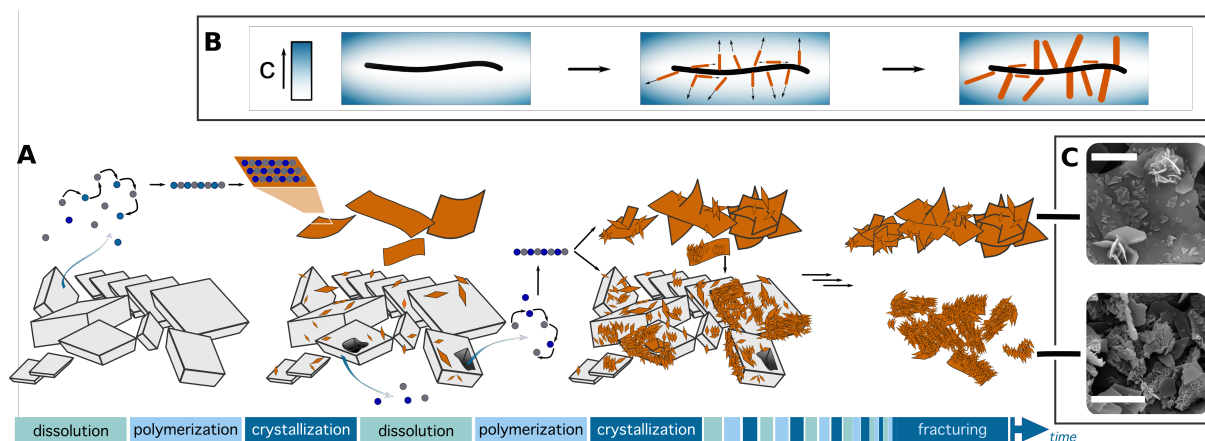


Figure 8: SEM micrographs of monomer salt and $\text{poly}(\text{PDA-PMA})$. A,B: $\text{poly}(\text{PDA-PMA})$ b -phase of $t_R = 3$ h (A), 8 h (B); C,D: $\text{poly}(\text{PDA-PMA})$ a -phase of $t_R = 1$ h (C), 12 h (D); E: monomer salt; F: $\text{poly}(\text{PDA-PMA})$ synthesized in m -cresol *via* PAAs and slowly cool down after reaction for comparison. Figure was reproduced from BAUMGARTNER.³⁵

To get deeper insight into the formation and crystallization process in HTP, we performed scanning electron microscopy (SEM). Micrographs of the b -phase synthesized at different reaction times exhibits a microflower morphology as well as larger sheets as depicted in **Fig. 8A-B**. These microflowers are composed of interstacked petals and are 5 - 10 μm in diameter, whereas the sheets are up to 50 μm in length. Presumably, the sheets act as nuclei for the microflowers. The a -phase shows a different morphology (*cf.* **Fig. 8D-E**). All crystallites obtained in the a -phase at various t_R are built up of densely packed platelets of approximately 1 μm in diameter. Note that these platelets are considerably smaller than the microflowers or sheets and seem to originate from them. Furthermore, we observed hollow particles, as shown in **Fig. 8C**, for short reaction times ($t_R < 3$ h; **Fig. 8C**), which exhibit similar rhombohedral shapes as the monomer salt (**Fig. 8E**). As the reaction progresses, the monomer salt crystals are consumed and act as nuclei for $\text{poly}(\text{PDA-PMA})$ crystallization. For longer reaction times ($t_R > 4$ h) the morphological similarity between monomer salt and polymer disappears.

Intriguingly, we found similarities of the obtained morphologies to so-called barite desert roses. The latter are formed by a geometrical selection mechanism. We correlated a related mechanism to *poly*(PDA-PMA) morphologies and proposed a formation hypothesis (**Fig. 10**). At ambient conditions, the monomer salt is insoluble in water but possesses a slight solubility in the HT regime. Therefore, the first step of the crystal growth mechanism is the dissolution of a small amount of monomer salt. In the second step, *poly*(PDA-PMA) is formed by polymerization in solution and crystallizes in the third step and forms large sheets, that act as seed for further crystallization (**Fig. 10A**). Due to the geometrical selection process, crystallites that grow perpendicular to the substrate, are able to reach regions with higher monomer concentration (**Fig. 10B**), and thus grow faster^{iv}. Whereas, crystallites that are oriented in parallel to the substrate cease growing, because of the consumption of monomer close to the substrate. This selection process leads to the flower-like particles, which act as nuclei for the densely packed platelets during the course of reaction. Consequently, the density of the more densely packed aggregates is higher as the density of microflowers from early stages of the reaction. Therefore, the densely packed platelets sink to the bottom of the reaction vessel and become the *a*-phase.



Scheme 10: Hypothesis of HT formation of *poly*(PDA-PMA). A: Polycrystalline monomer salt dissolves partially, polymerizes and as formed *poly*(PDA-PMA) crystallizes; B: Formation of microflowers by geometrical selection: Nuclei with a perpendicular orientation to the seed *poly*(PDA-PMA) sheet continue growing, whereas nuclei oriented parallel cease growing. This is due to the monomer concentration increasing to higher distances from the sheet. C: Representative SEM images of *a*- and *b*-phase; scale bar is 5 μm . Scheme was reproduced from BAUMGARTNER.³⁵

However, the surface of the monomer salt acts as site of nucleation as well. As a result of consecutive dissolution of the initial monomer salt crystallites, and rapid crystallization of *poly*(PDA-PMA) near the surface of the monomer salt lead ultimately to hollow rhombohedral particles (**Fig. 8C**). These particles are decorated with small *poly*(PDA-PMA) crystallites and replicate

^{iv}HTP is performed in non-stirred autoclaves, allowing for this formation process.

the external shape of the initial monomer salt crystals. At longer reaction times ($t_R > 5$ h) the hollow replica fracture and lose their morphological resemblance to the monomer salt.

Furthermore, monomer salts are able to form PIs directly *via* solid-state polymerization (SSP),^{33,34} which leads to the exact copies of the monomer salt crystals. This polymerization mechanism could occur, because the monomer salt is presumably not fully dissolved in the HT regime and can therefore undergo SSP in dispersion. Since we do not find morphologies related to the initial monomer salt, we believe this potential pathway to be basically inexistent in the case of *poly*(PDA-PMA).

To clarify if the observed morphologies are an intrinsic feature of chemical bonding in *poly*(PDA-PMA) or if it is a consequence of HTP and its reaction conditions, we synthesized *poly*(PDA-PMA) by the classical pathway, *i.e.* *via* the corresponding PAA, in analogy to previous reports (see **section 6.5** for experimental details).⁶ The *poly*(PDA-PMA) dispersion obtained from the classical two-step procedure was separated into two fractions: one part was rapidly precipitated into cold methanol, whereas the other part was allowed to slowly cool down to room temperature, thereby potentially allowing for higher crystallinity.⁷¹ For both PI products, FT-IR-ATR spectra confirmed the formation of *poly*(PDA-PMA) (see **section 7.7**). However, SEM analysis revealed a striking difference from *poly*(PDA-PMA) synthesized hydrothermally: As shown in **Fig. 8F**, page 23, representative for both conventionally synthesized PIs, no platelet-like crystallites were observed, but spherical aggregates of roundish particles and fibers. Subsequently, the conventionally synthesized *poly*(PDA-PMA) was subjected to HT conditions (200 °C, 12 h) in order to exclude the possibility of hydrothermal recrystallization. SEM analysis showed no morphological change by HT treatment).

This result indicates that (i) *poly*(PDA-PMA) molecules do not dissolve at 200 °C in the HT regime, thus *poly*(PDA-PMA) morphologies obtained from HTP do not originate from a recrystallization process and (ii) the dissolved monomers polymerize and crystallize in one step. Therefore, we conclude a dissolution-polymerization-crystallization formation process during HTP.

Sharp edges and recurrent angles in the obtained morphologies are indicative for a highly ordered material, hence we carried out powder X-ray diffraction (PXRD) in order to determine the crystallinity of *poly*(PDA-PMA). As depicted in **Fig. 9A** (see **section 7.8** for PXRD pattern of *b*-phase) neither *poly*(PDA-PMA) synthesized hydrothermally nor *poly*(PDA-PMA) synthesized conventionally show any reflections related to unreacted monomers. Classically synthesized *poly*(PDA-PMA) is semicrystalline and exhibits two broad amorphous halos centered around 19

$^{\circ}(2\theta)$ and $27 - 29^{\circ}(2\theta)$, whereas *a*- and *b*-phase of *poly*(PDA-PMA) obtained *via* HTP are highly crystalline. Indexing of the PXRD patterns for the *a*- and *b*-phase of *p*(PDA-PMA) gives an orthorhombic unit cell with $a = 5.390 \text{ \AA}$, $b = 8.341 \text{ \AA}$, and $c = 12.365 \text{ \AA}$. Both synthetic routes lead to patterns with all principal $(00l)$ reflections for this unit cell at $7.1, 14.3, 21.5, 28.8, 36.3$ and $43.9^{\circ}(2\theta)$. This nicely illustrates the effect of molecular stiffness of the repeating unit in *poly*(PDA-PMA). The 12.365 \AA repeat corresponds to the strut length (*i.e.* the repeating unit) of *poly*(PDA-PMA) as seen in **Fig. 9D**, hence we confirm that the principal polyimide chain has been formed *via* both synthesis methods.

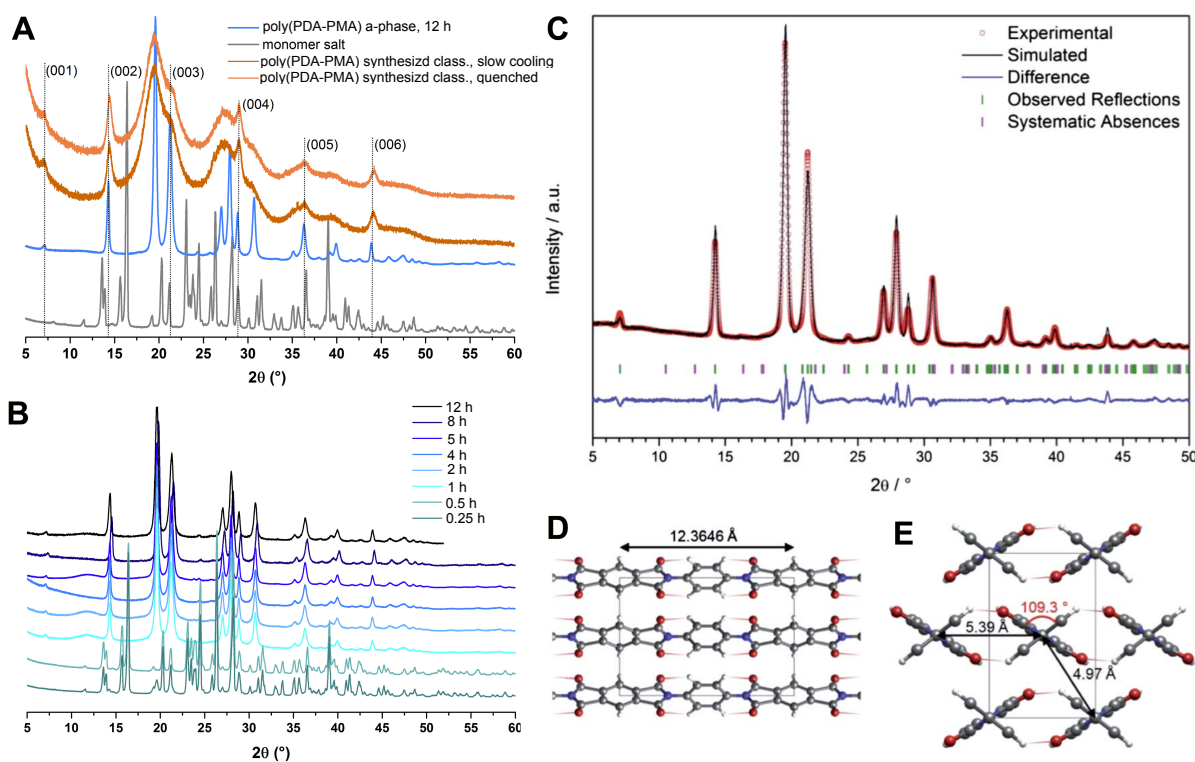


Figure 9: **A-B:** PXRD patterns of *poly*(PDA-PMA): **A:** monomer salt compared with *poly*(PDA-PMA) synthesized *via* HTP and conventionally in *m*-cresol with characteristic $(00l)$ Bragg peak positions of *poly*(PDA-PMA) marked as dotted lines; **B:** *poly*(PDA-PMA) synthesized at various t_R . **C-E:** Rietveld fit performed on the PXRD pattern of *poly*(PDA-PMA) synthesized hydrothermally: ($R_{wp} = 6.70 \%$, $R_p = 4.60 \%$) with the observed pattern in red, a refined profile in black, a difference plot in blue, and Bragg peak positions in green (observed) and pink (absent)(**C**); **E-D:** Projection along the *a*-axis (**D**) and the *c*-axis (**E**) of *poly*(PDA-PMA). O-H bonds are shown as red-to-white gradient lines ($l(\text{O-H}) = 2.661 \text{ \AA}$, at 132.6°). The parameters of the orthogonal unit cell (*Pbam*, no. 55) are $a = 5.390 \text{ \AA}$, $b = 8.341 \text{ \AA}$, and $c = 12.365 \text{ \AA}$. Figure has been adapted from BAUMGARTNER.³⁵

However, the (hkl) - and $(hk0)$ -reflections can only be distinguished in the PXRD profiles of *poly*(PDA-PMA) synthesized *via* HTP, while they appear as broad and featureless for the conventionally synthesized *poly*(PDA-PMA). Structural refinement of the XRD pattern of *poly*(PDA-

PMA) synthesized hydrothermally (*a*-phase, 12 h, 200 °C, see **Fig. 9C-E**) suggests that the aryl-linkers are twisted at 109.3° out of the plane of the imide bond. Due to this asymmetric twist, chain-to-chain distances are 5.39 Å, along the *a*-axis and 4.97 Å, along the *ab*-vector. Thereby, close contacts of 2.661 Å, between oxygen and hydrogen atoms of neighboring chains are observed which have been described as weak hydrogen bonds in literature (**Fig. 9E**).⁷² Therefore, we believe that the outstanding crystallinity of *poly*(PDA-PMA) is a result of this close-packing of chains and the formation of weak hydrogen-bonds.

Fig. 9B depicts PXRD patterns of *poly*(PDA-PMA) synthesized hydrothermally at 200 °C at various reaction times ($t_R = 0.25 - 12$ h). PXRD patterns obtained at short reaction times $t_R < 1$ h show mainly unreacted monomer salt reflections. This is a result of the long heating time until the autoclave reaches the final reaction temperature. We estimate the heating time until the reaction mixture reaches 200 °C to be *ca.* 30 - 40 min. Hence for experiments with $t_R = 15 - 30$ min 200 °C is not reached during the experiment. *Poly*(PDA-PMA) synthesized for $t_R > 1$ h the reaction appears to be complete, since no monomer salt reflections are visible anymore. Moreover, we do not observe a notable change in crystallinity for $t_R > 8$ h.

In summary, we could show that HT processes can be applied to PIs. The polymerization time in HTP is much reduced compared to conventional polycondensations: we obtain fully condensed products after only 1 h at 200 °C. Furthermore, as HT mineral formation leads to crystalline materials, HTP of PMA and PDA yields highly crystalline *poly*(PDA-PMA).

4.2 Benzophenonetetracarboxylic Acid-Based Polyimides: Systems with Increased Flexibility

The previously described PI system, *poly*(*p*-phenylene pyromellitimide), showed outstanding crystallinity. This is most likely due to the stiff monomers that facilitates crystallization.⁶⁹ In general, more flexible polymer chains, *i.e.* polymers with less stiff monomers, are more difficult to crystallize because they offer higher degrees of freedom. But what if less stiff monomers are polymerized *via* HTP?

We choose two benzophenone-3,3',4,4'-tetracarboxylic acid (BTA) based systems (see **Fig. 10**, page 28) in combination with two different diamine monomers, *p*-phenylene diamine (PDA) and benzidine (Bz). This leads to following alterations: (*i*) their dianhydride comonomers are less stiff and therefore the corresponding PIs are probably easier to process compared to *poly*(PDA-PMA), (*ii*) they are reported to be amorphous polymers when classically synthesized,^{73,74} and

(iii) their monomer salts are to a small extent soluble below 100 °C. As a result of the solubility of the monomer salt in the subhydrothermal regime (< 100 °C, sHT) we find less crystalline PIs (amorphous background for both systems in PXRD diffractograms) and unknown morphologies. These new findings encouraged us to perform an intensive set of experiments to develop a mechanistic picture of HTP (see **section 6.4** for list of experiments). The outcome of HTP experiments with BTA-based monomers are discussed in this section.

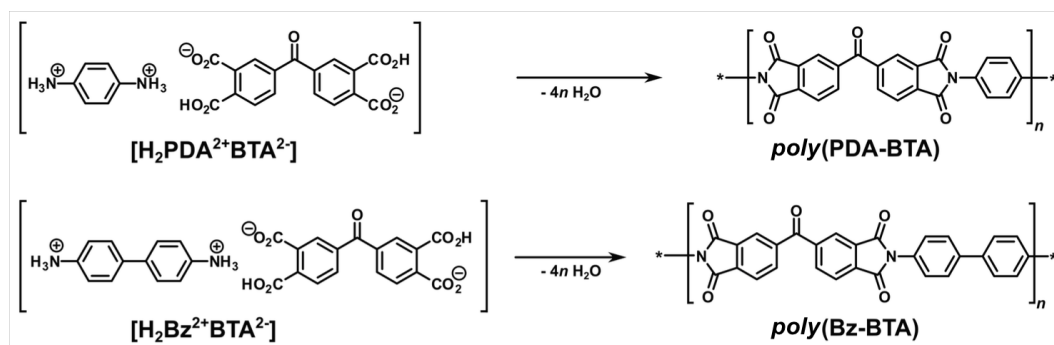


Figure 10: BTA-based monomer salts and PIs. Monomer salt of BTA and PDA, thus $[H_2PDA^{2+}BTA^{2-}]$, and the resulting PI $poly(PDA-BTA)$ and the monomer salt of BTA and Bz, thus $[H_2Bz^{2+}BTA^{2-}]$, and the resulting PI $poly(Bz-BTA)$.

4.2.1 Benzophenonetetracarboxylic Acid-based Monomer Salts

Initially, we synthesized PIs according the previously established route (see **section 4.1**), *i.e.* we prepared the monomer salts by vigorous stirring of the respective diamine with an equimolar amount of BTA in water at 80 °C for 4 h. Interestingly both monomer salts had started to oligomerize at these conditions (presence of imide modes in FR-IR-ATR, in coexistence with monomer salt modes, see **section 6.3** for FT-IR-ATR spectra). The presence of imide modes indicates that both monomer salts had already started to dissolve and imidize at 80 °C. Therefore, the monomer salts were then prepared at room temperature (see **section 6.3** for protocol), which led to the desired monomer salts without imide modes in FT-IR-ATR spectra (see **section 7.3**). Similar to $poly(PDA-PMA)$'s monomer salt, the BTA-based monomer salts were soluble in several protic and aprotic polar solvents (for solubility experiments see **section 7.1**), thereby allowing for solution NMR analysis (see **section 7.2**). From 1H -NMR, we find good agreement with a equimolar ratio of BTA to each diamine, respectively, and exclusively peaks related to ammonium protons, but no remaining amine signals. Therefore, both monomer salts are diamminium-dicarboxylate-dicarboxylic acid salts ($[H_2PDA^{2+}BTA^{2-}]$ or $[H_2Bz^{2+}BTA^{2-}]$, respectively).

4.2.2 HTP of Benzophenone Tetracarboxylic acid-based PIs

According to our previous protocol (see **section 6.4** for experiments), we performed HTP for different reaction times ($t_R = 1$ h, 2 h, 4 h and 12 h) at 200 °C. Similar to *poly*(PDA-PMA) products we found two product phases in the glass liner: a major yellowish *a*-phase and a minor brown *b*-phase for *poly*(PDA-BTA) and yellow-greenish *b*-phase for *poly*(Bz-BTA). The brownish color of *poly*(PDA-BTA)'s *b*-phase as well as its reddish supernatant can be attributed to the oxidation products of PDA (see **section 7.4** for photographs). The solubility tests showed that the BTA-based PI systems are insoluble in any solvent other than *conc.* sulfuric acid (see **section 7.5** for solubility tests).

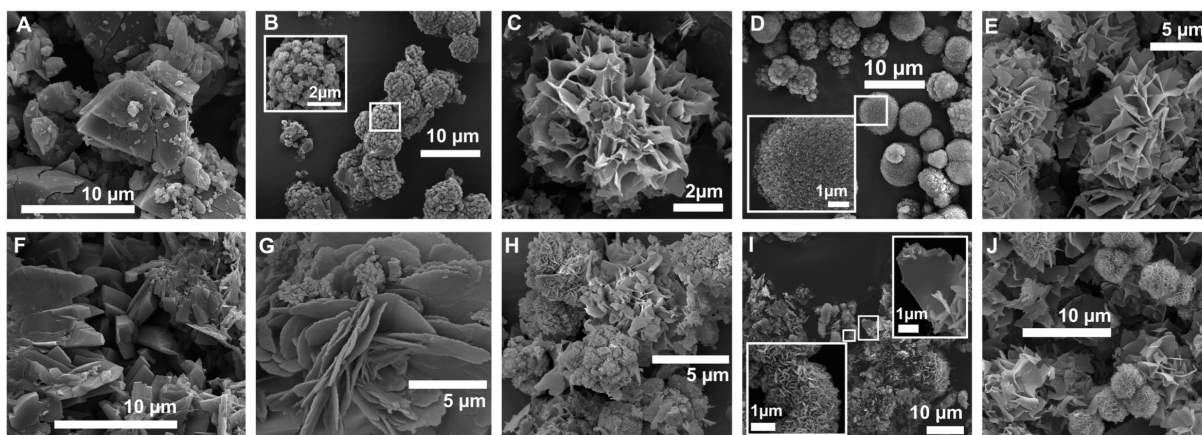


Figure 11: SEM images of monomer salts synthesized at room temperature and PIs synthesized at 200 °C. **A:** $[\text{H}_2\text{PDA}^{2+}\text{BTA}^{2-}]$; **B-C:** *poly*(PDA-BTA), $t_R = 2$ h, *a*-phase (**B**), *b*-phase (**C**); **D-E:** *poly*(PDA-BTA); $t_R = 12$ h, *a*-phase (**D**), *b*-phase (**E**); **F:** $[\text{H}_2\text{Bz}^{2+}\text{BTA}^{2-}]$; **G-H:** *poly*(Bz-BTA), $t_R = 2$ h, *a*-phase (**G**), *b*-phase (**H**); **I-J:** *poly*(Bz-BTA); $t_R = 12$ h, *a*-phase (**I**), *b*-phase (**J**). Figure was reproduced from BAUMGARTNER.³⁶

SEM images in **Fig. 11A** and **F** show the morphology of monomer salts, $[\text{H}_2\text{PDA}^{2+}\text{BTA}^{2-}]$ and $[\text{H}_2\text{Bz}^{2+}\text{BTA}^{2-}]$, respectively. Evidently, the monomer salts show a striking morphological difference to both PI products. Intergrown aggregates can be observed for both monomer salts, whereas, *poly*(PDA-BTA) synthesized for $t_R = 2$ h and 12 h (**Fig. 11B-E**) depicts dense roundish cauliflower-like shapes and spherical particles decorated with nanocrystallites in the *a*-phase (**Fig. 11B,D**), and microflower morphology in the *b*-phase (**Fig. 11C,E**) similar to *poly*(PDA-PMA), for all tested t_R . For longer t_R it seems that morphologies of higher homogeneity are observed in the *a*-phase, while the morphology of the *b*-phase is not influenced by t_R . *Poly*(Bz-BTA) shows a similar morphological behaviour: The *a*-phase evolves with t_R . For $t_R = 1$ h, we find aggregates of platy crystallites of *ca.* 1 μm in diameter and narrow size distribution. Products synthesized for $t_R = 12$ h show flat flower-shaped crystallites with rounded petals,

which are decorated with smaller crystallites exclusively on the petals' rims. For the longest reaction times ($t_R = 12$ h) we find rounded interstacked flowers. However, for the b -phase we do not find a morphological variation with t_R . As previously discussed, the b -phase polymerizes and crystallizes in solution in the HT regime. The a -phase is composed of PI that also polymerizes in solution, but crystallizes on earlier formed PI crystallites, which leads to denser particles. Furthermore, we stated a polymerization-crystallization process by relating products of a geometrical selection process to PIs formed by HTP. Thus, we were able to explain the previous reported morphologies except for the cauliflower-like morphologies. Their roundish shape suggests the growth of PI crystallites on spherical objects. As discussed in **section 4.3**, HTP at lower temperatures lead to these spherical PI particles, that act as macroscopic nuclei.

PXRD revealed high degrees of crystallinity for both a - and b -phase as indicated by ordered morphologies depicted in SEM images. The PXRD pattern of both systems synthesized at $t_R = 12$ h are depicted in **Fig. 12**. As reported previously, crystalline $poly(\text{PDA-BTA})$ was synthesized by KIMURA and co-workers *via* phase-separation techniques.²⁹ Intriguingly, $poly(\text{PDA-BTA})$ obtained by HTP exceeds their reported crystallinity, which is substantiated by additional reflections in the PXRD pattern (highlighted by blue arrows, **Fig. 12A**).

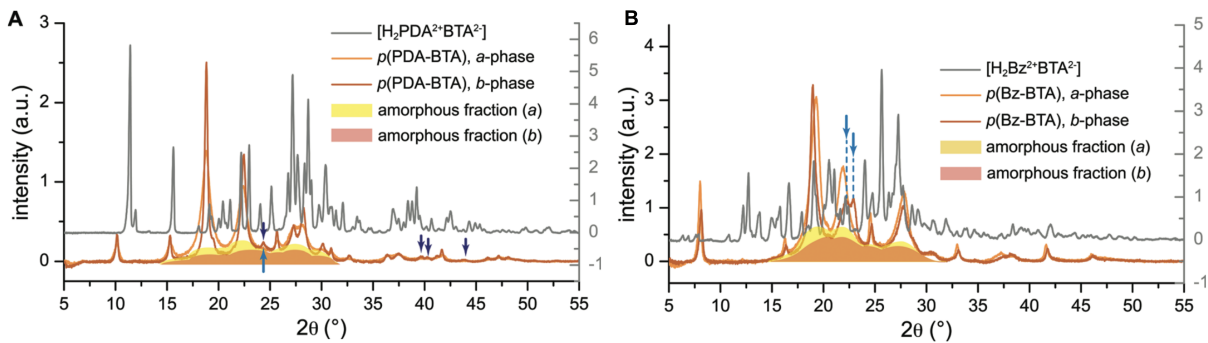


Figure 12: PXRD patterns of the monomer salts and dried a - and b -phase after HTP ($T_R = 200$ °C, $t_R = 12$ h); the amorphous fractions are illustrated by yellow areas. **A:** $poly(\text{PDA-BTA})$; **B:** $poly(\text{Bz-BTA})$. Dark blue arrows indicate additional reflections compared to previously reported $poly(\text{PDA-BTA})$,²⁹ light blue arrows indicate additional reflections which are not found in the a -phase. Figure was reproduced from BAUMGARTNER.³⁶

In agreement with the improvement of the morphological homogeneity of both PI systems, respectively, crystallinity of the a -phases increases with higher t_R at $T_R = 200$ °C. While the crystallinity of both b -phases remains unchanged for different t_R . From PXRD we find three major differences between the a - and the b -phase: (i) The b -phase shows sharper reflections and a smaller amorphous background; (ii) Additional reflections can be observed in the patterns of the b -phases, which are not present in the pattern of the a -phase (at 24 °(2θ) for $poly(\text{PDA-BTA})$ and at 22 °(2θ) for $poly(\text{Bz-BTA})$; Emphasized by light blue arrows in **Fig. 12**); (iii) At

shorter reaction times ($t_R < 2$ h) the *b*-phase shows reflections of unreacted monomer salt. The reaction is complete at $t_R > 2$ h.

In conclusion, all mentioned findings confirm that the *b*-phase exclusively forms *via* the previously stated polymerization-crystallization process. Since the reaction is complete at $t_R > 2$ h, the *b*-phases morphology nor the crystallinity is affected by t_R .

Despite the impressive crystallinity of both BTA-based PIs, our observations deviate from our previous reports for *poly*(PDA-PMA): We find amorphous backgrounds (illustrated as colored areas in **Fig. 12**) in the PXRD patterns of both systems.

The following sections provide explanations for the amorphous fractions of the BTA-based PIs by deeper insight into physicochemical properties of the starting compounds as well as by identifying several polymerization mechanisms occurring in HTP. Furthermore, the relationship between crystallinity and reaction temperature and heating rate will be discussed.

4.3 Global Picture: General Ongoing in Hydrothermal Polymerization

As detailed in the following sections, we conclude that the observed amorphous backgrounds in both BTA-based PI systems are consequences of (i) the solubility and reactivity of the monomer salt at lower temperatures, namely in the subhydrothermal regime (sHT, $T_R < 100$ °C) and lower HT regime (lHT, $T_R < 150$ °C) (**section 4.3.1** and **section 4.3.2**). (ii) Solid-state polymerization taking place in dispersion in the HT regime (**section 4.3.4**). Furthermore, we were able to relate the polymerization parameters (T , t , p , c) to the obtained PI crystallinity and morphology (**section 4.3.5**). It appears that the heating time t_h to reach the reaction temperature T_R is affecting the properties of the final PI product, as it is discussed within **section 4.3.3**.

4.3.1 Consequences of the Physicochemical Properties of the Monomer Salt for HTP

As discussed in the previous sections, we performed HTP with three different PI system. Syntheses were carried out according to the same protocol (in autoclaves, $T_R = 200$ °C, $t_R > 2$ h), still the obtained products differ for each systems. As a result of the similarity of the chemical structure, one would expect highly crystalline PI products as found for *poly*(PDA-PMA). So, what are the origin for the morphology and crystallinity differences between PMA- and BTA-based PIs?

One main difference is the reactivity of the monomer salt at lower temperatures ($T_R < 100$ °C).

As mentioned earlier, the BTA-based monomer salts, $[\text{H}_2\text{PDA}^{2+}\text{BTA}^{2-}]$ and $[\text{H}_2\text{Bz}^{2+}\text{BTA}^{2-}]$, respectively, had imidized (imide modes found in FT-IR-ATR spectra), when prepared at 80 °C, whereas the monomer salt of *poly*(PDA-PMA) ($[\text{H}_2\text{PDA}^{2+}\text{PMA}^{2-}]$) had not. Thus, we conclude that the BTA-based monomer salts are to a small amount soluble in water at lower temperature and can undergo reactions in solution (*e.g.* polymerization, oligomerization, imidization or recrystallization of the monomer salt). While the monomer salt of *poly*(PDA-PMA) is virtually insoluble in water at temperatures below 100 °C. But why is $[\text{H}_2\text{PDA}^{2+}\text{PMA}^{2-}]$ less soluble than $[\text{H}_2\text{PDA}^{2+}\text{BTA}^{2-}]$ and $[\text{H}_2\text{Bz}^{2+}\text{BTA}^{2-}]$? An attempt to answer this question is made by a fundamental consideration of solubility. There are two energetic contributions that have to be considered when dissolving an organic salt: (*i*) the energy required to break up the salt crystal (lattice energy), which has to be supplied; And (*ii*) the solvation energy of the organic ions when dissolved, which is released. The solvation energy corresponds to the number and strength of bonds that are formed between the solute and the dissolved molecule. In the case of dissolving organic salts, H-bonds are formed between the organic ions and water. On the other hand, the energy required to break the monomer salt's crystal lattice depends on how strongly the organic ions in the lattice are bound to each other (H-bonds, VAN DER WAALS interactions, π - π interactions). Thus, one would expect the smaller ions of $[\text{H}_2\text{PDA}^{2+}\text{PMA}^{2-}]$ to be solvated more effectively. Nonetheless, KRIECHBAUM AND CERRÓN-INFANTES *et al.* could determine the crystal structure of $[\text{H}_2\text{PDA}^{2+}\text{PMA}^{2-}]$, which exposed an outstandingly high crystal density as compared to similar organic salts.³⁴ As crystal density can be related to lattice energy (more effective packing), we believe the lattice energies of the BTA-based monomer salts to be smaller, which leads to their higher solubility and reactivity at lower temperatures. Generally speaking, a precise prediction of to what extent a monomer salt is soluble at lower temperatures depends strongly on the impact of the energetic contributions.

Usually, we perform HTP experiments at > 180 °C, so why would one be interested in the reactivity of the monomer salt at lower temperatures? Since we are using autoclaves that are placed in a preheated oven, the monomer salt dispersion inevitably passes the sHT and lHT regime. Due to the dissimilarity of the materials used in our autoclaves (steel, glass, PTFE), thermal conduction between these materials has to occur. Given the temperature difference of 175 °C (for $T_R = 200$ °C) and the different materials present, we estimate the heating time t_h until the reaction mixture reaches T_R to be *ca.* 30 - 40 min.

During this time, reactions in the sHT regime can occur. To determine the influence of subhydrothermal reactions (sHTR) we refluxed the BTA-based monomer salts for 1 h and 12 h,

respectively, in water and analyzed the crude products by FT-IR-ATR and PXRD. The obtained FT-IR-ATR spectra for both systems (**Fig. 13**, page 33) show the typical ammonium modes ($\tilde{\nu}_{\text{as}}(\text{Ar-NH}_3^+) \approx 2830 \text{ cm}^{-1}$, $\tilde{\nu}_{\text{s}}(\text{Ar-NH}_3^+) \approx 2580 \text{ cm}^{-1}$), which correspond to the monomer salt, as well as the characteristic imide modes ($\tilde{\nu}_{\text{as}}(\text{C=O}) \approx 1775 \text{ cm}^{-1}$, $\tilde{\nu}_{\text{s}}(\text{C=O}) \approx 1720 \text{ cm}^{-1}$ and $\tilde{\nu}_{\text{s}}(\text{C-N}) \approx 1365 \text{ cm}^{-1}$). Thus, both systems had already started to react in the sHT regime. This experiment was not carried out with $[\text{H}_2\text{PDA}^{2+}\text{PMA}^{2-}]$, since its preparation is performed at $80 \text{ }^\circ\text{C}$ for several hours, leading exclusively to the pure monomer salt and thus no premature polymerization ($< 100 \text{ }^\circ\text{C}$).

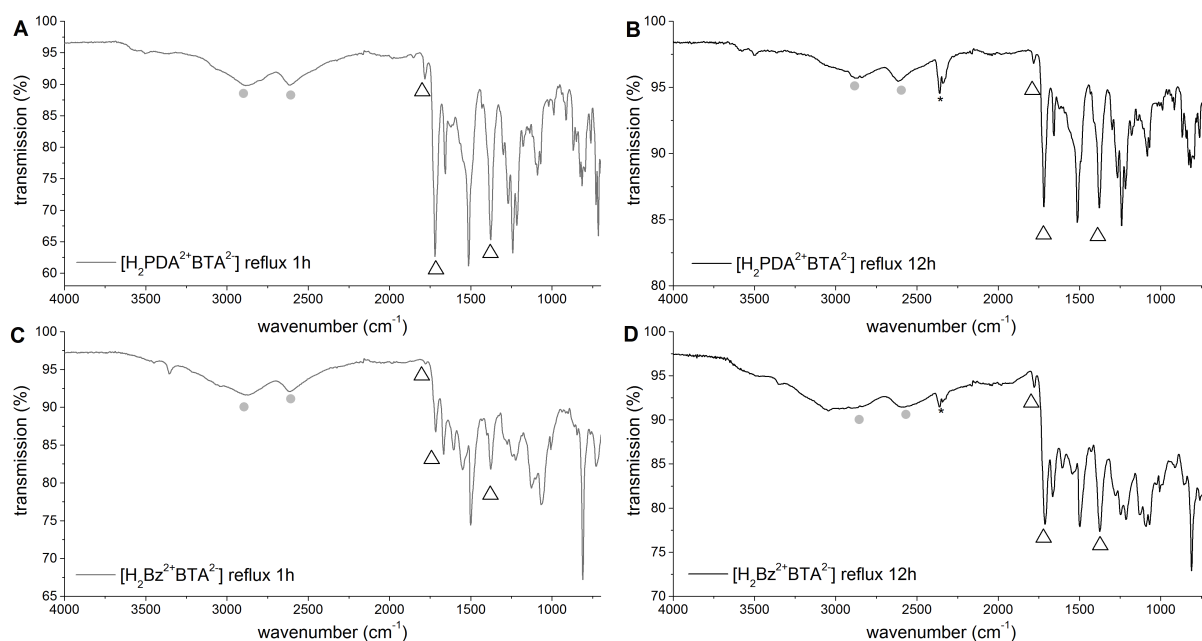


Figure 13: FT-IR-ATR spectra of BTA-based monomer salts refluxed for 1 h and 12 h in water. **A:** $[\text{H}_2\text{PDA}^{2+}\text{BTA}^{2-}]$ refluxed for 1 h, **B:** $[\text{H}_2\text{PDA}^{2+}\text{BTA}^{2-}]$ refluxed for 12 h, **C:** $[\text{H}_2\text{Bz}^{2+}\text{BTA}^{2-}]$ refluxed for 1 h, **D:** $[\text{H}_2\text{Bz}^{2+}\text{BTA}^{2-}]$ refluxed for 12 h. The relevant modes are emphasized as follows: • = typical monomer salt modes ($\tilde{\nu}_{\text{as}}(\text{Ar-NH}_3^+) \approx 2830 \text{ cm}^{-1}$, $\tilde{\nu}_{\text{s}}(\text{Ar-NH}_3^+) \approx 2580 \text{ cm}^{-1}$, $\tilde{\nu}(\text{C=O, Ar-COOH}) \approx 1690 \text{ cm}^{-1}$) Δ = characteristic imide modes ($\tilde{\nu}_{\text{as}}(\text{C=O}) \approx 1775 \text{ cm}^{-1}$, $\tilde{\nu}_{\text{s}}(\text{C=O}) \approx 1720 \text{ cm}^{-1}$ and $\tilde{\nu}_{\text{s}}(\text{C-N}) \approx 1365 \text{ cm}^{-1}$). Figure was reproduced from BAUMGARTNER.³⁶

PXRD revealed strong monomer salt reflections after 1 h of reflux (emphasized by gray boxes in **Fig. 14**, page 34), whereas, reflections related to the monomer salt are less prominent in PXRD patterns after 12 h of reflux. Interestingly, we find reflections that cannot be attributed to the monomer salt neither to the PI product. Additional reflections are observed at $13, 14, 21$ and $26^\circ (2\theta)$ for *poly*(PDA-BTA) and at $6, 10$ and $18^\circ (2\theta)$ for *poly*(Bz-BTA). Furthermore, note that all reflux experiments lead to broad amorphous halos, especially for $[\text{H}_2\text{Bz}^{2+}\text{BTA}^{2-}]$ in **Fig. 13D**.

Since we found ammonium modes in the FT-IR-ATR spectra of all samples, basically, potential

sources for these additional reflections might be (i) another polymorph of the monomer salt, (ii) a hydrate of the monomer salt, or (iii) short, crystalline oligomers formed from the monomer salt.

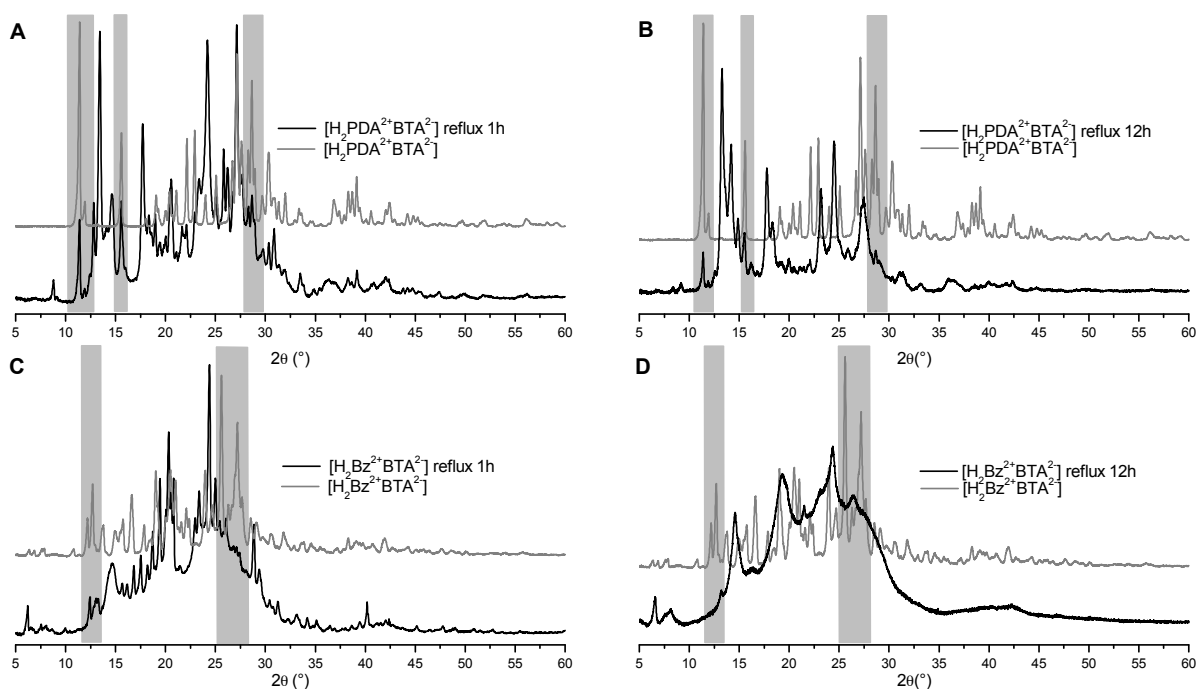


Figure 14: PXRD patterns of BTA-based monomer salts after reflux for 1 h and 12 h superimposed with the corresponding monomer salt patterns (gray). **A-B:** $[\text{H}_2\text{PDA}^{2+}\text{BTA}^{2-}]$ after 1 h (A) and 12 h (B) of reflux in water. **C-D:** $[\text{H}_2\text{Bz}^{2+}\text{BTA}^{2-}]$ after 1 h (C) and 12 h (D) of reflux in water. Gray boxes emphasize monomer salt reflections in the pattern of reflux experiments. Figure was reproduced from BAUMGARTNER.³⁶

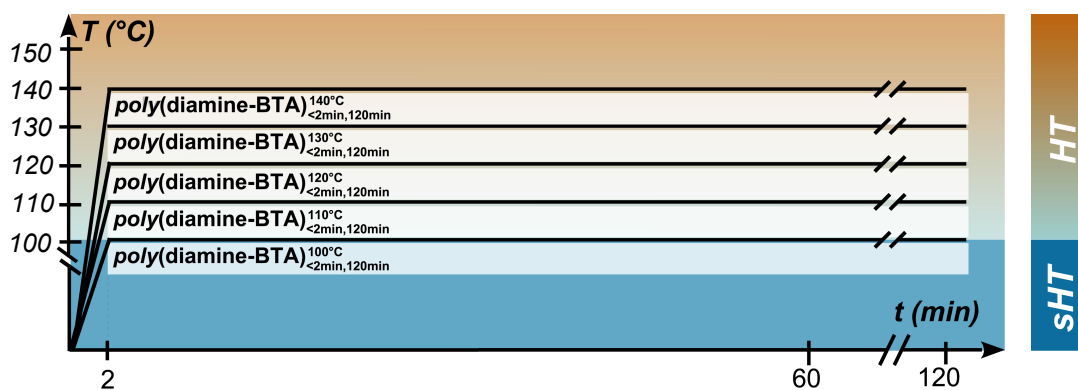
$^1\text{H-NMR}$ and LC/MS proved the presence of zwitterionic dimers $dimer(\text{PDA-BTA})$ and $dimer(\text{Bz-BTA})$ (see **section 7.6** for ^1NMR spectra), containing one BTA and one PDA or Bz unit, respectively, and ionic end groups (NH_3^+ and CO_2^-).

SEM images of the crude products after refluxing for 12 h show big pieces with a few roundish particles. Hence, we conclude, that these spherical particles are formed by classical solution polycondensation, which leads in general to amorphous products. Therefore, we attribute the amorphous background in the PXRD patterns to products of this polymerization mechanism. The finding of initial condensation intermediates, which form in the sHT regime, indicate that the PI formation in HTP is closely related to classical AA/BB step-growth polymerizations.

4.3.2 Influence of Reaction Temperature T_R in Lower HT regime

As previously discussed, reactions in the sHT regime lead amongst others to amorphous products. Since the typical HTP experiment is carried out in autoclaves, the reaction mixture inevitably passes lower temperature regimes while heating up. Thus, time is spent at undesirable sHT conditions. In order to avoid undesirable temperature conditions and control the heating time t_h , we used a microwave reactor for all further experiments. This enabled to reach the desired reaction temperature T_R in $t_h < 2$ min as well as to precisely control t_h for any $t_h > 2$ min. In order to estimate the effect of T_R in the lower HT regime, we performed HTP experiments at $T_R = 100, 110, 120, 130$ and 140 °C with $t_h < 2$ min for $t_R = 120$ min (see **scheme 11** for temperature-time profiles of experiments).

In order to summarize the different parameters (T_R, t_R, t_h), we use the following nomenclature to clearly name the experiments: $poly(\text{diamine} - \text{BTA})_{t_h, t_R}^{T_R}$ with diamines PDA and Bz.



Scheme 11: Temperature-time profiles of experiments in the lower HT regime carried out at $t_h = 2$ min and $t_R = 120$ min. White columns illustrate the time the reaction mixture is kept at T_R , $t_R - t_h$, and give the experiment codes. Scheme was adapted from BAUMGARTNER.³⁷

We characterized the crude products by FT-IR-ATR and PXRD. FT-IR-ATR analysis proved the presence of imide modes as well as characteristic ammonium modes for all obtained products. The PXRD pattern of both PIs obtained in the LHT regime are depicted in **Fig. 15**. *Poly*(PDA-BTA) obtained at $T_R = 100$ °C shows already a crystalline PXRD pattern with reflections that neither correspond to the monomer salt nor to the PI product. We find the same reflections as in the reflux experiments, and consequently attribute the pattern to the dimer *dimer*(PDA-BTA). Higher T_R leads to bigger amorphous backgrounds and from 120 °C on we observe typical *poly*(PDA-BTA) reflections, *i.e.* with the most intense reflections at 10, 19, 22 and 26° (2θ). These increase in sharpness and intensity with increasing T_R .

In order to characterize the increasing amorphous fraction, the samples were immersed in DMSO at room temperature: $poly(PDA-BTA)_{2min,120min}^{100^{\circ}C}$ dissolved entirely and $poly(PDA-BTA)_{2min,120min}^{110^{\circ}C}$, $poly(PDA-BTA)_{2min,120min}^{120^{\circ}C}$, $poly(PDA-BTA)_{2min,120min}^{130^{\circ}C}$ dissolved partially and an insoluble brown residue remained.

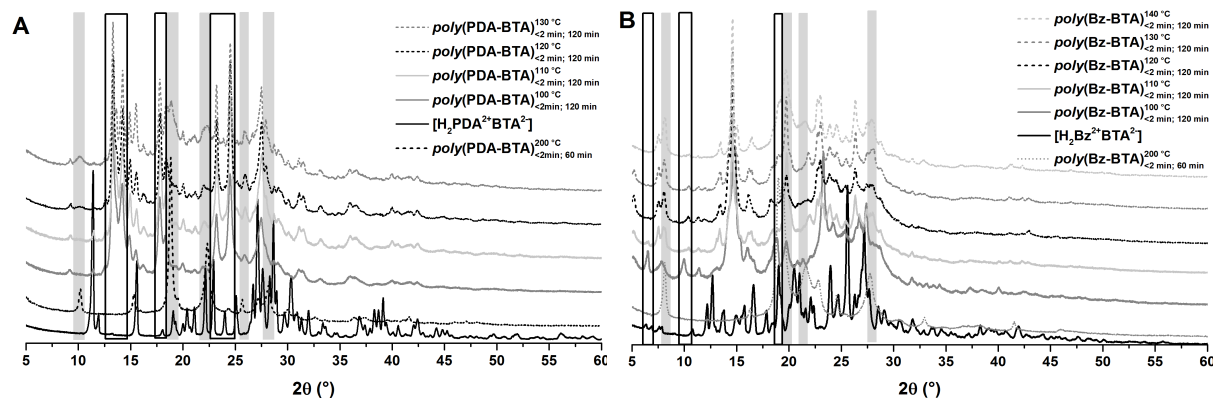


Figure 15: Normalized PXRD patterns of $poly(PDA-BTA)$ and $poly(Bz-BTA)$ synthesized at $t_h = 2$ min and $t_R = 120$ min in the IHT regime, leading to short oligomers. **A:** $poly(PDA-BTA)$; **B:** $poly(Bz-BTA)$; Gray areas highlight additional reflections not present in this reference pattern, white boxes emphasize monomer salt reflections. Figure was reproduced from BAUMGARTNER.³⁷

This residue was separated and washed with distilled water. The FT-IR-ATR spectra of the dried residues show no ammonium modes, thus, all dimer was removed by the washing step and the residues consist of longer oligomers or polymers. PXRD reveals $poly(PDA-BTA)$ reflections on top of broad amorphous halos, without additional reflections associated with the corresponding dimer or monomer salt (**Fig. 16A**). Furthermore, the addition of water to the DMSO solutions of all samples lead to the precipitation of off-white powders. These were dried and analyzed by 1H -NMR and LC/MS, which confirmed the structure of $dimer(PDA-BTA)$. We quantified the amounts of $dimer(PDA-BTA)$ by weighing the residues which are: quantitative ($poly(PDA-BTA)_{2min,120min}^{100^{\circ}C}$), ca. 90 wt% ($poly(PDA-BTA)_{2min,120min}^{110^{\circ}C}$), ca. 65 wt% ($poly(PDA-BTA)_{2min,120min}^{120^{\circ}C}$), and ca. 55 wt% ($poly(PDA-BTA)_{2min,120min}^{130^{\circ}C}$). The decrease of the dimer weight fractions indicates that longer oligoimides are formed with increasing T_R .

Similar to $poly(PDA-BTA)$, we revealed the formation of a dimer, $dimer(Bz-BTA)$, in HTP experiments in the IHT regime for $poly(Bz-BTA)$ (**Fig. 15B**). At the lowest reaction temperature, $T_R = 100$ °C, no reflections of pure $poly(Bz-BTA)$ are observed, but reflections that can be associated with $dimer(Bz-BTA)$ were found at 6, 10 and 18°(2θ). For $poly(Bz-BTA)_{2min,120min}^{110^{\circ}C}$, we find reflections that can be associated to $poly(Bz-BTA)$, specifically at 15, 20, 23 and 26°(2θ) that become more prominent for higher T_R . Reflections associated with $dimer(Bz-BTA)$ fade with increasing T_R and are not visible anymore in the PXRD pattern

of $poly(\text{Bz-BTA})_{2\text{min},120\text{min}}^{130^\circ\text{C}}$. The fractionation of $poly(\text{Bz-BTA})_{2\text{min},120\text{min}}^{T_R}$, was done according to the same protocol as for $poly(\text{PDA-BTA})$, *i.e.* by dissolving in DMSO and reprecipitation in water. Again, we confirmed the presence of $dimer(\text{Bz-BTA})$ by $^1\text{H-NMR}$ and LC-MS. In PXRD we found broad amorphous halos with reflections corresponding to the final $poly(\text{Bz-BTA})$ product (**Fig. 16B**). We determined the weight fractions, which gave: quantitative amounts for $poly(\text{Bz-BTA})_{2\text{min},120\text{min}}^{100^\circ\text{C}}$, 80 wt% ($poly(\text{Bz-BTA})_{2\text{min},120\text{min}}^{110^\circ\text{C}}$), 80 wt% ($poly(\text{Bz-BTA})_{2\text{min},120\text{min}}^{120^\circ\text{C}}$), 40 wt% ($poly(\text{Bz-BTA})_{2\text{min},120\text{min}}^{130^\circ\text{C}}$) and 35 wt% ($poly(\text{Bz-BTA})_{2\text{min},120\text{min}}^{140^\circ\text{C}}$). The findings in PXRD correlate with the observations in SEM: For $poly(\text{PDA-BTA})$ we find mixtures of small amounts of crystalline platelets likely to be related to the presence of monomer salt, with sponge-like, fibrous particles suspected to be associated with $dimer(\text{PDA-BTA})$ and starting from $T_R = 120^\circ\text{C}$, spherical flower-like particles associated with the appearance of crystalline $poly(\text{PDA-BTA})$. At higher T_R , morphologies associated with the monomer salt vanish, whereas the amount of flower-shaped $poly(\text{PDA-BTA})$ crystallites increases. For $poly(\text{Bz-BTA})$, we also find a coexistence of morphologies that can be associated with monomer salt, $dimer(\text{Bz-BTA})$ and $poly(\text{Bz-BTA})$. Again, morphologies associated to $poly(\text{Bz-BTA})$ become more prominent at higher temperatures, while monomer salt related morphologies strongly decrease at *ca.* 140°C .

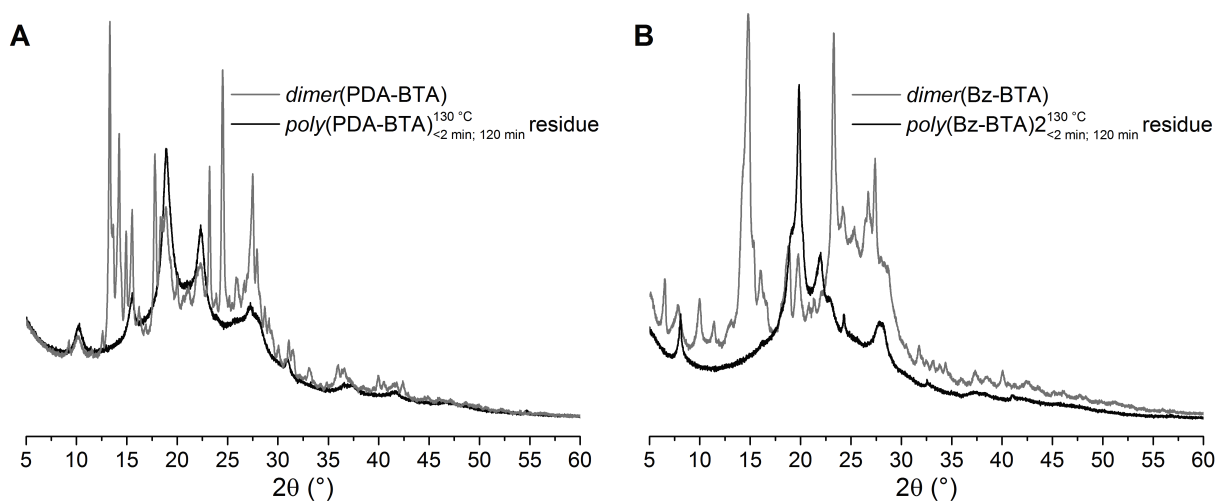


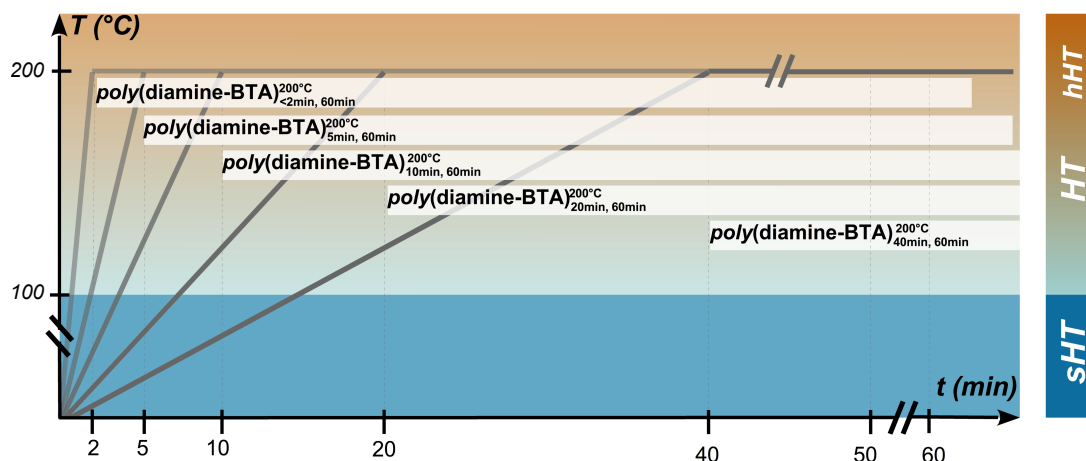
Figure 16: Normalized PXRD patterns of $dimer(\text{PDA-BTA})$ (**A**) and $dimer(\text{Bz-BTA})$ (**B**) and their respective residues, as obtained from reactions $poly(\text{PDA-BTA})_{2\text{min},120\text{min}}^{130^\circ\text{C}}$ and $poly(\text{Bz-BTA})_{2\text{min},120\text{min}}^{130^\circ\text{C}}$. Figure was reproduced from BAUMGARTNER.³⁷

For HTP in the LHT regime we find crystalline dimer species, whose amount decreases with higher T_R , while the amount of amorphous fraction increases. These results could be related to morphologies found in SEM. In conclusion, reactions in the LHT regime influence the degree of crystallinity and the morphological homogeneity of the PI product. Since, HTP experiments are usually performed at $T_R > 180^\circ\text{C}$ (higher HT regime, hHT), the reaction mixture passes the

LHT regime while heating up and therefore, is affected by reactions occurring in LHT regime. To determine the impact of reactions while passing the LHT regime, we carried out HTP experiments under hHT conditions with different heating times, *i.e.* different dwell times in this regime. The outcome of this set of experiments is discussed in the following section.

4.3.3 Effect of Heating Rate t_h in Higher HT Regime

In the following section the results of the different heating protocols at $T_R = 200\text{ }^\circ\text{C}$ with respect to crystallinity, morphology and completeness of the transformation are discussed. The time required to heat the reactor (t_h) reflects the dwell time of the reaction mixture at temperature below T_R , and thus also in the sHT and LHT regime. Consequently, t_h should have an effect on the observed final crystallinity of the PI products. A set of experiments with different t_h (2, 5, 10, 20 and 40 min) and a final reaction temperature $T_R = 200\text{ }^\circ\text{C}$ for both BTA-based systems was carried out. For all experiments, the reaction mixture was kept at T_R for 60 minutes. As we showed in the previous sections, the monomer salt dispersion starts to react at lower temperatures, we define t_R as overall time of reaction, which is thus 62, 65, 70, 80 and 100 min, respectively. The temperature-time profiles of these experiments are shown in **scheme 12**.



Scheme 12: Temperature-time profiles of experiments carried out at $T_R = 200\text{ }^\circ\text{C}$. Dark blue background illustrates the subhydrothermal (sHT) regime, turquoise to red background illustrates the hydrothermal regime, which is divided in lower hydrothermal (LHT) and higher hydrothermal (hHT) regime. White columns illustrate the time the reaction mixture is kept at T_R and give the experiment codes. Scheme was adapted from BAUMGARTNER.³⁷

All experiments were carried out according to the previous protocols (see **section 6.4**) and were characterized by FT-IR-ATR, PXRD and SEM. All products of $poly(\text{PDA-BTA})_{t_h, 60\text{ min}}^{200\text{ }^\circ\text{C}}$ and $poly(\text{Bz-BTA})_{t_h, 60\text{ min}}^{200\text{ }^\circ\text{C}}$ no matter t_h show the characteristic imide modes and very weak

amminium modes, that are associated with unreacted monomer salt or short oligomers (see **section 7.7** for spectra). PXRD patterns revealed outstanding crystallinity for all $poly(\text{PDA-BTA})_{t_h,60min}^{200^\circ\text{C}}$. Furthermore, no additional reflections corresponding to the monomer salt or $dimer(\text{PDA-BTA})$ were observed, except for $poly(\text{PDA-BTA})_{40min,60min}^{200^\circ\text{C}}$, the experiment with the longest dwell time in the sHT and lHT regime. $Poly(\text{PDA-BTA})_{40min,60min}^{200^\circ\text{C}}$ shows additional reflections at 13, 14, 17, 21 and 27° (2θ) that can be associated with $dimer(\text{PDA-BTA})$ and at 16° (2θ), that correspond to the monomer salt (see **section 7.8** for diffractograms). SEM analysis revealed morphologies similar to the previous reported $poly(\text{PDA-BTA})$ morphologies (**Fig. 17**): All samples are composed of thin platelets of *ca.* 5 - 10 μm in diameter that are inter-grown into flower-like aggregates, with the exception of $poly(\text{PDA-BTA})_{40min,60min}^{200^\circ\text{C}}$, where we find spherulitic, lath-like monomer salt morphologies in coexistence with platy crystallites. This observations correlate with the PXRD patterns, where $poly(\text{PDA-BTA})_{40min,60min}^{200^\circ\text{C}}$ is the only sample where we find monomer salt and dimer reflections.

The $poly(\text{Bz-BTA})_{t_h,60min}^{200^\circ\text{C}}$ series shows the same reflections and extent of amorphicity, no matter t_h . It is noteworthy, that two reflections centered around 19° (2θ) vary in relative intensities in the diffractograms of all samples. This is likely to be related to orientational disorder of the most certainly anisotropic crystallite domains. Furthermore, we do not observe additional reflections that can be associated to $dimer(\text{Bz-BTA})$ nor remaining monomer salt. Morphological studies carried out *via* SEM (**Fig. 18**), show flower-like particles of *ca.* 5 μm in diameter and very narrow size-distribution for $poly(\text{Bz-BTA})_{2min,60min}^{200^\circ\text{C}}$, $poly(\text{Bz-BTA})_{5min,60min}^{200^\circ\text{C}}$, $poly(\text{Bz-BTA})_{10min,60min}^{200^\circ\text{C}}$ and $poly(\text{Bz-BTA})_{20min,60min}^{200^\circ\text{C}}$. In $poly(\text{Bz-BTA})_{60min,60min}^{200^\circ\text{C}}$ we find less homogeneous morphologies than for the rest of the series. We find aggregates covered with platelets, but still larger particles that seem to be less ordered.

In summary, the heating time t_h until T_R is reached has less effect on the overall crystallinity and morphological homogeneity for $t_h < 40$ min. Until now, we did not consider the possibility of solid-state polymerization (SSP) of the monomer salt in dispersion in the HT regime. The set of experiments in this section was performed at $T_R = 200$ °C, which is higher than the solid-state polymerization temperature T_P of the monomer salts. Since SSP yields amorphous to semicrystalline products, it is favorable to avoid SSP by performing HTP experiments at $T_R > T_P$. The results of this experiments are discussed in the following section.

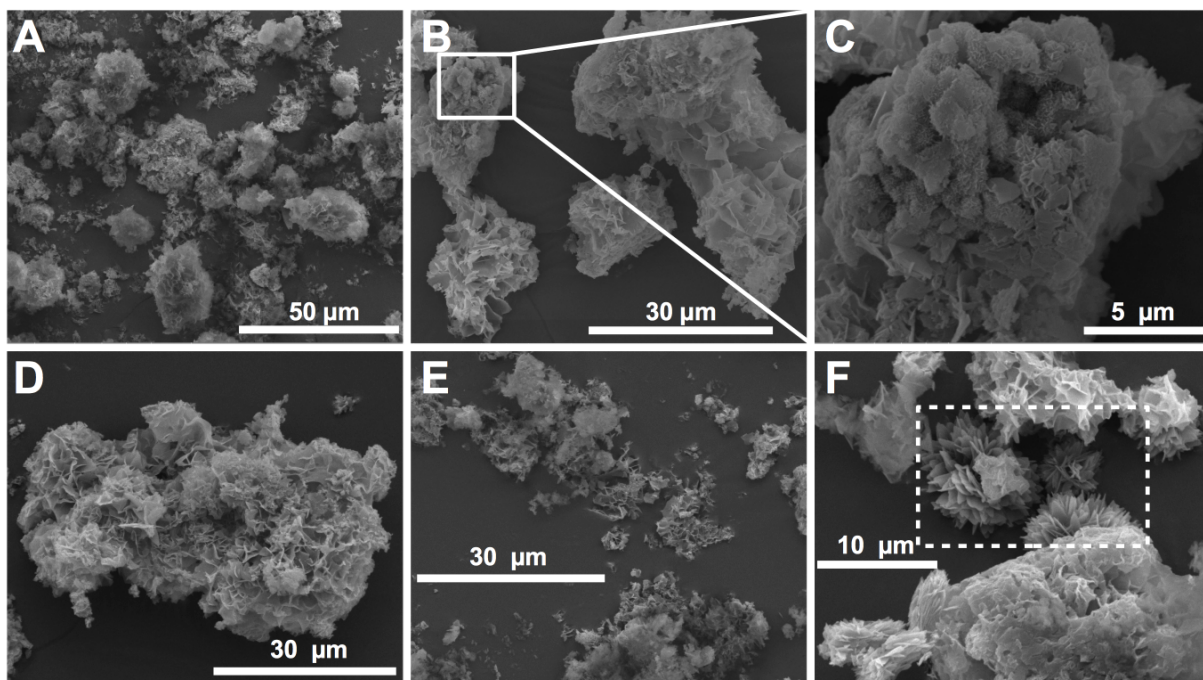


Figure 17: SEM images of *poly*(PDA-BTA) synthesized at $T_R = 200\text{ }^\circ\text{C}$ and different t_h . **A:** *poly*(PDA-BTA) $_{2\text{min},60\text{min}}^{200^\circ\text{C}}$; **B:** *poly*(PDA-BTA) $_{5\text{min},60\text{min}}^{200^\circ\text{C}}$; **C:** close-up image of *poly*(PDA-BTA) $_{5\text{min},60\text{min}}^{200^\circ\text{C}}$; **D:** *poly*(PDA-BTA) $_{10\text{min},60\text{min}}^{200^\circ\text{C}}$; **E:** *poly*(PDA-BTA) $_{20\text{min},60\text{min}}^{200^\circ\text{C}}$; **F:** *poly*(PDA-BTA) $_{40\text{min},60\text{min}}^{200^\circ\text{C}}$; with dotted rectangle indicates platy ellipsoidal crystallites of the monomer salt $[\text{H}_2\text{PDA}^{2+}\text{BTA}^{2-}]$. Figure was reproduced from BAUMGARTNER.³⁷

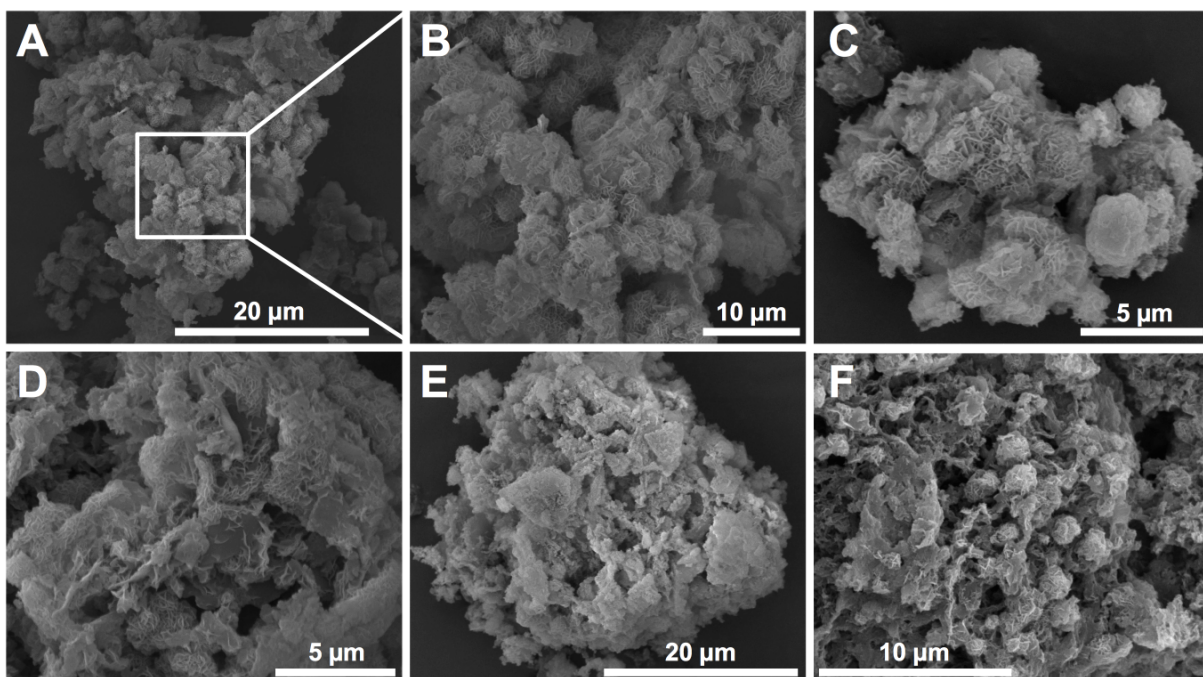


Figure 18: SEM images of *poly*(Bz-BTA) synthesized at $T_R = 200\text{ }^\circ\text{C}$ and different t_h . **A:** *poly*(Bz-BTA) $_{2\text{min},60\text{min}}^{200^\circ\text{C}}$; **B:** close-up images of *poly*(Bz-BTA) $_{2\text{min},60\text{min}}^{200^\circ\text{C}}$; **C:** *poly*(Bz-BTA) $_{5\text{min},60\text{min}}^{200^\circ\text{C}}$; **D:** *poly*(Bz-BTA) $_{10\text{min},60\text{min}}^{200^\circ\text{C}}$; **E:** *poly*(Bz-BTA) $_{20\text{min},60\text{min}}^{200^\circ\text{C}}$; **F:** *poly*(Bz-BTA) $_{40\text{min},60\text{min}}^{200^\circ\text{C}}$. Figure was reproduced from BAUMGARTNER.³⁷

4.3.4 Solid-State Polymerization in HT Regime

Due to the fact that the monomer salts are of diamminium-dicarbonylate dicarboxylic acid type, they can undergo SSP when they are heated to their specific polymerization temperature T_P .^{33,34} The characterization of T_P is carried out *via* TGA, where one observes a mass loss that corresponds to the liberation of two equivalents of H₂O per imide ring. However, SSP is a reaction, where T_P depends on the amount of provided energy instead of a defined transition temperature.⁷⁵ This fact results in different outcomes for TGA measurements performed at different heating rates. Thus, T_P indicates the ease of a specific monomer to undergo SSP.

We determined the T_P for all three monomer salts by TGA, which lead to $T_P(\text{PDA-PMA}) = 210$ °C, $T_P(\text{PDA-BTA}) = 149$ °C and $T_P(\text{Bz-BTA}) = 172$ °C at a heating rate of 10 K min⁻¹. In combination with differential scanning calorimetry (DSC) measurements with several heating and cooling cycles, we identified the mass loss at T_P as a reaction peak only present in the first heating ramp. Subsequent heating cycles showed a flat curve, that clearly underlines the mass loss at T_P is associated with an irreversible reaction.³³ For *poly*(PDA-PMA) we were operating below T_P . Since, previously performed HTP experiments with both BTA-based monomer salts were carried out at $T_R > T_P$, SSP of non-dissolved monomer salt in dispersion in the medium water could be a possible mechanism. Moreover, we found copies of the monomer salt crystals, that act as nuclei for HTP crystallization and angled shapes decorated with crystalline PI platelets in SEM analysis, that could evidence the occurrence of SSP. In general, PIs obtained *via* SSP are less crystalline than HTP PIs.³³ SSP of the BTA-based monomer salts was carried out at 200 °C for 12 h, to determine the crystallinity of their SSP PI products (see **section 7.8** for diffractograms). We found fully amorphous halos for *poly*(PDA-BTA) and a semicrystalline pattern for *poly*(Bz-BTA) in PXRD analysis.

In conclusion, it is possible that BTA-based systems undergo SSP at $T_R = 200$ °C if undissolved monomer salt is present. This polymerization mechanism lead to semicrystalline PI products at best, and could therefore contribute to an amorphous fraction of our hydrothermally synthesized PIs. In order to avoid SSP two approaches are thinkable. The first and more obvious approach is to perform HTP at $T_R < T_P$ ($T_R = 145$ °C for *poly*(PDA-BTA) and $T_R = 165$ °C for *poly*(Bz-BTA)). The resulting PXRD patterns of both systems are depicted in **Fig. 19**. Interestingly, the amorphous backgrounds are tremendously bigger for *poly*(PDA-BTA) and slightly bigger for *poly*(Bz-BTA) synthesized at $T_R < T_P$. Moreover, reflections of *poly*(PDA-BTA) and *poly*(Bz-BTA) synthesized at $T_R = 200$ °C are sharper than those synthesized at $T_R < T_P$. Overall, it

becomes clear that for both BTA-based PI systems, the extent of crystallinity scales with the overall reaction temperature and is higher for $T_R = 200\text{ }^\circ\text{C}$ than for $T_R < T_P$. Therefore, the suppression of SSP at $T_R < T_P$ and HTP with increasing T_R are counteracting events.

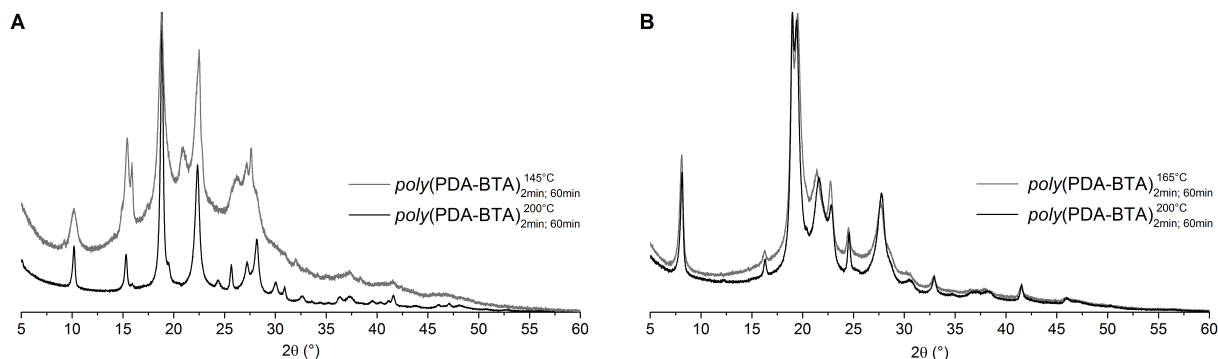


Figure 19: Superimpositions of normalized PXRD patterns of *poly*(PDA-BTA) (A) and *poly*(Bz-BTA) (B) synthesized at $T_R < T_P$ (gray) and $T_R = 200\text{ }^\circ\text{C}$ (black). Figure was reproduced from BAUMGARTNER.³⁷

The second possibility to avoid SSP is to lower the monomer salt concentration and therefore, decrease the amount of undissolved monomer salt. Since SSP can only occur, if solid, undissolved monomer salt is present, we should be able to suppress this polymerization mechanism. Note that a small concentration should lead to the complete dissolution of the respective monomer salt, but not to its complete reaction in sHT and lHT: the extent of these pathways is - as in any reaction - limited by the reaction rate. Thus, if all monomer salt dissolves in sHT and/or lHT regime, it will only react to some extent *via* sHTR or lHTP. We performed HTP experiments at lower (0.015 mol L^{-1}) and higher (0.05 mol L^{-1}) concentration than our typical concentration of 0.03 mol L^{-1} , but worked again at $T_R > T_P$.

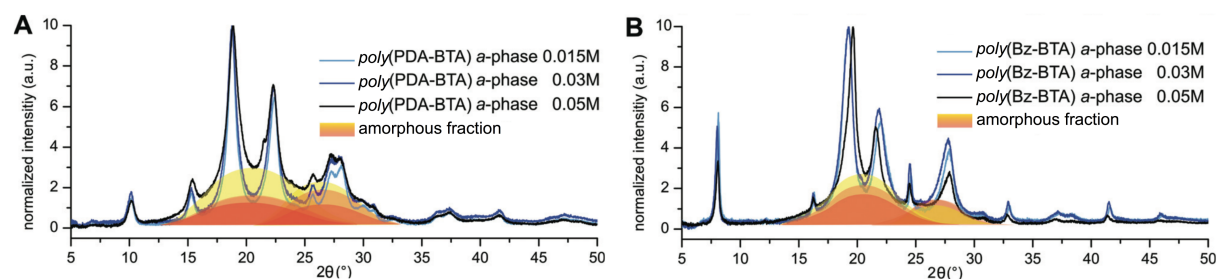


Figure 20: Powder-diffractograms of dired a- and b-phases after HTP at $T_R < T_P$ ($t_R = 12\text{ h}$) and at different concentrations. A: *poly*(PDA-BTA); B: *poly*(Bz-BTA). Amorphous fractions are emphasized in yellow to red areas. Figure was reproduced from BAUMGARTNER.³⁶

It is worth mentioning, that we were not able to determine the solubility of the monomer salt in the HT regime until now. Therefore, the chosen concentration are just bench marks to proof the hypothesis, that lower concentrations lead to an increase of crystallinity (as carried out at relatively high $T_R = 200\text{ }^\circ\text{C}$) and the achievement of higher morphological homogeneity (by

suppressing of SSP and avoiding amorphous PI nuclei of broad size and shape distribution). Indeed, we found impressive morphological homogeneity in SEM and higher crystallinity in PXRD for lower monomer salt concentrations (**Fig. 20**).

The theoretical background, *i.e.* thermodynamics and the impact of the properties of water, that explains these results are discussed in **section 4.3.6**. Furthermore, we could relate the different polymerization mechanisms and reactions occurring during HTP experiments to their morphologies, which is discussed in the following section.

4.3.5 Morphology in HTP: Effect of sHTR, IHTP and SSP Pathways

In the previous sections we introduced new polymerization and reaction pathways occurring during the HTP experiment, namely sHT reactions, IHTP, hHTP and SSP. In this section presents the relationship between these new mechanisms with respect to the observed morphologies.

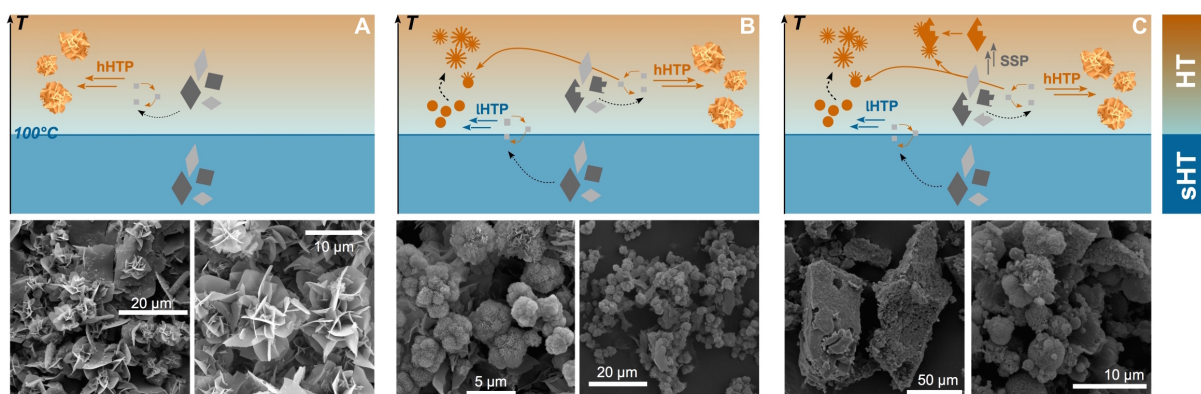


Figure 21: Different morphologies occurring in HTP with respect to different polymerization mechanisms. **A:** The geometrical selection process in HTP leads exclusively to microflower-like morphology. **B:** Spherical particles formed by solution polymerization and act as nuclei for HTP as result in cauliflower-like PI particles. **C:** SSP leads to polymerized copies of the monomer salt crystals, that act as nuclei for HTP and angled shapes decorated with crystalline PI platelets are observed.

In HTP the monomer salt might dissolve during heating, but exclusively polymerizes in the hHTP regime. Due to a geometrical selection process (as explained in **section 4.1**), HTP leads to microflower morphology (see **Fig. 21A**). PIs formed *via* hHTP are prone to crystallize on an external nucleus. Reactions in the autoclave lead to long t_h , which impart the possibility for the monomer salt to dissolve and react in the sHT and IHT regime. We find, amongst other reactions, polymerization in solution that lead to amorphous spherical particles. As solution polymerization takes place in a rather narrow time window (t_h is estimated to be 30 - 40 min), the amorphous PI particles have themselves a narrow size distribution. These particles act as nuclei for HTP crystallization and result in cauliflower-like PI particles (see **Fig. 21B**). We have

previously shown that SSP of monomer salts leads to precise copies of the monomer salt crystallite shapes.^{33,34} We prepare the monomer salt *via* precipitation, which leads to inhomogeneous sizes and shapes of both monomer salts (*cf.* **Fig. 11A,F**, page 29), copying these particles by SSP leads to a broad size and shape distribution of the resulting PIs. Those act as well as nuclei for HTP crystallization and angled shapes decorated with crystalline PI platelets are observed in SEM (see **Fig. 21C**).

Another way to suppress undesirable reactions in terms of morphological inhomogeneity is to perform HTP in a microwave reactor instead of an autoclave to reduce the heating time to $t_h < 2$ min. This results in mainly microflower-like morphologies with narrow size distribution.³⁷

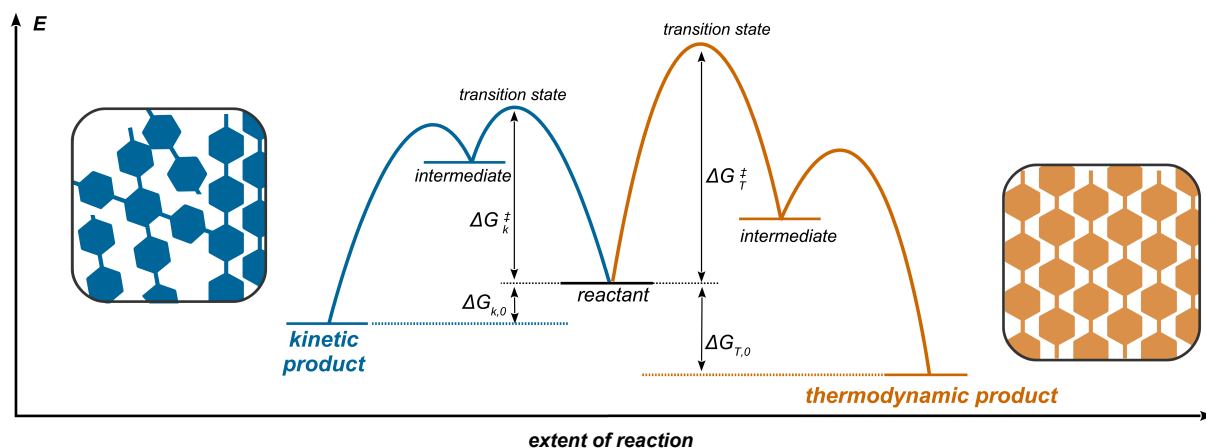
In conclusion, the outcome of the experiments carried out with controlled heating time t_h , lower concentration and at $T_R < T_P$ of each BTA-based system, lead to the following insights: (i) shorter t_h lead to outstanding crystallinity and morphological homogeneity, (ii) less morphological homogeneous PIs are obtained at longer t_h (iii) SSP occurs at $T_R > T_P$ if $t_h > 40$ min, (iv) SSP accounts to a small extent for the amorphous product, (v) higher crystallinity of the final PI is achieved with increasing temperature in the hydrothermal regime. In the next section, we will relate these findings with physical parameters of water as well as with kinetics and thermodynamics of HTP.

4.3.6 Outstanding Crystallinity via HTP: A Hypothesis

The observation that polymerization in the lower HT regime leads an amorphous to semicrystalline PI, while HTP at $T_R > 180$ °C yields a crystalline product is indeed curious. Why are higher temperatures better in terms of crystallinity?

In order to tackle this question, one needs to first compare the crystalline to the amorphous product. A crystalline linear PI can be best understood as chains of a homogeneous conformation that are arranged in an ordered array over a long-range. An amorphous PI is best described as an array of chains of inhomogeneous conformation (*i.e.* irregularly kinked chains). These inhomogeneities of the chain conformations leads to PI chains that cannot pack in a long-range order, but rather arrange randomly (**scheme 13**). The crystalline PI product is considered as the thermodynamic product, while the amorphous counterpart is the kinetic product. Hence, the fact that lHTP leads to amorphous PIs, while hHTP yields crystalline PIs indicates that hHTP conditions (≈ 200 °C) might favor the thermodynamic product, and that the crystalline PI is

formed under thermodynamic reaction control. YAGHI and co-workers established the concept of thermodynamic *vs.* kinetic reaction control for crystalline *vs.* amorphous covalent organic and metal organic frameworks (COFs and MOFs).^{69,76,77} The synthesis of both, MOFs and COFs, relies on dynamic covalent bonds, *i.e.* reversible linkages, between monomeric units. At first, the amorphous product is formed, but the dynamic bonds allow for the monomeric unit to detach



Scheme 13: Thermodynamic *vs.* kinetic reaction control for crystalline *vs.* amorphous PIs. **Left:** The amorphous PI represents the kinetic product. Reaching the kinetic product requires an activation energy ΔG_K^\ddagger , and the overall free energy difference between the starting compounds and the kinetic product is $\Delta G_{K,0}$. **Right:** The crystalline PI represents the thermodynamic product. The activation energy towards the thermodynamic product ΔG_T^\ddagger is higher than ΔG_K^\ddagger , and the overall free energy gain when reaching the thermodynamic product, $\Delta G_{T,0}$ also exceeds $\Delta G_{K,0}$.

However, the cyclic imide linkage in PIs is essentially irreversible,³⁵ and the concept of linker reversibility does thus not apply here. The hydrothermal irreversibility was proven by attempting to recrystallize PIs *via* HT conditions, which was not successful.³⁵ This showed that the cyclic imide bond is irreversible even under HT conditions. HTP of PIs is closely related to the natural formation of silicates by polycondensation of silicic acid species. HT synthesis of silicates also yields crystalline products, and most interestingly, the Si-O bond is also essentially irreversible. Thus, the direct formation of the thermodynamic product in polycondensations with water as byproduct is likely possible. Little is understood about the underpinnings, but we believe that the increased temperatures and pressures (and consequently increased number of molecular collisions), in combination with the fact that the monomers are dissolved in HTP, might allow for overcoming the activation energy towards the thermodynamic product directly. The activation energy towards the kinetic product is smaller, and the moderate temperature and pressure in the LHT regime might only allow for yielding the kinetic, amorphous PI. A second explanation for better results in experiments in the higher HT regime with respect to crystallinity and

morphology is found in the properties of water within this regime. How do physicochemical properties of the reaction medium influence HTP experiments at low and at high temperatures? For one, the solubility of all intermediates (monomer salt, dimer,.. oligomers, *etc.*) scales with the temperature. At the same time, longer reactions times at a given temperature can overcome even low solubilities, as freshly dissolved species react when dissolved and subsequently precipitate, which allows further low-molecular-weight species to dissolve. However, there are more properties than dissolving power of water that change at higher temperatures and autogeneous pressures as mentioned in **section 3.1**, page 18. **Fig. 5A** and **B** shows the temperature dependency of the density ρ and the viscosity η of water. Although, both decrease with increasing temperature, their impact on HTP is moderate. The dielectric constant ϵ is a measure for the polarity of a medium, and thus of importance to HTP, as oligomers of increasing length become increasingly apolar compared to monomer salt ions or dimers. ϵ is $\approx 80 \text{ A}\cdot\text{s V}^{-1}\cdot\text{m}^{-1}$ and decreases to $\approx 45\text{--}55 \text{ A}\cdot\text{s V}^{-1}\cdot\text{m}^{-1}$ for the lower HT regime, and to even $35 \text{ A}\cdot\text{s V}^{-1}\cdot\text{m}^{-1}$ at $200 \text{ }^\circ\text{C}$ (**Fig. 5C**). This important change of the polarity of water certainly favors the dissolution of longer oligomers and their polymerization to macromolecules of higher molecular weights. Furthermore, the ionic product of water K_W has to be considered: The latter is a measure for the autodissociation of H_2O into OH^- and H_3O^+ ions. K_W increases from $0 \text{ }^\circ\text{C}$ until it reaches its maximum at $\approx 250 \text{ }^\circ\text{C}$. Typically, polycondensations are acid- or base-catalyzed (classical PI synthesis was carried out in the presence of isoquinoline as base catalyst, see **section 6.5** for protocol). Therefore, the fact that K_W is increasing with increasing T is most beneficial for HTP. The ionic product increases with temperature: $K_W \approx 10^{-14} \text{ mol}^2 \text{ kg}^{-2}$ at room temperature and becomes $10^{-11.2} \text{ mol}^2 \text{ kg}^{-2}$ at $200 \text{ }^\circ\text{C}$ (**Fig. 5D**). Therefore, the ionic product (and thus the concentration of OH^- and H_3O^+ ions) of water is at $200 \text{ }^\circ\text{C}$ by a factor of 1000 higher than at room temperature. In fact, water at high temperatures has been shown to act as both acid and base catalyst in the synthesis of small organic molecules.⁷⁸

The maximum for K_W is at $10^{-11.1} \text{ mol}^2 \text{ kg}^{-2}$ which is only slightly higher than at $200 \text{ }^\circ\text{C}$. Consequently, the chosen reaction conditions are with $T_R = 200 \text{ }^\circ\text{C}$ already in an optimal range for HTP: while the important ionic product guarantees acid-/base-catalyzed polycondensations, the dielectric constant of $\approx 35 \text{ A}\cdot\text{s V}^{-1}\cdot\text{m}^{-1}$ enables the solubility and thus further condensation of low to medium molecular weight oligoimides.

Summarizing all gathered results on HTP, experiments could be designed to lead to crystalline BTA-based PIs that crystal structures could be refined by PXRD data which is shown in the following section.

4.3.7 Experimental Design of Crystalline PIs and their Crystal Structure

Section 4.3.2 presented the formation of zwitterionic dimers in the IHT regime which coexist with amorphous PI fractions. One might suspect that the amorphous fractions formed in the IHT regime are not yet highly condensed products, but rather oligomers that can still dissolve at 200 °C and then further polymerize to highly crystalline PIs. As mentioned in the previous section, the attempt to recrystallize PIs failed, but the used PI was likely of considerably higher molecular weights.³⁵ The question is: Is it possible to recrystallize PIs that formed in the IHT regime under higher temperatures and pressures, *i.e.* in the hHT regime?

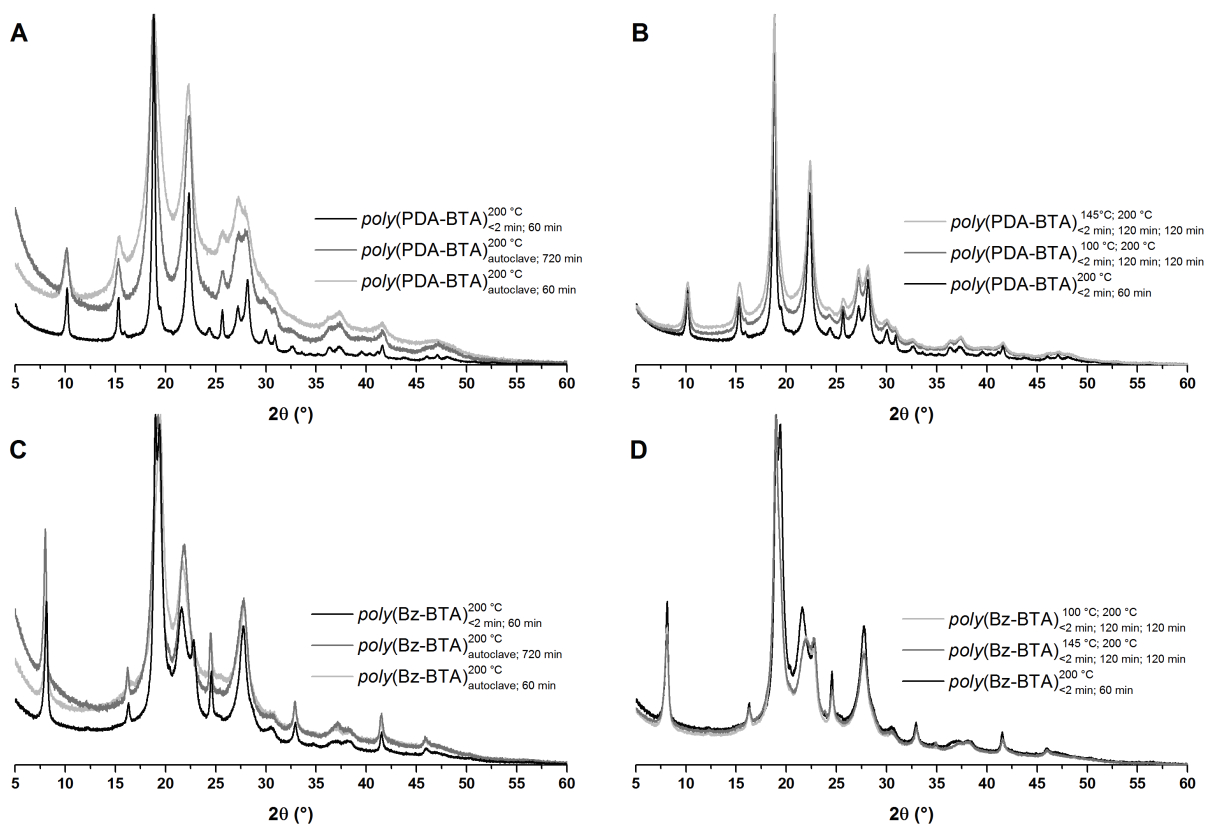


Figure 22: Superimposition of PXRD patterns of *poly*(PDA-BTA) and *poly*(Bz-BTA) synthesized with different heating protocols at $T_R = 200$ °C. **A,B:** *poly*(PDA-BTA), **C,D:** *poly*(Bz-BTA). Figure was reproduced from BAUMGARTNER.³⁷

performed: rapid heating to a low first T_R (100 °C or 145 °C) at which the vessel was kept for 2 h and then a second rapid heating to high second T_R (200 °C) at which the mixture was kept for another 2 h. These heating protocols were applied to both PIs, *poly*(PDA-BTA) and *poly*(Bz-BTA), The experiments were therefore: (a) $t_{h1} = 2$ min, $T_{R1} = 100$ °C, $t_R = 122$ min, $t_{h2} = 2$ min, $T_{R2} = 200$ °C, $t_{R2} = 122$ min; (b) (a) $t_{h1} = 2$ min, $T_{R1} = 145$ °C, $t_{R1} = 122$ min, $t_{h2} = 2$ min, $T_{R2} = 200$ °C, $t_{R2} = 122$ min; and named as *poly*(diamine-BTA) $_{th,tR1,tR2}^{TR1,TR2}$. The PXRD patterns of the PIs resulting from these heating protocols are shown in **Fig. 22**. For

comparison, we performed short and long HTP experiments in autoclaves ($t_R = 60$ min and 720 min, respectively). *Poly*(PDA-BTA) synthesized at $T_R = 200$ °C for $t_R = 60$ min with $t_h = 2$ min yields much higher crystallinity than autoclave synthesis of uncontrolled t_h at the same T_R for both, short (60 min) and long reaction times (720 min), as depicted in **Fig. 22A**. Most interestingly, the experiment with $T_{R1} = 100$ °C ($poly(\text{PDA-BTA})_{2\text{min},122\text{min},122\text{min}}^{100^\circ\text{C},200^\circ\text{C}}$) outmatches the experiment with $T_{R1} = 145$ °C ($poly(\text{PDA-BTA})_{2\text{min},122\text{min},122\text{min}}^{145^\circ\text{C},200^\circ\text{C}}$) in terms of crystallinity. This indicates that amorphous oligoimides formed in the IHT regime are already of considerable average molecular weight and cannot be redissolved in the hHT regime.

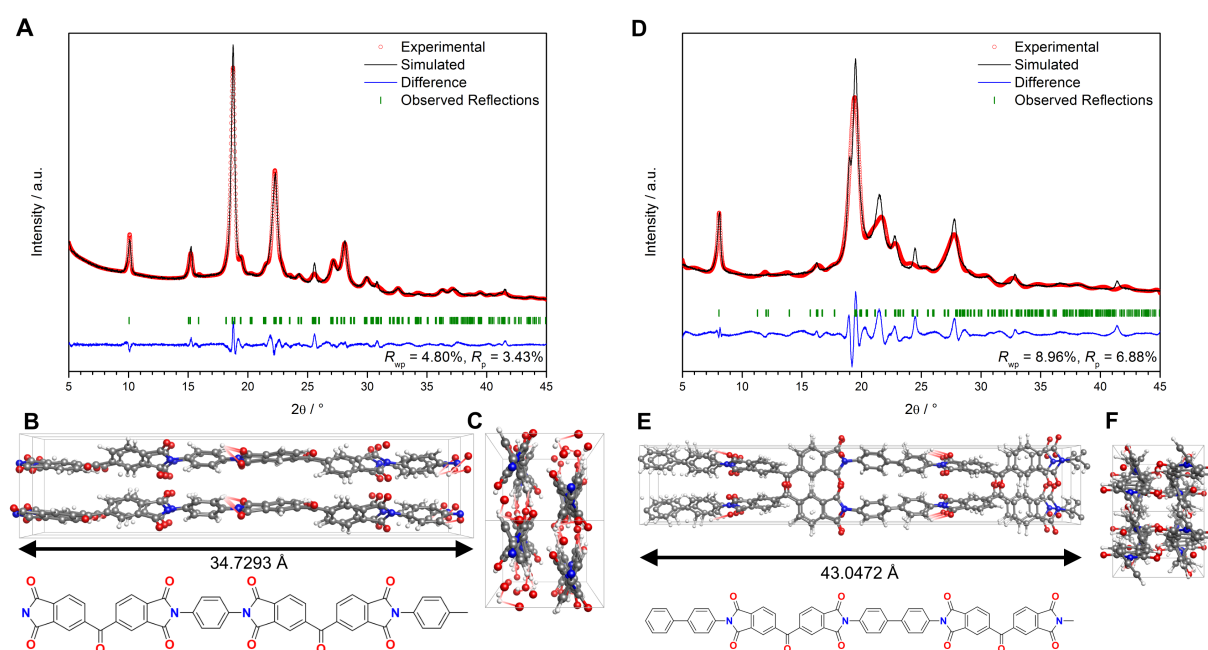


Figure 23: Rietveld fit performed on the PXR D pattern of *poly*(PDA-BTA) (**A**) ($R_{wp} = 4.80\%$, $R_p = 3.43\%$) and *poly*(Bz-BTA) (**D**) ($R_{wp} = 8.96\%$, $R_p = 6.88\%$) with the observed profile as continuous lines, refined profile as dashed line, and observed Bragg peak positions as dashed line. Projection along the b -axis (**B**, and **E**) and c -axis (**C**, and **F**) of *poly*(PDA-BTA) and *poly*(Bz-BTA), respectively, showing the length of the repeat unit per unit cell below. The parameters of the orthogonal unit cells are as follows: *poly*(PDA-BTA) (*PCA21*, no. 29) are $a = 7.9616$ Å, $b = 5.8412$ Å, $c = 34.7292$ Å, and *poly*(Bz-BTA) (*PCC2*, no. 27) are $a = 7.7321$ Å, $b = 5.5875$ Å, $c = 43.0472$ Å. Figure was reproduced from BAUMGARTNER.³⁷

However, for *poly*(Bz-BTA), the results are less striking. $poly(\text{Bz-BTA})_{2\text{min},60\text{min}}^{200^\circ\text{C}}$ outmatches HTP carried out in autoclaves for both short and long reaction times (**Fig. 22C**). For *poly*(Bz-BTA), there is no difference in crystallinity for $poly(\text{PDA-BTA})_{2\text{min},122\text{min},122\text{min}}^{100^\circ\text{C},200^\circ\text{C}}$ vs. $poly(\text{Bz-BTA})_{2\text{min},122\text{min},122\text{min}}^{145^\circ\text{C},200^\circ\text{C}}$, but the pattern obtained from $poly(\text{PDA-BTA})_{2\text{min},60\text{min}}^{200^\circ\text{C}}$ shows slightly more defined reflections at 19° and $21^\circ(2\theta)$. Furthermore, the PXR D patterns of $poly(\text{PDA-BTA})_{2\text{min},60\text{min}}^{200^\circ\text{C}}$ and $poly(\text{Bz-BTA})_{2\text{min},60\text{min}}^{200^\circ\text{C}}$ were of sufficiently high crystallinity to attempt an

ab initio structure solution and Rietveld refinement.

The *c*-axes of the respective unit cells (34.7293 Å for *poly*(PDA-BTA), and 43.0472 Å for *poly*(Bz-BTA), respectively) corresponds to the length of two periodic repeats of the 1D PI chains of both *poly*(PDA-BTA) and *poly*(Bz-BTA). Due to the helical twists into the PI chains of both PI systems *via* the carbonyl (C=O) group of the benzophenone-moiety a double-length per unit cell is necessary. The torsion between both aromatic groups bridged by the carbonyl (Ar-(C=O)-Ar) is 52° for *poly*(PDA-BTA), and 63° for *poly*(Bz-BTA), respectively. The additional degree of freedom introduced into *poly*(Bz-BTA) *via* the biphenyl linker causes a considerable amount of uncertainty regarding the unit cell. Rotation around the biphenyl linker is accompanied with differences in overall chain energy on the order of magnitude of thermal drift at room temperature (as established by CASTEP).⁷⁹ Hence, a number of *poly*(Bz-BTA) chain conformations are possible each of which would necessitate integral multiples or slight deviations of the length of the *c*-axis. This is reflected in the appreciable width and anomalous shape of peaks containing an *l*-component in the PXRD profile of *poly*(Bz-BTA) (**Fig. 23D**), in particular the (004)-peak at 8.2°(2θ), and in the overlapping region around 19° to 20°(2θ).

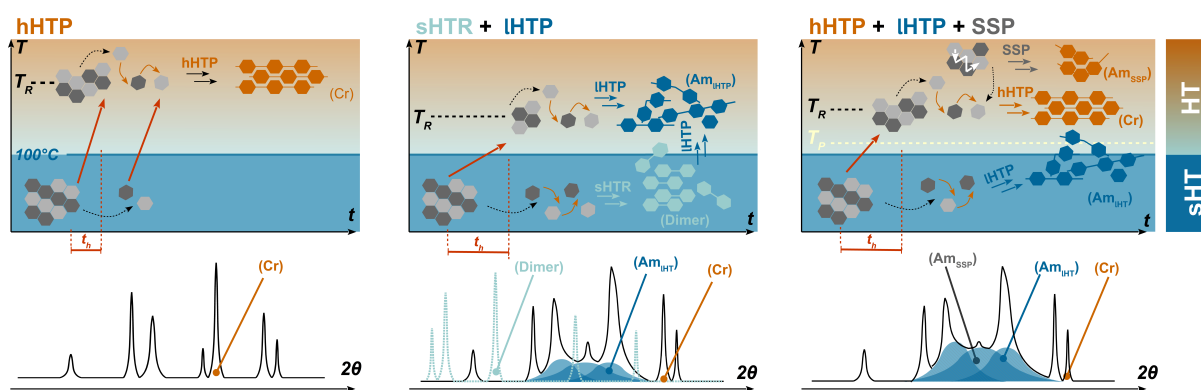
The chain-to-chain distances in *poly*(PDA-BTA) are 5.00 Å along the *ab*-vector and 5.84 Å along the *a*-axis. These values are comparable to *poly*(PDA-PMA) mentioned in **section 4.1.2**. Furthermore, structural refinement predicts close contacts on the order of magnitude of 1.96 Å between oxygen and hydrogen atoms of adjacent chains. For *poly*(Bz-BTA) on the other hand, larger overall distances between adjacent chains of 5.80 Å along the *ab*-vector and 5.59 Å along the *a*-axis are found. No close contacts between chains are apparent, and hydrogen bonding can only arise in the form of intrachain contacts of 1.96 and 2.35 Å between hydrogens of biphenyl-linkers and adjacent imide-oxygens.

In analogy to *poly*(PDA-PMA), higher degrees of crystallinity are observed for systems with fewer degrees of freedom and more polar functional groups. The FWHM value is a useful indicator of relative crystallinity (and particle size) and varies as follows: 0.25 for *poly*(PDA-PMA), 0.26 for *poly*(PDA-BTA), and 0.30 for *poly*(Bz-BTA). In that respect, *poly*(Bz-BTA) is the most challenging system to crystallize.

5 Conclusion

This master thesis presents the detailed study of hydrothermal polymerization of three polyimide systems: *poly(p*-phenylene pyromellitimide), *poly(p*-phenylene benzophenone imide) and *poly*(4,4'-biphenyl benzophenone imide). The facile process yields outstanding crystallinity for all three polyimides. Furthermore, polymerization and crystallization appears to be complete after only 2 h at 200 °C. A careful analysis of the morphological evolution over time, allows for proposition that PI crystallites grow *via* a dissolution–polymerization–crystallization process.

A benzophenone-moiety was introduced into the backbone of two PI systems to increase flexibility of the corresponding polymeric chain and thus to enhance processability. Although the two benzophenone tetracarboxylic acid-based polyimides are structurally closely related to the stiffer, third investigated system (*poly*(PDA-PMA)), the obtained PIs seemed to be less crystalline. We believe that, in contrast to *poly*(PDA-PMA), the BTA-based monomer salts possess a higher solubility in the lower HT regime. As a consequence, HTP of the latter lead to three different products and corresponding polymerization mechanisms. These polymerization mechanisms that all take place during the HTP experiment (lower hydrothermal polymerization, lHTP, hydrothermal polymerization, HTP, and solid-state polycondensation, SSP, see **scheme 14**) were related to the final PI products in terms of crystallinity and morphological homogeneity. HTP in hHT regime leads highly crystalline PIs. Reactions in the subhydrothermal regime yield dimeric species that further react to amorphous PIs in the lower HT regime that form *via* solution polymerization. SSP takes place in dispersion and yields semicrystalline to amorphous products.



Scheme 14: Polymerization mechanisms occurring in HT experiments. hHTP leads to crystalline PIs, also by polymerization in solution at high T_R ; lHTP leads to amorphous PIs by polymerization in solution in the lower HT regime; At < 100 °C dimeric species form that further react to PI; Solid-state polycondensation (SSP) takes place in nondissolved monomer salt particles and leads to amorphous (or semicrystalline) PIs.

Experiments to circumvent this pathway were designed and showed to successfully enhance the

crystallinity of the PI products. Moreover, we could show that the time until the final reaction temperature is reached has an impact on the resulting crystallinity. Hence, microwave-assisted HTP experiments were performed, allowing for control over the heating time. Experiments at different heating times broaden the understanding of HTP. We could show that (i) Lower HT regime ($\approx 100 - 130$ °C) yields dimeric species and semicrystalline PIs; (ii) Dimers indicate that the PI formation in HTP is closely related to classical AA/BB step-growth polycondensations. (iii) Crystallinity scales with reaction temperature: The range at which HTP generates highly crystalline PIs is situated > 180 °C. Within this temperature range (180 - 200 °C), the physicochemical properties of the medium water are beneficial for polycondensations as the strongly enhanced autoprotolysis of water allows for acid/base catalysis. Furthermore, the important decline of the static dielectric constant of water most likely enables the dissolution of oligoimides, and thus further polymerization. Nonetheless, the formation of the imide bond is an irreversible reaction. We could show that IHTP yields PIs of inferior crystallinity, even if subsequently polymerized/crystallized at higher temperatures, *i.e.* in the higher HT regime. Finally, we were able to transfer this understanding to design HTP experiments yielding products of sufficiently high crystallinity to refine the crystal structure from powder diffraction data.

We conclude that the hydrothermal process presents a simple and rapid route for the synthesis of highly ordered aromatic polyimides. Compared to conventional polycondensation, this novel route is particularly environmentally friendly as no toxic solvents or catalysts are required. By revealing the possibility of hydrothermal polymerization of PIs, we paved the way for a novel and benign synthetic route towards high-performance polymers. As HTP is inspired by its inorganic counterpart (*i.e.* hydrothermal condensation of silicic acids to silica), we believe that numerous other inspirations can be gathered from inorganic hydrothermal syntheses, such as for instance the use of water-soluble additives for generating porosity (templating).

6 Experimental Section

6.1 General Methods

FT-IR-ATR spectra were recorded on a Bruker Tensor 27 working in ATR MicroFocusing MVP-QL with a diamond crystal, using OPUS (version 4.0) software for data analysis. Resolution was set to 2 - 4 cm^{-1} , and spectra were recorded from 4000 to 600 cm^{-1} .

^1H and ^{13}C solution NMR spectra were recorded on a Bruker AVANCE 250 (250.13 MHz) and a Bruker AVANCE DPX 300 spectrometer (300.13 MHz) equipped with a 5 mm inverse - broad probe head and z-gradient unit.

Scanning electron microscopy was carried out with a Quanta 200F FEI microscope. Typically the samples were measured at 5 kV or 10 kV, with a working distance of 9 - 10 mm and spot size 2.0 or 2.5. Prior to imaging, samples were loaded on carbon-coated stubs and coated by sputtering with a 17 nm thick layer of Au/Pd 60/40 alloy with a Quorum Q105T S sample preparation system.

Thermogravimetric analysis was carried out using a Netzsch TG 209 analyzer at a heating rate of 10 $\text{K}\cdot\text{min}^{-1}$ under nitrogen atmosphere, equipped with NETZSCH Proteus (Version 4.3) software.

Powder X-ray diffraction data was collected with a PANalytical X'Pert Pro multi-purpose diffractometer (MPD) in Bragg Brentano geometry operating with a Cu anode at 40 kV, 40 mA, and an X-Celerator multichannel detector was used. Samples were ground and mounted as loose powders on silicon single crystal sample holders. The diffraction patterns were recorded between 5 and 60° (2θ) with 69.215 s/step and a step size of 0.0050134°, sample holders were rotated during the measurement with 4 s/turn.

HPLC-MS/MS measurements were performed *via* an Agilent 1100 + HCT ultra (Bruker Daltonics) system using acetonitrile/water as mobile phase and a RP-C18 column (Phenomenex 4.6 x 250 mm, 10 μm , 100 Å) as stationary phase at 40 °C and a constant flow rate of 1 $\text{mL}\cdot\text{min}^{-1}$. Syringe filtered (0.45 μm PTFE) samples with a concentration of 1 $\text{mg}\cdot\text{mL}^{-1}$ in DMSO/water (50:50; v/v) were injected (5 μL) and eluted using following gradients: 3-74 % ACN in water from $t = 3$ to $t = 15$ (BB254) 10-90 % ACN in water from $t = 3$ to $t = 15$ (BB249). A continuous split (1:1000) of chromatographed analytes was transferred to the spectrometer *via* a 10 $\mu\text{L}\cdot\text{min}^{-1}$ ACN carrier flow. ESI was performed at 35 psi nebulizer nitrogen pressure, 10 $\text{L}\cdot\text{min}^{-1}$ drying gas flow und 365 °C drying temperature at -110 V.

Polymer structures for initial structural refinement were constructed from 4 to 8 repeat-units and were optimized using CASTEP code (B3LYP functional).⁸⁰ Structural refinement and Le Bail fitting was carried out using the TOPAS-Academic software.⁸¹

6.2 Chemicals

p-phenylene diamine (PDA, 97 %, Sigma Aldrich) and benzidine (Bz, 98 %, Sigma Aldrich) were purified *via* sublimation; pyromellitic dianhydride (PMDA, 97 % Sigma Aldrich) recrystallized from distilled water, *m*-cresol (99 %, Merck) purified *via* vacuum distillation; isoquinoline (97 %, Sigma Aldrich) used as received; methanol (Merck, 99 %), benzophenone-3,3',4,4'-tetracarboxylic dianhydride (BTDA, Sigma Aldrich), ethanol (Sigma Aldrich, 99.5 %) and dimethylsulfoxide (99.5 %, Sigma-Aldrich) were used as received.

6.3 Monomer Salt Synthesis

Monomer Salt Synthesis at Room Temperature

In a 3-neck-flask under inert atmosphere equipped with a reflux condenser 0.48 g (1.5 mmol) BTDA was hydrolyzed to benzophenone-3,3',4,4'-tetracarboxylic acid (BTA) by stirring in 15 mL distilled water at 80 °C for 20 min. The clear solution was cooled down to room temperature and an equimolar amount of diamine (either PDA or Bz) was added. The suspensions were stirred over night at room temperature. The off-white salts were separated by filtration, washed with distilled water and dried in the desiccator over silica gel.

[**H₂PDA²⁺BTA²⁻**]: ¹H NMR (d₆-DMSO, 250.13 MHz) d: 3.35 (s, 6H, NH³⁺), 6.77 (s, 4H, Ar), 8 (m, 6H, Ar) ¹³C NMR (d₆-DMSO 300.13 MHz) d: 119.22, 131.14, 132.03, 134.00, 138.31, 167.75, 168.27, 194.45

[**H₂Bz²⁺BTA²⁻**]: ¹H NMR (d₆-DMSO, 250.13 MHz) d: 3.3 (s, 6H, NH³⁺), 6.63 (d, J=10 Hz, 4H, Ar), 7.23 (d, J=10 Hz, 4H, Ar), 7.95 (m, 6H, Ar) ¹³C NMR (d₆-DMSO, 300.13 MHz) d: 115.96, 126.67, 129.67, 130.31, 130.69, 132.49, 133.01, 137.90, 138.30, 167.85, 168.65, 194.02

(for spectra and assignment see **Fig. 25**)

Monomer salt synthesis at 80 °C

Benzophenone tetracarboxylic acid-based monomer salts: In a 3-neck-flask under inert atmosphere, equipped with a reflux condenser 0.48 g (1.5 mmol) BTDA was hydrolysed by

stirring in 15 mL deionized water at 80 °C for 20 min. To the clear solution an equimolar amount of diamine (either PDA or Bz) was added. The suspensions were stirred over night at 80 °C. The gray (PDA) or yellow (Bz) salts were separated by filtration, washed with water and dried in a desiccator over silica gel.

Pyromellitic acid-based monomer salt: In a 3-neck-flask under inert atmosphere, equipped with a reflux condenser 0.33 g (1.5 mmol) PMDA was hydrolysed by stirring in 15 mL deionized water at 80 °C for 20 min. To the clear solution 0.16 g (1.5 mmol) PDA was added. The suspension was stirred over night at 80 °C. The white salt was separated by filtration, washed with water and dried in a desiccator over silica gel.

[H₂PDA²⁺PMA²⁻]: ¹H NMR (d₆-DMSO, 250.13 MHz) d: 6.78 (s, 6H, Ar), 8.42 (s, 2H, Ar)

Monomer salt refluxation

In a flask, equipped with a reflux condenser 0.1 g of each BTA-based monomer salt was suspended in 15 mL distilled water and refluxed for 1 h or 12 h, respectively. The resulting suspensions were gray for [H₂PDA²⁺BTA²⁻] and green for [H₂Bz²⁺BTA²⁻]. They were separated by filtration, washed with methanol and dried in the desiccator over silica gel.

6.4 HTP experiments

Autoclave experiments: The freshly prepared salt dispersion was transferred to a glass liner (V = 27 mL). The liner was then put into PTFE-lined autoclave (V = 45 mL). The autoclave was placed in an oven at different temperatures (140 °C, 150 °C, 160 °C, or 200 °C) and kept there for various reaction times (0.25 h - 60 h). At the end of the reaction, the autoclave was quickly cooled back to room temperature by quenching in cold tap water. The different PI phases were isolated, washed several times with distilled water and dried *in vacuo* over silica gel overnight. We used only cold water for washing and dried the PI products in innocuous environment in order to be able to properly evaluate *e.g.* remaining monomer salt, which would be removed by washing with other solvents or undergo SSP with remaining monomer salt by drying at elevated temperatures. All other hydrothermal polymerizations were carried out accordingly (see **Tab. 1**, page 56).

Microwave-assisted experiments: The dried monomer salt was re-dispersed in distilled water in a microwave glass vial (V = 30 mL), that was closed with a PTFE septum. The dispersion was heated by microwave irradiation to various reaction temperatures T_R (100 °C, 110 °C, 120 °C,

130 °C, 140 °C, 145 °C, 165 °C or 200 °C) with different heating rates t_h (heating to T_R in various times; 2 min, 5 min, 10 min, 20 min, 40 min or 60 min*) and kept there for different times (0.5 h, 1 h, 2 h). At the end of the reaction, the glass vial was cooled back to room temperature. The PI product was isolated, washed several times with distilled water and dried *in vacuo* over silica gel. All other microwave-assisted hydrothermal polymerizations were carried out accordingly and are summarized in **Tab. 2**, page 57.

Table 1: Overview of HTP Experiments performed in autoclaves. Given are concentration, reaction temperature, reaction time and pressure. The autogenous pressures were calculated using Wexler's equation.^{82,83}

	Concentration (mol L ⁻¹)	T _R (°C)	t _R (h)	pressure (bar)
<i>poly</i> (PDA-PMA)	0.1	150	12	4.7
	0.1	200	12	16.7
	0.1	250	12	40.0
	0.1	200	0.25	16.7
	0.1	200	0.5	16.7
	0.1	200	1	16.7
	0.1	200	2	16.7
	0.1	200	3	16.7
	0.1	200	4	16.7
	0.1	200	5	16.7
	0.1	200	6	16.7
	0.1	200	7	16.7
	0.1	200	8	16.7
	0.1	200	60	16.7
	0.05	200	12	16.7
<i>poly</i> (PDA-BTA)	0.030	200	1	16.7
	0.030	200	2	16.7
	0.030	200	4	16.7
	0.030	200	12	16.7
	0.015	200	1	16.7
	0.015	200	12	16.7
	0.05	200	1	16.7
	0.030	140	12	3.6
<i>poly</i> (Bz-BTA)	0.030	200	1	16.7
	0.030	200	2	16.7
	0.030	200	4	16.7
	0.030	200	12	16.7
	0.015	200	1	16.7
	0.015	200	12	16.7
	0.05	200	1	16.7
	0.030	160	12	6.2

Table 2: Overview of HTP Experiments performed in microwave reactor. Given are concentration, reaction temperature, reaction time, heating time and pressure. The autogenous pressures were calculated using Wexler's equation.^{82,83}

	concentration (mol L ⁻¹)	T _R (°C)	t _R (min)	t _h (min)	pressure (bar)
<i>poly</i> (PDA-BTA)	0.030	200	60	< 2	16.7
	0.030	200	60	5	16.7
	0.030	200	60	10	16.7
	0.030	200	60	20	16.7
	0.030	200	60	40	16.7
	0.030	145	30	2	4.1
	0.030	145	60	2	4.1
	0.030	145	120	2	4.1
	0.030	145	60	5	4.1
	0.030	145	69	10	4.1
	0.030	145	60	20	4.1
	0.030	145	60	40	4.1
	0.030	145	60	60	4.1
	0.030	100	120	2	1
	0.030	110	120	2	1.2
	0.030	120	120	2	2.3
	0.030	130	120	2	2.7
	0.030	100/200	120/120	2	16.7
	0.030	145/200	120/120	2	16.7
<i>poly</i> (Bz-BTA)	0.030	200	60	2	16.7
	0.030	200	60	5	16.7
	0.030	200	60	10	16.7
	0.030	200	60	20	16.7
	0.030	200	60	40	16.7
	0.030	165	30	2	4.1
	0.030	165	60	2	4.1
	0.030	165	120	2	4.1
	0.030	165	60	5	4.1
	0.030	165	60	10	4.1
	0.030	165	60	20	4.1
	0.030	165	60	40	4.1
	0.030	165	60	60	4.1
	0.030	100	120	2	1
	0.030	110	120	2	1.2
	0.030	120	120	2	2.3
	0.030	130	120	2	2.7
	0.030	140	120	2	2.7
	0.030	100/200	120/120	2	16.7
	0.030	145/200	120/120	2	16.7

6.5 Classical PI Synthesis

1 g PMDA (4.6 mmol) and 0.49 g PDA (4.6 mmol) were dispersed in 40 mL of freshly distilled *m*-cresol under inert atmosphere. Then 2 mL of dry toluene, and 0.1 mL of isoquinoline were added to the reaction mixture. The orange dispersion was stirred at 80 °C for 1 h. The resulting PAA dispersion was heated to 200 °C and kept at this temperature for 6 h. The condensate (water) was continuously removed with a Dean-Stark trap. One part of the *poly*(PDA-PMA) dispersion was quenched in methanol and the other part was allowed to slowly cool down to room temperature. The products from both fractions were isolated *via* filtration, washed three times with ethanol and dried under high vacuum.

6.6 Solid-State Polymerization

0.2 g of each monomer salt was placed in a flask and heated up to 200 °C or 250 °C, respectively, in a sandbath and kept at this temperature overnight. Yellow to brownish PIs were obtained.

7 Appendix

7.1 Solubility tests of monomer salts

The solubility of all monomer salts was tested in various solvents according to the following procedure: 10 mL of the respective solvent was added to 125 mg of the respective solid. The resulting dispersion was heated up to the boiling temperature of the respective solvent. The dispersion was kept at reflux for several hours. **Tab. 3** shows the used solvents and the outcome of the solubility tests for different monomer salts.

Table 3: Solubility experiments of the monomer salts $[\text{H}_2\text{PDA}^{2+}\text{PMA}^{2-}]$, $[\text{H}_2\text{PDA}^{2+}\text{BTA}^{2-}]$ and $[\text{H}_2\text{Bz}^{2+}\text{BTA}^{2-}]$. Used solvents and boiling points: acetone (bp = 56 °C), MeOH = methanol (bp = 65 °C), EtOH = ethanol (bp = 78 °C), THF = tetrahydrofuran (bp = 66 °C), i-PrOH = isopropanol (bp = 83 °C), DMSO = dimethylsulfoxide (bp = 189 °C), DMF = dimethylformamide (bp = 152 °C).

	$[\text{H}_2\text{PDA}^{2+}\text{PMA}^{2-}]$	$[\text{H}_2\text{PDA}^{2+}\text{BTA}^{2-}]$	$[\text{H}_2\text{Bz}^{2+}\text{BTA}^{2-}]$
acetone	no	no	yes
MeOH	yes	yes	yes
EtOH	no	no	no
THF	no	no	no
i-PrOH	no	no	no
DMSO	yes	yes	yes
DMF	yes	yes	yes

7.2 NMR analysis of monomer salts

Since the monomere salts are soluble in a number of protic and aprotic polar solvents, solution NMR analysis could be carried out.

The ^1H spectra of dried **PMA-based monomer salt** is shown in **Fig.24**.

Integral ratios: Expected ratio for $[\text{H}_2\text{PDA}^{2+}\text{PMDA}^{2-}]$ is $\int\text{H}_a : \int\text{H}_b = 2:4$ obtained ratio = 2:6.2. For $[\text{H}_2\text{PDA}^{2+}\text{PMDA}^{2-}]$ we find a 1:1.5 stoichiometry according to ^1H NMR. This is most likely due to proton exchange processes. However, the stoichiometric ratio of this system was confirmed *via* PXRD by comparison of PXRD data of single crystals with proven 1:1 stoichiometry.³⁴

The ^1H spectra of dried **BTA-based monomer salts** are shown in **Fig. 25**, page 61. Both spectra show broad singlets between 3 and 4 ppm, which correspond to the protons of the ammonium group. Furthermore, the peaks of the ionized monomers are shifted to higher ppm

values compared to the neutral BTA and diamines. For the monomer salts $[\text{H}_2\text{PDA}^{2+}\text{BTA}^{2-}]$ and $[\text{H}_2\text{Bz}^{2+}\text{BTA}^{2-}]$ very broad singlets between 8 and 11 ppm are hardly visible, which correspond to the acidic proton of BTA. The two protonated acidic BTA groups are hardly visible in the spectra due to rapid proton exchange processes (with nondeuterated solvent impurities or deuterated solvent with traces of H_2O , and between the species themselves) which broaden peak extremely.⁸⁴

Since there are no amine-groups (singlet between 4 and 6 ppm) visible, we conclude a stoichiometric ratio 1:1 of BTA: to each diamine (see **Fig. 25**). The ratio of integrals related to BTA^{2-} and each respective ammonium fit reasonably well, the deviations from the expected ratios are related to the proton exchange processes.

Integral ratios:

Expected ratio for $[\text{H}_2\text{PDA}^{2+}\text{BTA}^{2-}]$ is $(\int\text{H}_d + \int\text{H}_e) : (\int\text{H}_a + \int\text{H}_b + \int\text{H}_c) = 4:6$ obtained ratio = 3.77:6.00.

Expected ratio for $[\text{H}_2\text{Bz}^{2+}\text{BTA}^{2-}]$ is $(\int\text{H}_d + \int\text{H}_e) : (\int\text{H}_a + \int\text{H}_b + \int\text{H}_c) = 6:8$ obtained ratio = 5.30:8.79

The ^{13}C -APT (Attached Proton Test) spectra of the two BTA-based monomer salts are depicted in **Fig. 26** and **27**, respectively. All signals are attributed in the figures (see molecule drawings). Quarternary carbon atoms and carbon atoms bearing two protons are pointing downwards, carbon atoms connected to one (CH) and three protons (CH_3) are pointing upwards.

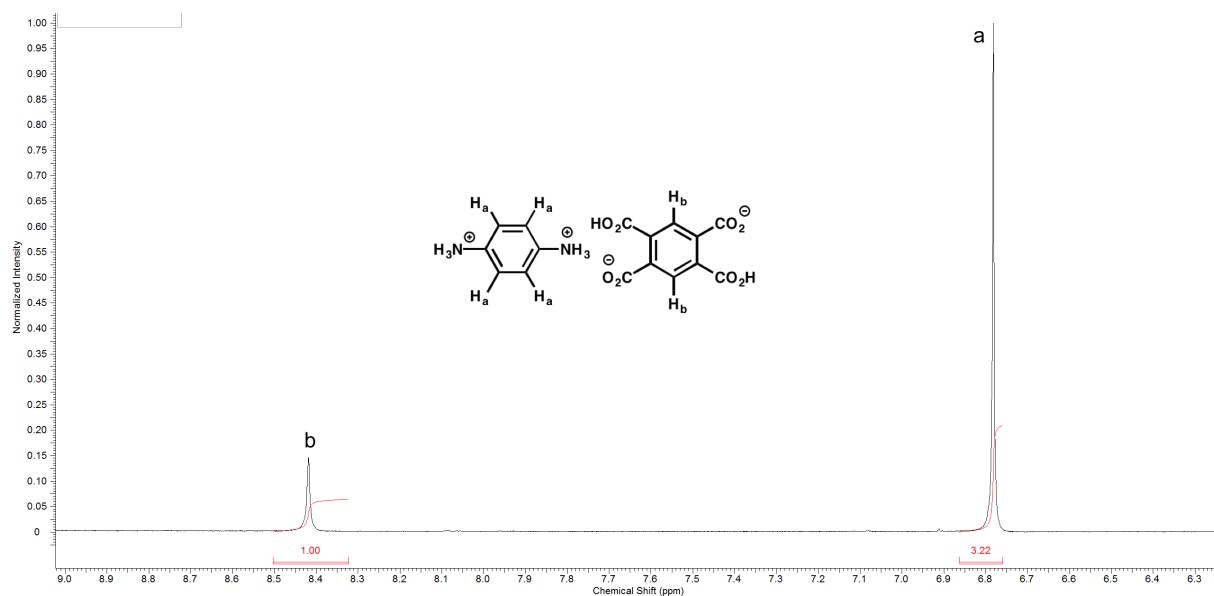


Figure 24: ^1H -NMR spectra of monomer salt $[\text{H}_2\text{PDA}^{2+}\text{PMA}^{2-}]$.

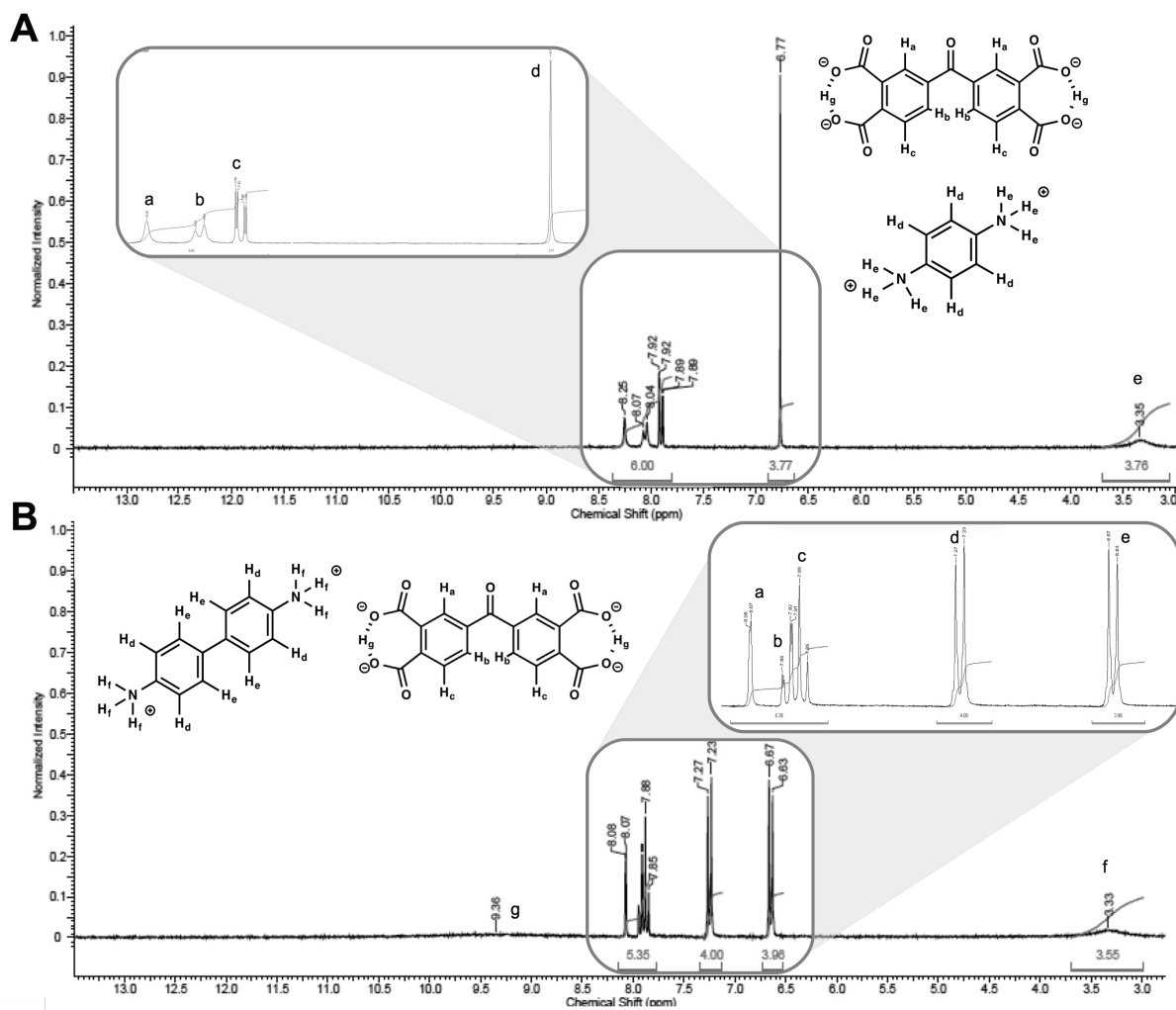


Figure 25: $^1\text{H-NMR}$ spectra of the monomer salt $[\text{H}_2\text{PDA}^{2+}\text{BTA}^{2-}]$ and $[\text{H}_2\text{Bz}^{2+}\text{BTA}^{2-}]$. Figure was reproduced from BAUMGARTNER.³⁶

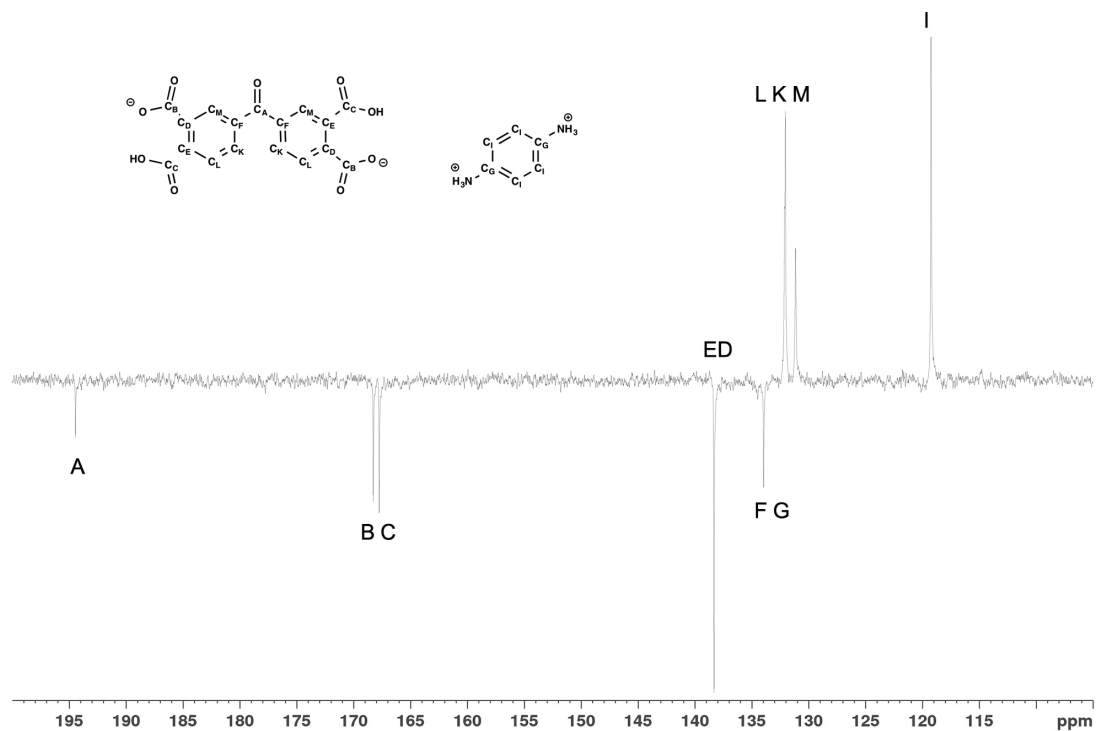


Figure 26: ^{13}C -NMR-APT spectra of the monomer salt $[H_2PDA^{2+}BTA^{2-}]$. Figure was reproduced from BAUMGARTNER.³⁶

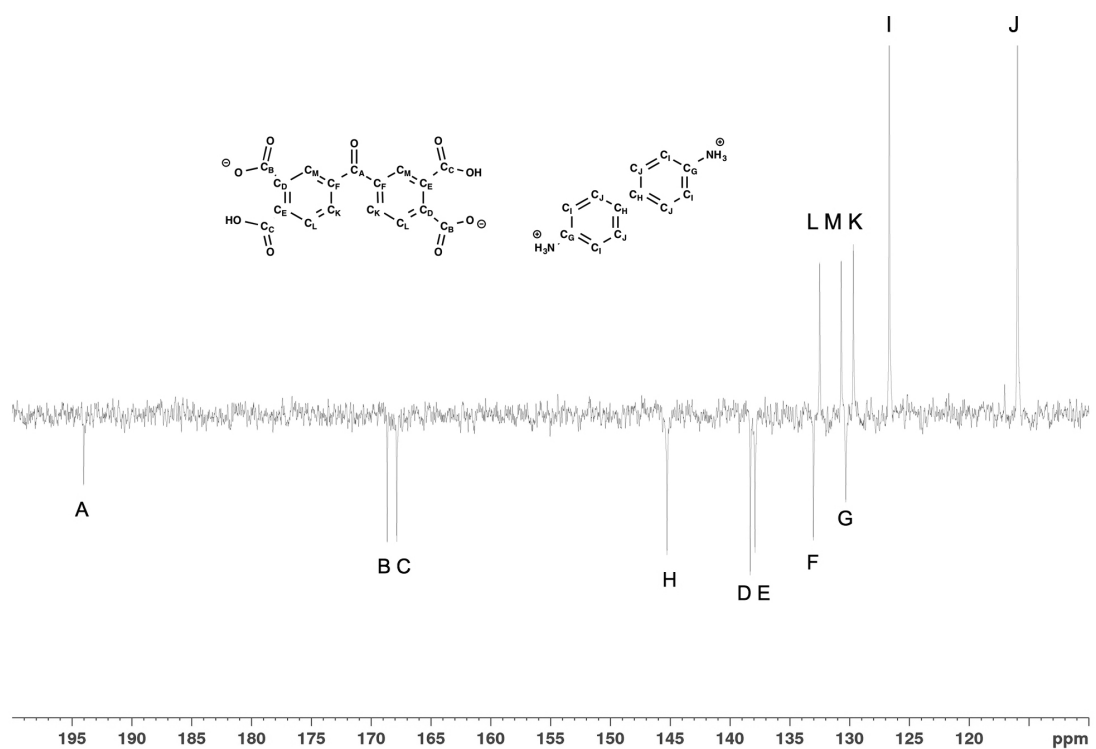


Figure 27: ^{13}C -NMR-APT spectra of the monomer salt $[H_2Bz^{2+}BTA^{2-}]$. Figure was reproduced from BAUMGARTNER.³⁶

7.3 FT-IR-ATR Analysis of Monomer Salts

FT-IR-ATR spectra of dried monomer salts $[\text{H}_2\text{PDA}^{2+}\text{BTA}^{2-}]$ and $[\text{H}_2\text{Bz}^{2+}\text{BTA}^{2-}]$ synthesized at 80 °C for 2 h are shown in **Fig. 28**. The spectra depict the typical monomer salt modes ($\nu_{\text{as}}(\text{Ar-NH}_3^+) \approx 2830 \text{ cm}^{-1}$, $\nu_{\text{s}}(\text{Ar-NH}_3^+) \approx 2580 \text{ cm}^{-1}$, $\nu(\text{C=O}, \text{Ar-COOH}) \approx 1680 \text{ cm}^{-1}$, $\nu_{\text{as}}(\text{C=O}, \text{Ar-COO}^-) \approx 1605 \text{ cm}^{-1}$ and $\nu_{\text{s}}(\text{C=O}, \text{Ar-COO}^-) \approx 1570 \text{ cm}^{-1}$) but also the characteristic imide modes ($\nu_{\text{as}}(\text{C=O}) \approx 1775 \text{ cm}^{-1}$, $\nu_{\text{s}}(\text{C=O}) \approx 1720 \text{ cm}^{-1}$ and $\nu_{\text{s}}(\text{C-N}) \approx 1365 \text{ cm}^{-1}$). Both systems show the coexistence of monomer salt and imide modes, as they had already started to polymerize/oligomerize.

FT-IR-ATR spectra of dried monomer salts $[\text{H}_2\text{PDA}^{2+}\text{BTA}^{2-}]$ and $[\text{H}_2\text{Bz}^{2+}\text{BTA}^{2-}]$ synthesized at RT for 1 d are shown in **Fig. 29**. The spectra depict the typical monomer salt modes and no characteristic imide modes.

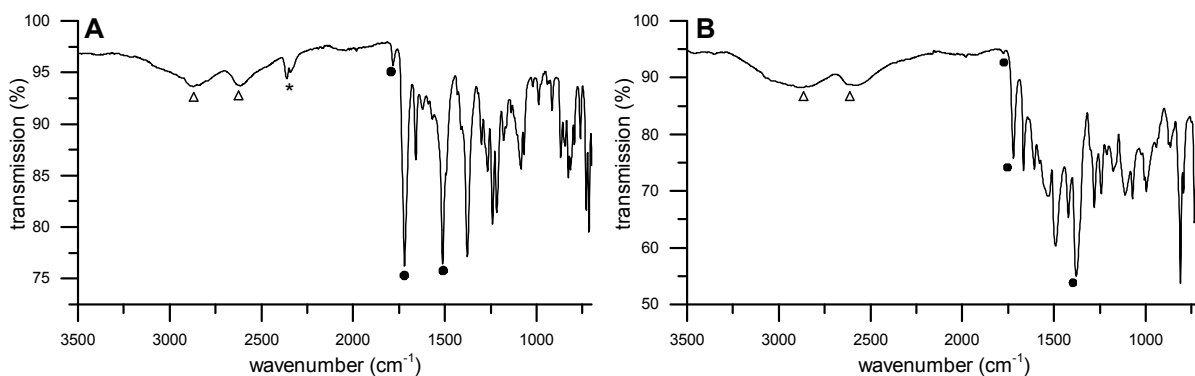


Figure 28: FT-IR-ATR spectra of the BTA-monomer salts synthesized at 80 °C. $[\text{H}_2\text{PDA}^{2+}\text{BTA}^{2-}]$ (A) and $[\text{H}_2\text{Bz}^{2+}\text{BTA}^{2-}]$. The relevant modes are emphasized as follows: Δ = typical monomer salt modes ($\tilde{\nu}_{\text{as}}(\text{Ar-NH}_3^+) \approx 2830 \text{ cm}^{-1}$, $\tilde{\nu}_{\text{s}}(\text{Ar-NH}_3^+) \approx 2580 \text{ cm}^{-1}$, $\tilde{\nu}(\text{C=O}, \text{Ar-COOH}) \approx 1690 \text{ cm}^{-1}$) \bullet = characteristic imide modes ($\tilde{\nu}_{\text{as}}(\text{C=O}) \approx 1775 \text{ cm}^{-1}$, $\tilde{\nu}_{\text{s}}(\text{C=O}) \approx 1720 \text{ cm}^{-1}$ and $\tilde{\nu}_{\text{s}}(\text{C-N}) \approx 1365 \text{ cm}^{-1}$) (B). Figure was reproduced from BAUMGARTNER.³⁶

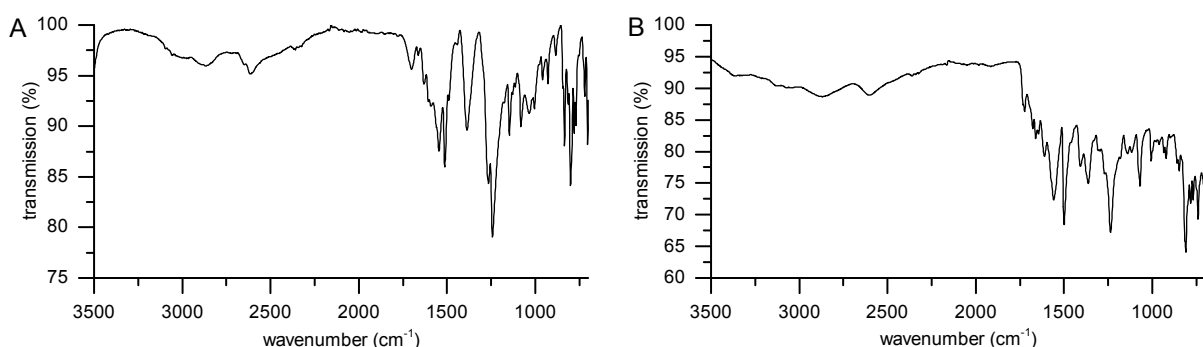


Figure 29: FT-IR-ATR spectra of the BTA-monomer salts synthesized at RT for 1 d. $[\text{H}_2\text{PDA}^{2+}\text{BTA}^{2-}]$ (A) and $[\text{H}_2\text{Bz}^{2+}\text{BTA}^{2-}]$ (B) with typical monomer salt modes ($\tilde{\nu}_{\text{as}}(\text{Ar-NH}_3^+) \approx 2830 \text{ cm}^{-1}$, $\tilde{\nu}_{\text{s}}(\text{Ar-NH}_3^+) \approx 2580 \text{ cm}^{-1}$, $\tilde{\nu}(\text{C=O}, \text{Ar-COOH}) \approx 1690 \text{ cm}^{-1}$). Figure was reproduced from BAUMGARTNER.³⁶

7.4 Aspect of PIs

The aspect of the crude BTA-based PI products after HTP (exemplarily for t_R) is depicted below (Fig. 30).

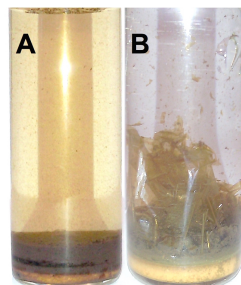


Figure 30: Aspect of crude PIs after HTP. **A:** *poly*(PDA-BTA); **B:** *poly*(Bz-BTA)

7.5 Solubility of PIs

The solubility of *a*- and *b*-phase of all PIs was tested in various solvents according to the following procedure: 10 mL of the respective solvent was added to 125 mg of the respective solid. The resulting dispersion was heated up to the boiling temperature of the respective solvent. The dispersion was kept at reflux for several hours. **Tab. 4** shows the used solvents and the outcome of the solubility tests for different PIs. The solubility behaviour of *a*- and *b*-phases for all systems is identical.

Table 4: Solubility experiments of PIs *poly*(PMA-PDA), *poly*(PDA-BTA) and *poly*(Bz-BTA). Used solvents and boiling points: acetone (bp = 56 °C), MeOH = methanol (bp = 65 °C), EtOH = ethanol (bp = 78 °C), THF = tetrahydrofuran (bp = 66 °C), ⁱ-PrOH = isopropanol (bp = 83 °C), NMP = N-methyl-2-pyrrolidone (bp = 202 °C), DMSO = dimethylsulfoxide (bp = 189 °C), DMF = dimethylformamide (bp = 152 °C), H₂SO₄ conc. = concentrated sulfuric acid (heated to 200 °C as it decomposes at bp).

	<i>poly</i> (PDA-PMA)	<i>poly</i> (PDA-BTA)	<i>poly</i> (Bz-BTA)
acetone	no	no	no
MeOH	no	no	no
EtOH	no	no	no
THF	no	no	no
ⁱ PrOH	no	no	no
NMP	no	no	no
DMSO	no	no	no
DMF	no	no	no
H ₂ SO ₄ , conc.	no	yes	yes

7.6 NMR Analysis of Dimers

Both dimers *dimer*(PDA-BTA) and *dimer*(Bz-BTA) were soluble in DMSO. Therefore, solution NMR could be carried out. The ^1H -NMR-spectra of dried *dimer*(PDA-BTA) is depicted in **Fig. 31**. The broad doublet of doublets between 7.1 - 6.6 ppm corresponds to the ring protons of the amino-phenyl moiety, whereas the signals between 8.2 - 7.8 ppm correspond to the aromatic ring protons of the benzophenone moiety. Since there are no amine-groups (which would appear as singlet between 4 and 6 ppm) or carboxylic acid-groups (which would appear at 10 - 12 ppm) visible, we conclude the structure of the zwitterionic monoimide *dimer*(PDA-BTA). The ^1H -NMR-spectra of *dimer*(Bz-BTA) is depicted in **Fig. 32**. Due to the different chemical environments of each of the 17 protons, an attribution was not possible.

***dimer*(PDA-BTA):** ^1H NMR (250 MHz, DMSO- d_6 , δ , ppm): 8.20 (d, 1 H), 8.06 - 8.15 (d, 1 H), 7.99 (d, $J = 9.61$ Hz, 1 H), 7.88 (d, $J = 7.93$ Hz, 1 H), 7.07 (d, $J = 8.54$ Hz, 2 H), 6.67 (d, $J = 8.54$ Hz, 2 H)

MS (ESI) m/z [M^+H] $^+$: calcd for $\text{C}_{23}\text{H}_{14}\text{N}_2\text{O}_7$ 429.08; found 428.9.

***dimer*(Bz-BTA):** MS (ESI) m/z [M^+H] $^+$: calcd for $\text{C}_{29}\text{H}_{18}\text{N}_2\text{O}_7$ 505.11; found 504.9.

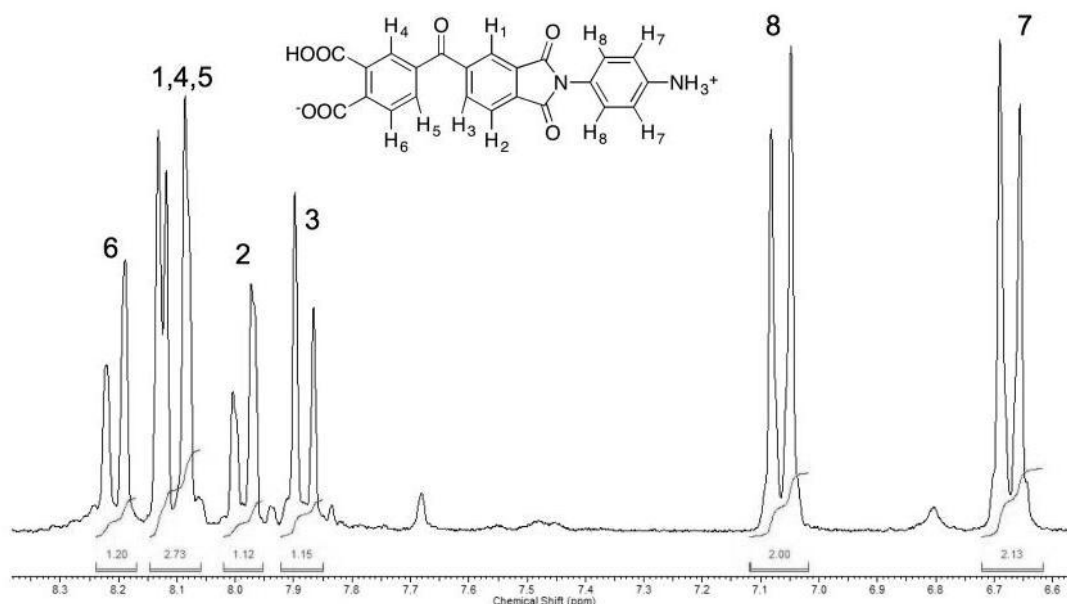


Figure 31: Relevant area of ^1H -NMR spectra of *dimer*(PDA-BTA). Figure was reproduced from BAUMGARTNER.³⁷

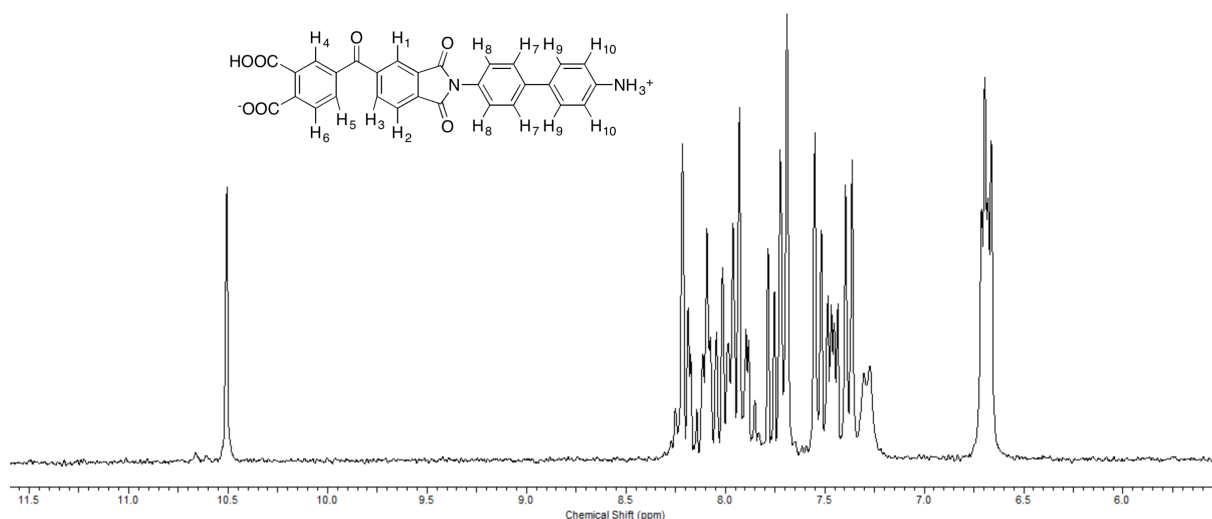


Figure 32: Relevant area of $^1\text{H-NMR}$ spectra of *dimer*(Bz-BTA). Figure was reproduced from BAUMGARTNER.³⁷

7.7 FT-IR-ATR Analysis of PIs

Fig. 33A shows a superimposition of normalized FT-IR-ATR spectra of dried monomer salt $[\text{H}_2\text{PDA}^{2+}\text{PMA}^{2-}]$, with the *poly*(PDA-PMA) *a*-phases at low reaction times ($t_R = 0.25$ h, 0.5 h and 1 h) obtained at 200 °C. The spectra of products obtained after 0.25 h and 0.5 h still strongly depict monomer salt modes, aside weak imide modes. The spectra from *poly*(PDA-PMA) obtained after 1 h does not show monomer salt modes at all, but appears to be fully imidized: the classical cyclic imide modes are present.

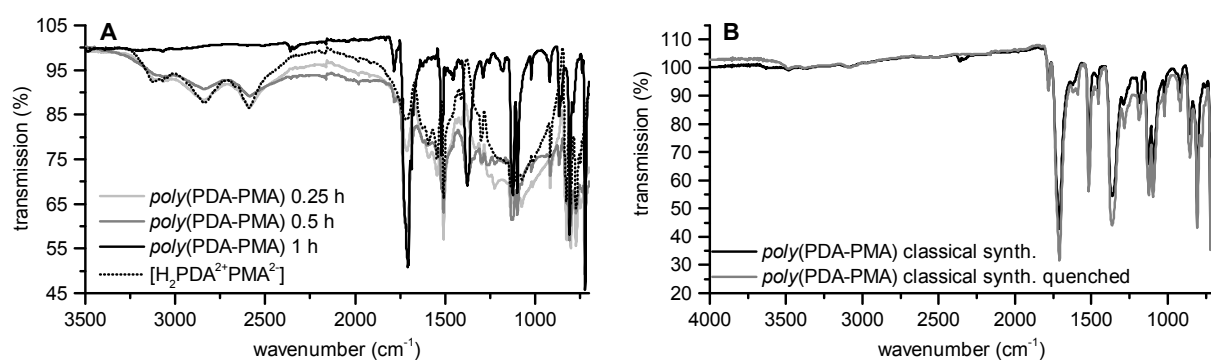


Figure 33: Superimposition of FT-IR-ATR spectra of **A**: $[\text{H}_2\text{PDA}^{2+}\text{PMA}^{2-}]$, with *poly*(PDA-PMA) *a*-phases obtained after different t_R at 200 °C: 0.25 h, 0.5 h and 1 h. **B**: conventionally synthesized *poly*(PDA-PMA). *poly*(PDA-PMA) conventionally synthesized allowed to cool slowly (black); *poly*(PDA-PMA) conventionally synthesized quenched (gray). Figure was reproduced from BAUMGARTNER.³⁵

Fig. 33B shows a superimposition of conventionally synthesized *poly*(PDA-PMA), which was

allowed to slowly cool down (black) and quenched by precipitation in methanol (gray). Both spectra show a fully imidized product lacking remainings of monomer modes, *poly*(amic acid) modes or endgroups (potentially amino-, carboxylic acid- or anhydride modes). Moreover, it can be concluded that the mode of cooling does not affect the chemical nature of the product.

The superimpositions of FT-IR-ATR spectra of the PIs *poly*(PDA-BTA) and *poly*(Bz-BTA) synthesized *via* HTP at different reaction times ($t_R = 1$ h, 2 h, 4 h and 12 h) at 200 °C are depicted in **Fig. 34**. The spectra of *poly*(PDA-BTA) and *poly*(Bz-BTA) obtained after 1 h do not show monomer salt modes at all, and are fully imidized: the classical cyclic imide modes are present.

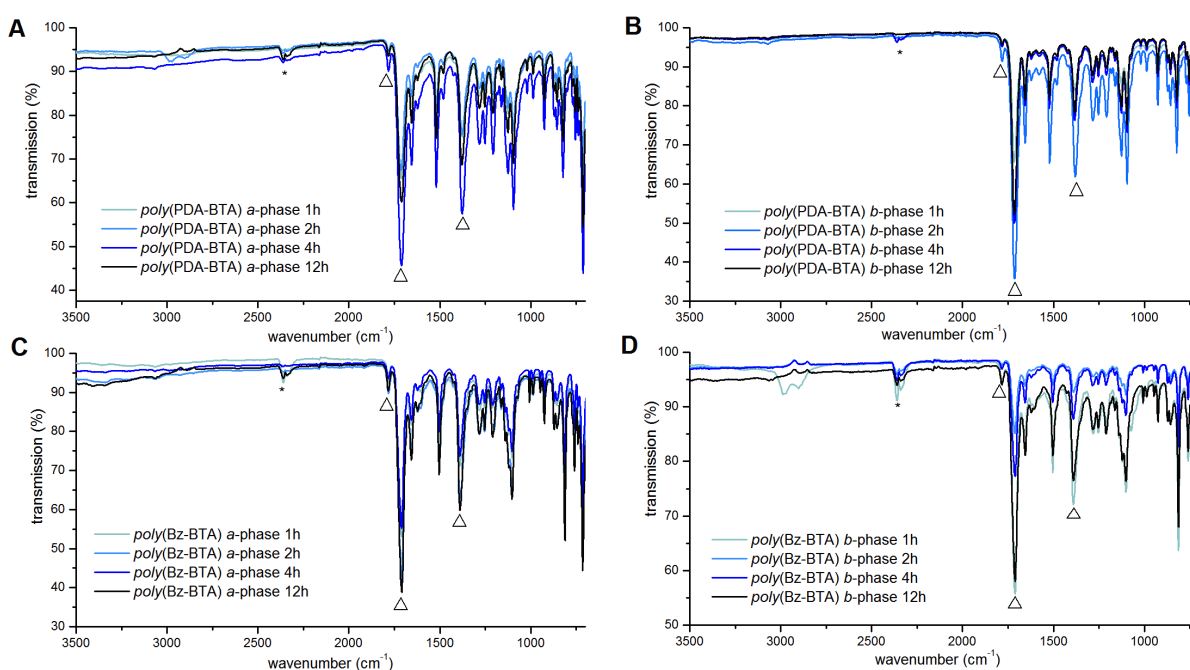


Figure 34: FT-IR-ATR spectra of PIs synthesized *via* HTP at 200 °C for different reaction times. In all panels: light blue for $t_R = 1$ h, blue $t_R = 2$ h, dark blue $t_R = 4$ h and black for $t_R = 12$ h. **A:** *poly*(PDA-BTA) *a*-phases; **B:** *poly*(PDA-BTA) *b*-phases; **C:** *poly*(Bz-BTA) *a*-phases; **D:** *poly*(Bz-BTA) *b*-phases. The relevant modes are emphasized by triangles ($\Delta =$ characteristic imide modes ($\tilde{\nu}_{as}(C=O) \approx 1775$ cm^{-1} , $\tilde{\nu}_s(C=O) \approx 1720$ cm^{-1} and $\tilde{\nu}_s(C-N) \approx 1365$ cm^{-1}). We find no typical monomer salt modes. *=atmospheric CO_2 . Figure was reproduced from BAUMGARTNER.³⁶

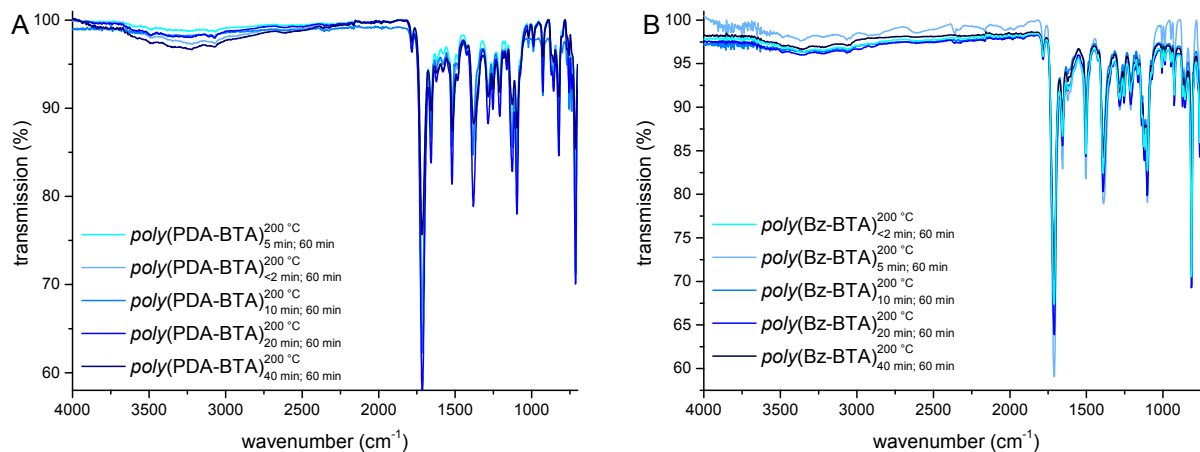


Figure 35: FT-IR-ATR spectra of PIs synthesized at $T_R = 200\text{ °C}$ with different heating times t_h . **A:** $\text{poly}(\text{PDA-BTA})$; **B:** $\text{poly}(\text{Bz-BTA})$. Figure was reproduced from BAUMGARTNER.³⁶

The superimpositions of FT-IR-ATR spectra of T_P and $\text{poly}(\text{Bz-BTA})$ synthesized *via* HTP at $t_R = 60\text{ min}$ with $T_R < T_P$ ($T_P(\text{poly}(\text{PDA-BTA})) = 149\text{ °C}$, $T_P(\text{poly}(\text{Bz-BTA})) = 172\text{ °C}$) and $T_R = 200\text{ °C}$ with different heating times ($t_h = 2\text{ min}$, 5 min , 10 min , 20 min , 60 min) are depicted in **Fig. 35** and **Fig. 36**. All PI spectra show the characteristic imide modes. $\text{poly}(\text{PDA-BTA})$ synthesized at 145 °C still shows slight ammonium modes ($\tilde{\nu}_{\text{as}}(\text{Ar-NH}_3^+) \approx 2830\text{ cm}^{-1}$, $\tilde{\nu}_{\text{s}}(\text{Ar-NH}_3^+) \approx 2580\text{ cm}^{-1}$).

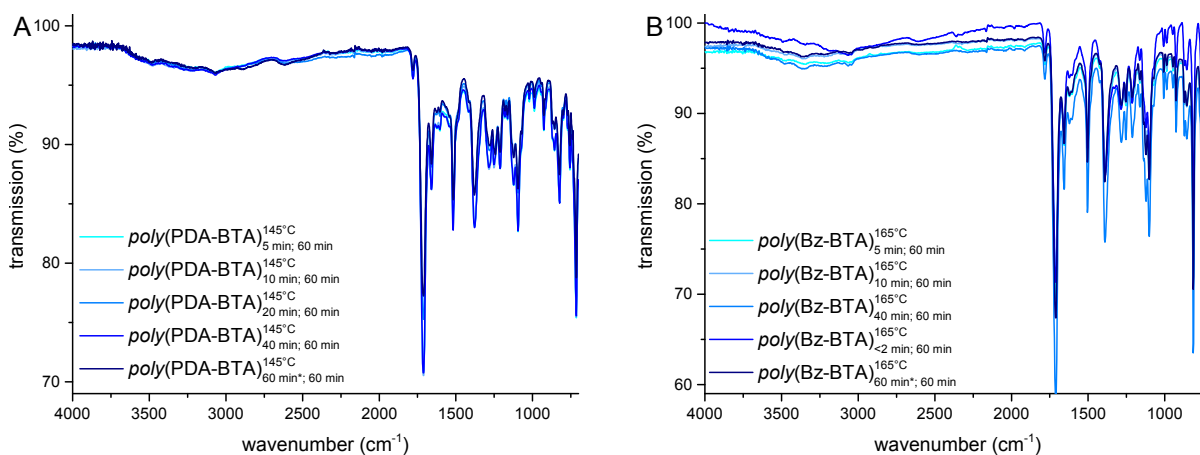


Figure 36: FT-IR-ATR spectra of PIs synthesized at $T_R < T_P$ with different heating times t_h . **A:** $\text{poly}(\text{PDA-BTA})$; **B:** $\text{poly}(\text{Bz-BTA})$. Figure was reproduced from BAUMGARTNER.³⁷

Superimpositions of FT-IR-ATR spectra of isolated *dimer*(PDA-BTA) *vs.* residue and *dimer*(Bz-BTA) *vs.* residue at $T_R = 130\text{ °C}$ for $t_R = 120\text{ min}$ and obtained *via* fractionation are depicted in **Fig. 37**. The dimer spectra show imide modes as well as ammonium modes. Their residues depict slightly visible ammonium modes.

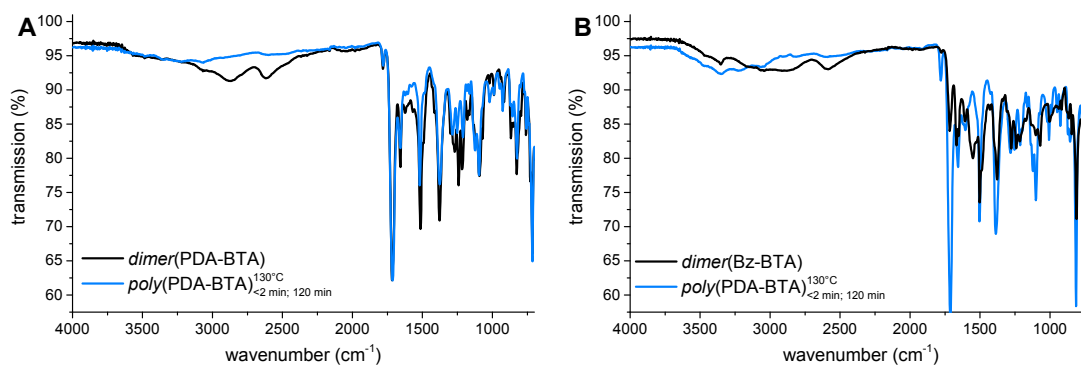


Figure 37: Exemplary FT-IR-ATR spectra of BTA-based dimers and PIs synthesized at 130 °C and their residue. **A:** *dimer*(PDA-BTA)/*poly*(PDA-BTA) **B:** *dimer*(Bz-BTA)/*poly*(Bz-BTA). Figure was reproduced from BAUMGARTNER.³⁷

The superimpositions of FT-IR-ATR spectra of the BTA-based reaction products synthesized at $t_R = 60$ min at different temperatures T_R are depicted in **Fig. 38**. The products are mixtures of $[\text{H}_2\text{PDA}^{2+}\text{BTA}^{2-}]$ /*dimer*(PDA-BTA)/*poly*(PDA-BTA) and *dimer*(Bz-BTA)/*poly*(Bz-BTA) in different ratios. All spectra show the characteristic ammonium-modes which belong to $[\text{H}_2\text{PDA}^{2+}\text{BTA}^{2-}]$ /*dimer*(PDA-BTA) and $[\text{H}_2\text{Bz}^{2+}\text{BTA}^{2-}]$ /*dimer*(Bz-BTA), respectively, and the characteristic imide modes.

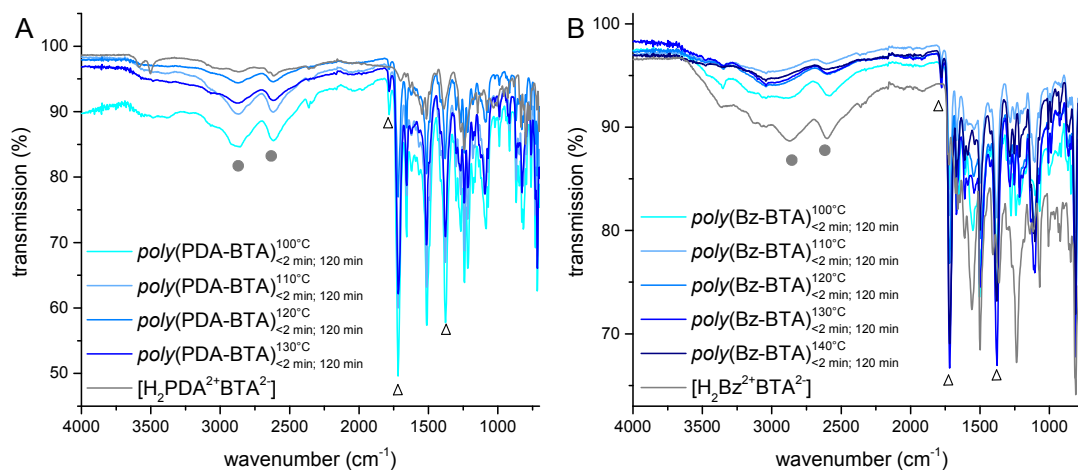


Figure 38: FT-IR-ATR spectra of PIs and dimers synthesized at $t_R = 120$ min at different temperatures. **A:** *poly*(PDA-BTA)/*dimer*(PDA-BTA); **B:** *poly*(Bz-BTA)/*dimer*(Bz-BTA); (● = typical ammonium modes: $\tilde{\nu}_{\text{as}}(\text{Ar-NH}_3^+) \approx 2830 \text{ cm}^{-1}$, $\tilde{\nu}_{\text{s}}(\text{Ar-NH}_3^+) \approx 2580 \text{ cm}^{-1}$) Δ = characteristic imide modes: $\tilde{\nu}_{\text{as}}(\text{C=O}) \approx 1775 \text{ cm}^{-1}$, $\tilde{\nu}_{\text{s}}(\text{C=O}) \approx 1720 \text{ cm}^{-1}$ and $\tilde{\nu}_{\text{s}}(\text{C-N}) \approx 1365 \text{ cm}^{-1}$. Figure was reproduced from BAUMGARTNER.³⁷

7.8 Powder X-ray Diffraction of PIs

Fig. 39 shows PXRD patterns of *poly*(PDA-PMA) *a*-phase obtained after $t_R = 12$ h at different reaction temperatures ($T_R = 150$ °C, 200 °C, 250 °C). Peaks attributed to unreacted monomer salt are present in the pattern of the sample obtained at 150 °C only and are denoted by an asterisk (*). The PXRD pattern of products obtained at 200 and 250 °C correspond to the typical *poly*(PDA-PMA) pattern.

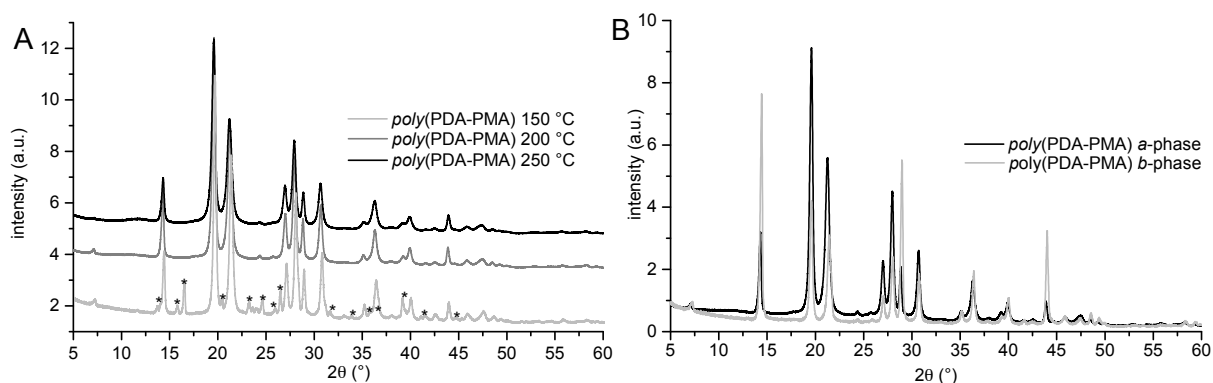


Figure 39: PXRD patterns of *poly*(PDA-PMA) **A:** PIs obtained at different reaction temperatures, at $t_R = 12$ h. $T_R = 150$, 200 or 250 °C. Peaks attributed to unreacted monomer salt are denoted by asterisks (*). **B:** *poly*(PDA-PMA) *a*- and *b*-phase obtained at $t_R = 12$ h. Figure was reproduced from BAUMGARTNER.³⁵

Superimpositions of the XRD patterns of *a*- and *b*-phases of *poly*(PDA-BTA) and *poly*(Bz-BTA), respectively, obtained after different t_R (1 h, 2 h, 4 h and 12 h) are shown in **Fig. 40**. The *a*- and *b*-phases of each BTA-based PI - for the same t_R - show identical major reflections. However, the *b*-phases are typically of higher crystallinity and show a few additional reflections (highlighted with gray arrows in **Fig. 40B** and **D**). In PXRD patterns, we still find reflections related to non-reacted monomer salt after $t_R = 1$ h, however only in the *b*-phases (highlighted with orange arrows in **Fig. 40B** and **D**).

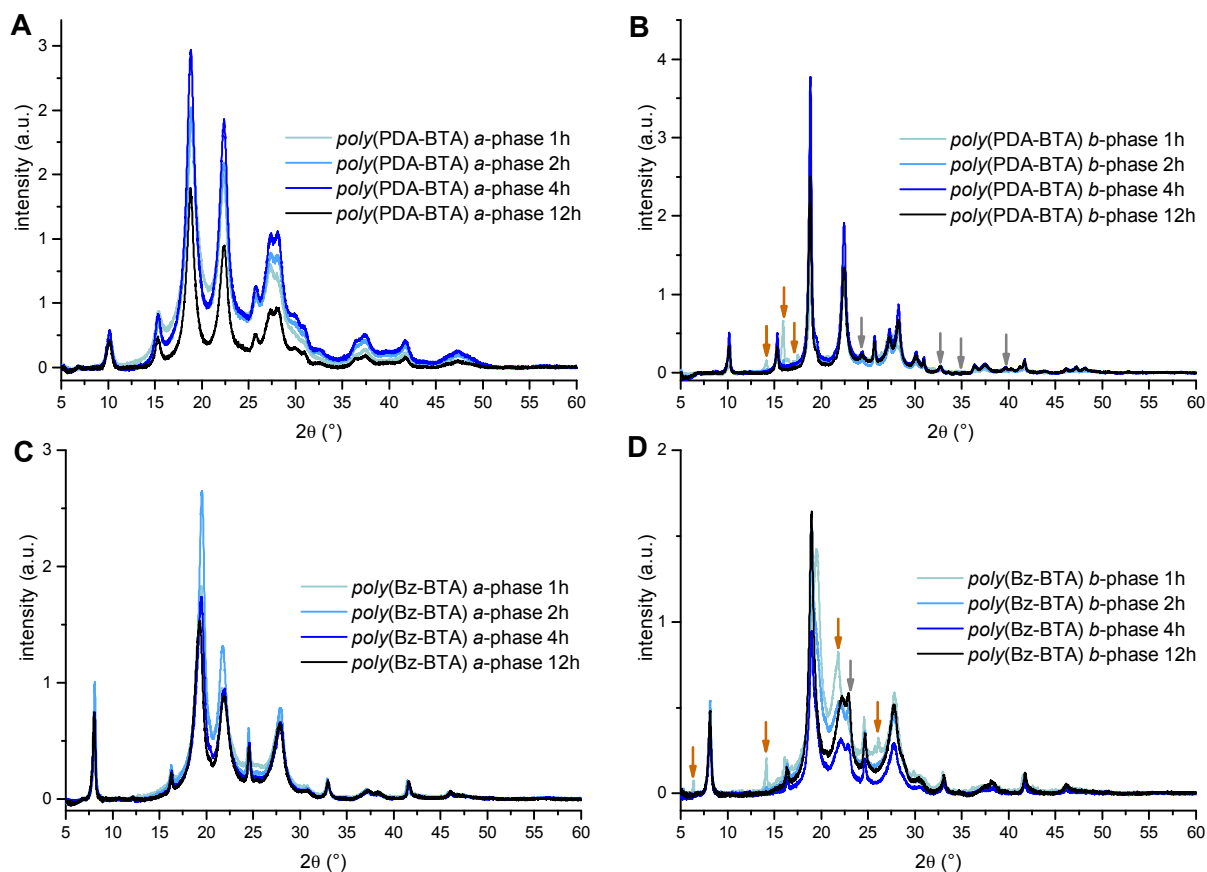


Figure 40: Diffractograms of *poly*(PDA-BTA) and *poly*(Bz-BTA) synthesized *via* HTP at 200 °C for different reaction times. For all panels: $t_R = 1$ h (light blue), $t_R = 2$ h (blue), $t_R = 4$ h (dark blue), and $t_R = 12$ h (black). **A:** a- phases of *poly*(PDA-BTA); **B:** b-phase of *poly*(PDA-BTA); **C:** a-phases of *poly*(Bz-BTA), and **D:** b-phases of *poly*(Bz-BTA). Figure was reproduced from BAUMGARTNER.³⁶

Solid-state polymerizations have been carried out for comparison (200 °C, 12 h). The diffractograms of BTA-based PIs obtained by SSP are depicted **Fig. 41**. The amorphous halos in **Fig. 41** are qualitatively emphasized as colored areas, and their centers are emphasized by dotted lines: the pattern of *poly*(PDA-BTA) shows amorphous halos centered at around 18° (2θ), 21° (2θ) and a very broad and weak halo around 43° (2θ). The diffractogram of *poly*(Bz-BTA) shows a semicrystalline product featuring amorphous halos centered at around 20°, 26° and 38° (2θ).

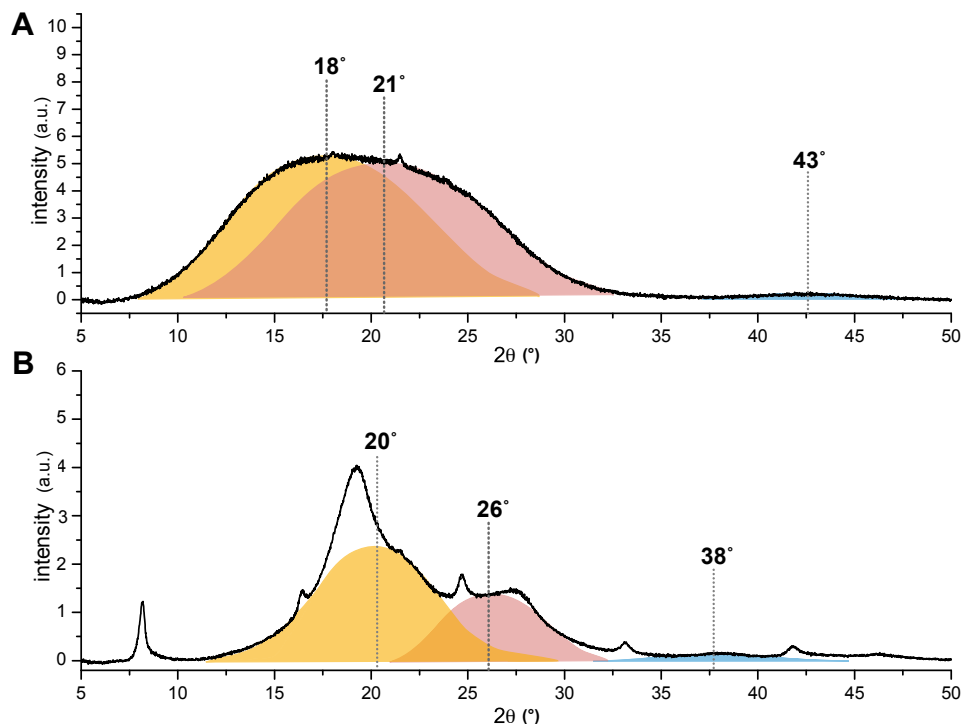


Figure 41: Diffraction patterns of PIs obtained by solid-state polycondensation of monomer salt $[\text{H}_2\text{PDA}^{2+}\text{BTA}^{2-}]$ (A) and $[\text{H}_2\text{Bz}^{2+}\text{BTA}^{2-}]$ (B) polymerized by solid-state polymerization at 200°C for 12 h. Figure was reproduced from BAUMGARTNER.³⁶

Normalized PXRD patterns of *poly*(PDA-BTA) and *poly*(Bz-BTA) synthesized at $T_R < T_P$ and different heating times t_h are depicted in **Fig. 42**. *poly*(PDA-BTA) synthesized with $t_h = 60$ min shows additional reflections at $13, 14, 16, 17, 21$ and 27° (2θ), that correspond to remaining monomer salt $[\text{H}_2\text{PDA}^{2+}\text{BTA}^{2-}]$ ($16^\circ(2\theta)$) and to *dimer*(PDA-BTA) ($13, 14, 17, 21, 27^\circ$ (2θ)). Superimpositions of normalized PXRD patterns of *poly*(PDA-BTA) and *poly*(Bz-BTA) synthesized $T_R = 200^\circ\text{C}$ and different t_h are shown in **Fig. 43**.

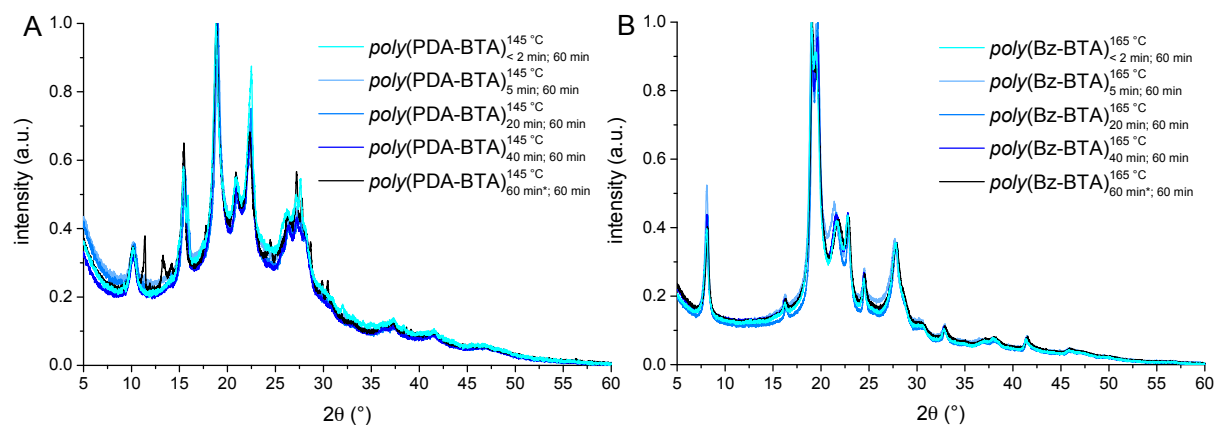


Figure 42: PXRD patterns of PIs synthesized $T_R < T_P$ at different heating times. **A**: *poly*(PDA-BTA); **B**: *poly*(Bz-BTA). Figure was reproduced from BAUMGARTNER.³⁷

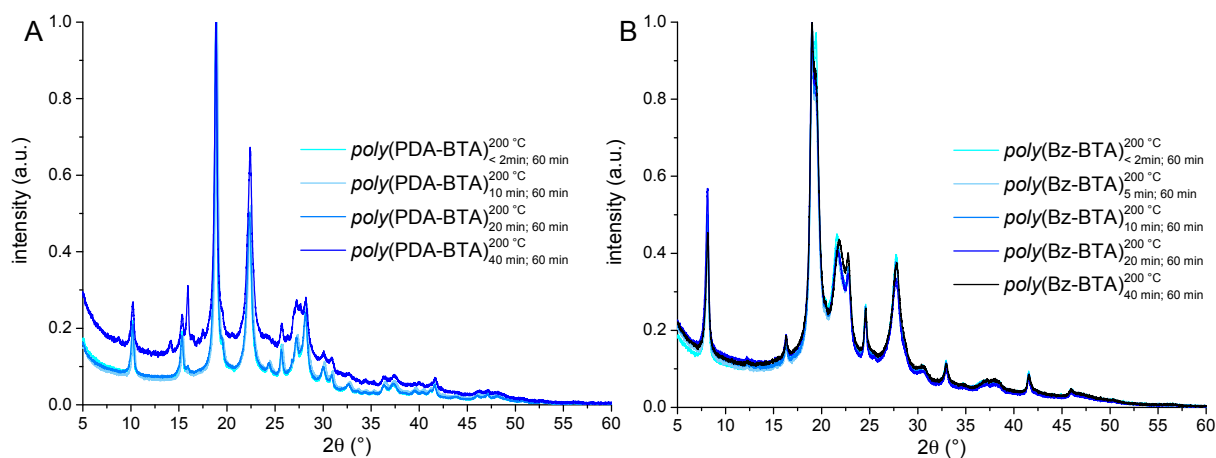


Figure 43: Normalized PXRD patterns of PIs synthesized $T_R < T_P$ at different heating times. **A**: *poly*(PDA-BTA); **B**: *poly*(Bz-BTA). Figure was reproduced from BAUMGARTNER.³⁷

7.9 Crystal Structure Data

For Unit-cell parameters and atomic coordinates in CIF-format see BAUMGARTNER *et al.*^{35,37}

7.10 Thermogravimetric Analysis of Monomer Salts and PIs

TGA of the dried monomer salt $[\text{H}_2\text{PDA}^{2+}\text{PMA}^{2-}]$ is depicted in **Fig. 44A**. The monomer salt depicts a polymerization point at 210 °C. **Fig. 44B** shows the thermogravimetric analysis of *poly*(PDA-PMA) *a*-phase, obtained after $t_R = 12$ h. The product is stable up to 640 °C.

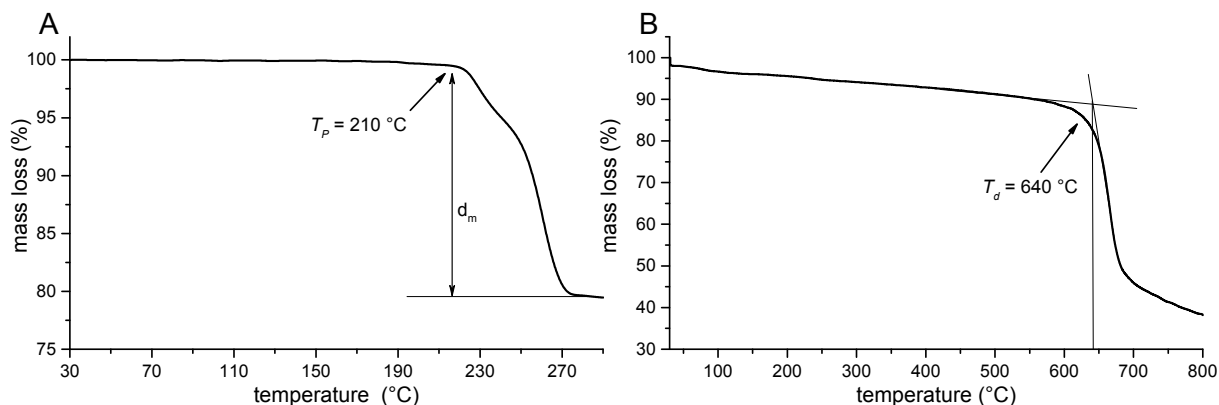


Figure 44: Thermogravimetric analysis of $[\text{H}_2\text{PDA}^{2+}\text{PMA}^{2-}]$ (**A**) and *poly*(PDA-PMA) (*a*-phase, $t_R = 12$ h) (**B**). The polymerization of the monomer salt starts at 210 °C and a mass loss of 20 % equals to the amount of condensated water. Figure was reproduced from BAUMGARTNER.³⁵

The TGA curves of the dried BTA-based monomer salts are depicted in **Fig. 45**. The monomer salts depict a polymerization point T_P at 149 °C for $[\text{H}_2\text{PDA}^{2+}\text{BTA}^{2-}]$ and 172 °C for $[\text{H}_2\text{Bz}^{2+}\text{BTA}^{2-}]$. The initial mass loss around 100 °C is due to physisorbed water.

The mass losses d_m determined *via* TGA are 20 % for $[\text{H}_2\text{PDA}^{2+}\text{PMA}^{2-}]$, 14 % for $[\text{H}_2\text{PDA}^{2+}\text{BTA}^{2-}]$ and 13 % for $[\text{H}_2\text{Bz}^{2+}\text{BTA}^{2-}]$. This corresponds well to two equivalents of water per imide ring, which are eliminated upon polymerization. The theoretical mass losses are 19.9 for $[\text{H}_2\text{PDA}^{2+}\text{PMA}^{2-}]$, 15.4 % for $[\text{H}_2\text{PDA}^{2+}\text{BTA}^{2-}]$ and 13.3 % for $[\text{H}_2\text{Bz}^{2+}\text{BTA}^{2-}]$ (calculated with **Eq. (13)**).

$$d_m = \frac{(M_{ms} - M_{RU})}{M_{ms}} \cdot 100 \quad (13)$$

With M_{ms} = molecular weight of the monomer salt, and M_{RU} = molecular weight of the corresponding polyimide's repeating unit.

$$\begin{aligned} M_{ms}([\text{H}_2\text{PDA}^{2+}\text{PMA}^{2-}]) &= 363.3 \text{ g/mol} & M_{RU}(\textit{poly}(\text{PDA-PMA})) &= 290.3 \text{ g/mol} \\ M_{ms}([\text{H}_2\text{PDA}^{2+}\text{BTA}^{2-}]) &= 466.4 \text{ g/mol} & M_{RU}(\textit{poly}(\text{PDA-PMA})) &= 394.4 \text{ g/mol} \\ M_{ms}([\text{H}_2\text{Bz}^{2+}\text{BTA}^{2-}]) &= 542.5 \text{ g/mol} & M_{RU}(\textit{poly}(\text{PDA-PMA})) &= 470.5 \text{ g/mol} \end{aligned}$$

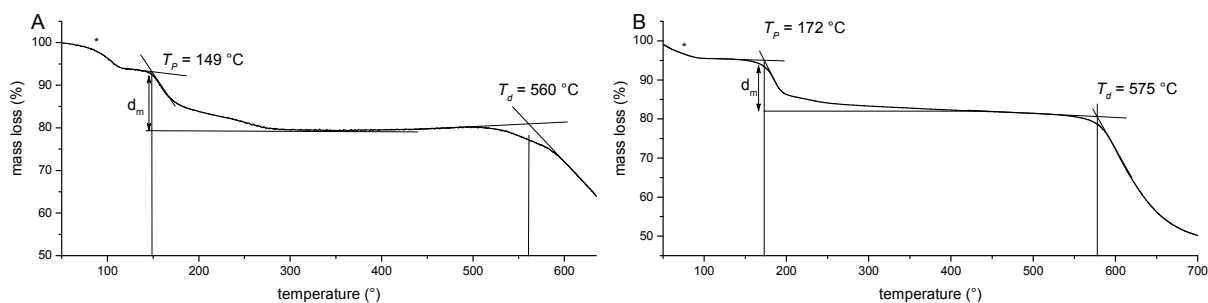


Figure 45: Thermogravimetric analysis of the BTA-based monomer salts. A: $[\text{H}_2\text{PDA}^{2+}\text{BTA}^{2-}]$, with $d_m = 14\%$, $T_P = 149\text{ °C}$ and $T_d = 517\text{ °C}$. B: $[\text{H}_2\text{Bz}^{2+}\text{BTA}^{2-}]$, with $d_m = 13\%$, $T_P = 172\text{ °C}$ and $T_d = 544\text{ °C}$. (*) indicates mass loss due to physisorbed water. Figure was reproduced from BAUMGARTNER.³⁶

7.11 Characterization of supernatant in PDA-based PIs

The *c*-phase of *poly*(PDA-PMA) was carefully removed from the product mixture with a pipette. The solvent water of all *c*-phases was then removed with a rotary evaporator. The remaining violet-brownish solid was redissolved in *d*-DMSO and ^1H solution NMR analysis was performed. The ^1H NMR spectra of dried *c*-phases after $t_R = 1\text{ h}$ and $t_R = 12\text{ h}$ are shown in **Fig. 47**. Both spectra show a singlet at 8.18 ppm, which corresponds to the aromatic protons of pyromellitic dianhydride. The removal of water under reduced pressure causes its dehydration to the anhydride, which we find *via* ^1H NMR. The triplets in **Fig. 47a** (7.31 ppm, 7.10 ppm, 6.90 ppm) and **Fig. 47b** (7.48 ppm, 7.27 ppm, 7.07 ppm) both exhibit a roof effect.

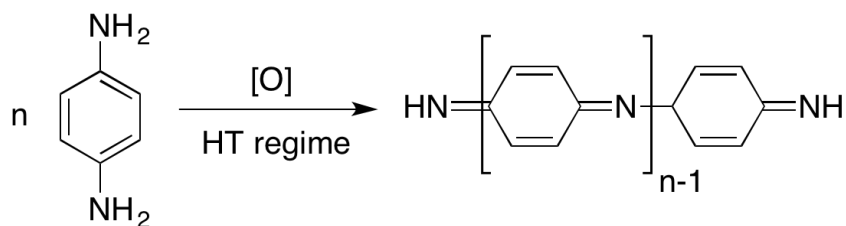
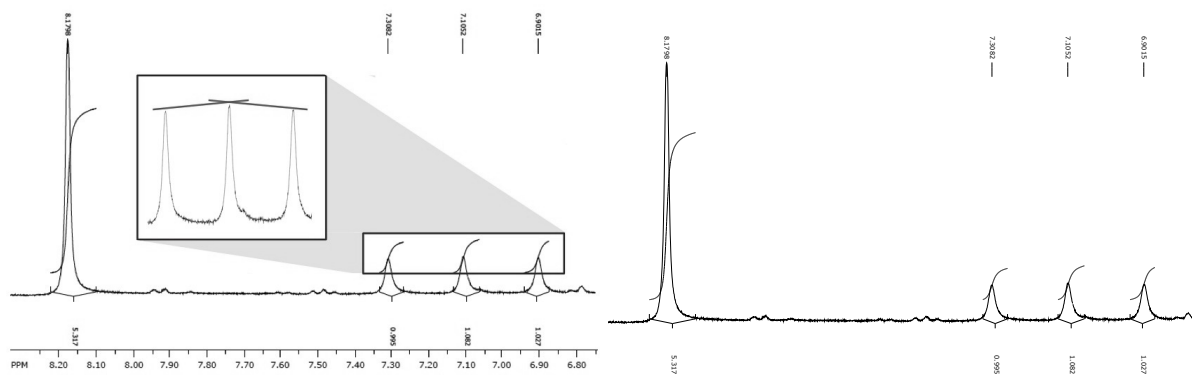


Figure 46: Oxidation of *p*-phenylene diamine, adapted from Lewis.⁸⁵ PDA forms strongly colored *para*-imino oligomers in the presence of oxygen.

These triplets are attributed to aromatic protons of oxidation oligomers of PDA (see **Fig. 46**). In the case of $t_R = 12\text{ h}$ (**Fig. 47b**), we find an additional peak at 6.75 ppm, which we attribute to imino protons. Note the decrease of integrals of the triplets at $t_R = 12\text{ h}$ compared to $t_R = 1\text{ h}$, which is due to PDA-derived oligomers growing longer after higher reaction times and joining the *b*-phase.



(a) $^1\text{H-NMR}$ of *poly*(PDA-PMA) *c*-phase ($t_R = 1$ h). (b) $^1\text{H-NMR}$ of *poly*(PDA-PMA) *c*-phase ($t_R = 12$ h)

Figure 47: Characterization of the *c*-phase by ^1H NMR. Figure was reproduced from BAUMGARTNER.³⁵

References

- [1] Elias, H.-G. *Makromoleküle Chemische Struktur und Synthese*; WILEY-VCH Verlag, 1999; Vol. 1.
- [2] Mitchell, B. S. *An Introduction to Materials Engineering and Science*; WILEY-VCH Verlag: Hoboken, 2003; p 969.
- [3] Ashby, M., Ed. *The CES EduPack Resoure Booklet 2*; CES EduPack: Cambridge, 2009.
- [4] Kalpakjian, S. *Manufacturing Processes for Engineering Materials*; Pearson Education, 1992.
- [5] Hergenrother, P. M. The Use, Design, Synthesis, and Properties of High Performance/High Temperature Polymers: an Overview. *High Perform. Polym.* **2003**, *15*, 3–45.
- [6] Ritter, N.; Senkovska, I.; Kaskel, S.; Weber, J. Towards Chiral Microporous Soluble Polymers—Binaphthalene-Based Polyimides. *Macromol. Rapid Commun.* **2011**, *32*, 438–443.
- [7] Unterlass, M. M.; Kopetzki, D.; Antonietti, M.; Weber, J. Mechanistic study of hydrothermal synthesis of aromatic polyimides. *Polym. Chem.* **2011**, *2*, 1744–1753.
- [8] Le Chatelier, H. Recherches expérimentales et théoriques sur les équilibres chimiques. *Ann. des Mines* **1888**, *13*, 157.
- [9] Anastas, P. T.; Warner, J. C. *Green Chemistry: Theory and Practice*; Oxford University Press, 1998.
- [10] Young, R. J.; Lu, D.; Day, R. J.; Knoff, W. F.; Davis, H. A. Relationship between structure and mechanical properties for aramid fibres. *J. Mater. Sci.* **1992**, *27*, 5431–5440.
- [11] McCullough, R. D.; Lowe, R. D. Enhanced electrical conductivity in regioselectively synthesized poly(3-alkylthiophenes). *J. Chem. Soc., Chem. Commun* **1992**, *1*, 70–72.
- [12] Sharma, P.; Damien, D.; Nagarajan, K.; Shaijumon, M. M.; Hariharan, M. Perylene-polyimide-Based Organic Electrode Materials for Rechargeable Lithium Batteries. *J. Phys. Chem. Lett.* **2013**, *4*, 3192–3197.
- [13] Shirota, Y. Organic materials for electronic and optoelectronic devices. *J. Mater. Chem.* **2000**, *10*, 1–25.
- [14] Flory, P. J. *Principles of Polymer Chemistry*; Cornell University Press, 1953.
- [15] Ballauff, M. Stiff-Chain Polymers: Structure, Phase Behavior, and Properties. *Angew. Chemie Int. Ed. English* **1989**, *28*, 253–267.
- [16] Carothers, W. H. Studies on polymerization and ring formation. I. An introduction to the general theory of condensation polymers. *J. Am. Chem. Soc.* **1929**, *51*, 2548–2559.
- [17] Carothers, W. H. Polymers and polyfunctionality. *Trans. Faraday Soc.* **1936**, *32*, 39–49.
- [18] Kardash, I.; Glukhoedov, N.; Ardashnikov, A. The nature of the equilibrium in the reaction of aromatic anhydrides with aromatic amines and its role in synthesis of polyimides. *Polym. Sci. USSR* **1971**, *15*, 2092–2100.

- [19] Kaas, R. L. Autocatalysis and equilibrium in polyimide synthesis. *J. Polym. Sci. Polym. Chem. Ed.* **1981**, *19*, 2255–2267.
- [20] Kendrick, J.; Robson, E.; McIntyre, S. Ab initio and molecular mechanics study of n-phenyl phthalimide and its crystal structure. *J. Comput. Chem.* **1992**, *13*, 408–413.
- [21] Dupont, DuPont Kapton: General Specifications. 2015.
- [22] Carraher, C. E.; Swift, G. *Functional Condensation Polymers*; Kulwer Academic, 2002.
- [23] Volksen, W.; Miller, R. D.; Dubois, G. Low Dielectric Constant Materials. *Chem. Rev.* **2010**, *110*, 56–110.
- [24] Shian, S.; Sandhage, K. H. A gas-tight Cu Ka x-ray transparent reaction chamber for high-temperature x-ray diffraction analyses of halide gas/solid reactions. *Rev. Sci. Instrum.* **2009**, *80*, 115108.
- [25] Hirai, T.; Cole, M. J.; Fujii, M.; Hasegawa, S.; Iwai, T.; Kobayashi, M.; Srama, R.; Yano, H. Microparticle impact calibration of the Arrayed Large-Area Dust Detectors in Interplanetary space (ALADDIN) onboard the solar power sail demonstrator IKAROS. *Planet. Space Sci.* **2014**, *100*, 87–97.
- [26] Vanherck, K.; Koeckelberghs, G.; Vankelecom, I. F. J. Crosslinking polyimides for membrane applications: A review. *Prog. Polym. Sci.* **2013**, *38*, 874–896.
- [27] Zhang, H.; Shen, P. K. Recent development of polymer electrolyte membranes for fuel cells. *Chem. Rev.* **2012**, *112*, 2780–2832.
- [28] Wilson, D.; Stenzenberger, H. D.; Hergenrother, P. M. *Polyimides*; Blackie and Son Ltd.: Glasgow, London, 1990.
- [29] Wakabayashi, K.; Kohama, S.-i.; Yamazaki, S.; Kimura, K. Morphology control of various aromatic polyimides by using phase separation during polymerization. *Polymer (Guildf)*. **2007**, *48*, 458–466.
- [30] Liaw, D.-J.; Wang, K.-L.; Huang, Y.-C.; Lee, K.-R.; Lai, J.-Y.; Ha, C.-S. Advanced polyimide materials: Syntheses, physical properties and applications. *Prog. Polym. Sci.* **2012**, *37*, 907–974.
- [31] Frank, H.; Ziener, U.; Landfester, K. Formation of polyimide nanoparticles in heterophase with an ionic liquid as continuous phase. *Macromolecules* **2009**, *42*, 7846–7853.
- [32] Kurita, K.; Suzuki, Y.; Enari, T.; Ishii, S.; Nishimura, S.-I. Polyisoimides: Synthesis and Evaluation as Efficient Precursors for Polyimides. *Macromolecules* **1995**, *28*, 1801–1806.
- [33] Unterlass, M. M.; Emmerling, F.; Antonietti, M.; Weber, J. From dense monomer salt crystals to CO₂ selective microporous polyimides via solid-state polymerization. *Chem. Commun.* **2014**, *50*, 430–432.
- [34] Kriechbaum, K.; Cerrón-Infantes, D. A.; Stöger, B.; Unterlass, M. M. 2015, DOI: 10.1021/acs.macromol.5b01545.
- [35] Baumgartner, B.; Bojdys, M. J.; Unterlass, M. M. Geomimetics for green polymer synthesis: highly ordered polyimides via hydrothermal techniques. *Polym. Chem.* **2014**, *5*, 3771–3776.

- [36] Baumgartner, B.; Puchberger, M.; Unterlass, M. M. Towards a general understanding of hydrothermal polymerization of polyimides. *Polym. Chem.* **2015**, *6*, 5773–5781.
- [37] Baumgartner, B.; Skrinjar, P.; Bojdys, M. J.; Unterlass, M. M. Design Strategies in Hydrothermal Polymerization of Polyimides. *Macromol. Chem. Phys.* **2015**,
- [38] Hsiao, S.-H.; Chen, Y.-J. Structure-property study of polyimides derived from PMDA and BPDA dianhydrides with structurally different diamines. *Eur. Polym. J.* **2002**, *38*, 815–828.
- [39] Ojeda, J. R.; Martin, D. C. High Resolution Microscopy of PMDA-ODA Poly(imide) Single Crystals. *Macromolecules* **1993**, *26*, 6557–6565.
- [40] Liu, J.; Rybnikar, F.; Geil, P. H. Lamellar and whisker single crystals of poly(2,6-oxynaphthoate). *J. Polym. Sci. Part B Polym. Phys.* **1992**, *30*, 1469–1482.
- [41] Liu, J.; Cheng, S. Z. D.; Harris, F. W. Crystal Structure, Morphology, and Phase Transitions in Aromatic Polyimide Oligomers. 1. Poly(4,4'-oxydiphenylene pyromellitimide). *Macromolecules* **1994**, *27*, 989–996.
- [42] Lin, L.; Ping, Y.; Cao, C.; Jin, Q.; Xu, G.-S.; Shen, Y.-H.; Yuan, Y.-P. Rapid microwave-assisted green production of a crystalline polyimide for enhanced visible-light-induced photocatalytic hydrogen production. *J. Mater. Chem. A* **2015**, *3*, 10205–10208.
- [43] Fang, Q.; Zhuang, Z.; Gu, S.; Kaspar, R. B.; Zheng, J.; Wang, J.; Qiu, S.; Yan, Y. Designed synthesis of large-pore crystalline polyimide covalent organic frameworks. *Nat. comm.* **2014**, *5*.
- [44] Byrappa, K.; Yoshimura, M. *Handbook of Hydrothermal Technology*; Elsevier, 2001; pp 161–197.
- [45] Schäfer, H. *Chemische Transportreaktionen*; Verlag Chemie, Weinheim, 1962.
- [46] Rabenau, P. D. A. The Role of Hydrothermal Synthesis in Preparative Chemistry. *Angew. Chemie Int. Ed.* **1985**, *24*, 1026–1040.
- [47] Nacken, R. Hydrothermal Synthese als Grundlage für Züchtung von Quarz-Kristallen. *Chem. Zeitung* **1950**, 745–749.
- [48] Schafhäutl, K. F. E. Die neuesten geologischen Hypothesen und ihr Verhältnis zur Naturwissenschaft überhaupt. *Gelehrt. Anzeigen Bayer. Akad.* **1845**, *72*, 557 – 592.
- [49] Chang, C.-C.; Wu, H.-L.; Kuo, C.-H.; Huang, M. H. Hydrothermal Synthesis of Monodispersed Octahedral Gold Nanocrystals with Five Different Size Ranges and Their Self-Assembled Structures. *Chem. Mater.* **2008**, *20*, 7570–7574.
- [50] Zhao, X.-Z.; Roy, R.; Cherian, K. A.; Badzian, A. Hydrothermal growth of diamond in metal-C-H₂O systems. *Nature* **1997**, *385*, 810–813.
- [51] Cundy, C. S.; Cox, P. A. The hydrothermal synthesis of zeolites: Precursors, intermediates and reaction mechanism. *Microporous Mesoporous Mater.* **2005**, *82*, 1–78.
- [52] Fujita, M.; Kwon, Y. J.; Washizu, S.; Ogura, K. Preparation, Clathration Ability, and Catalysis of a Two-Dimensional Square Network Material Composed of Cadmium(II) and 4,4'-Bipyridine. *J. Am. Chem. Soc.* **1994**, *116*, 1151–1152.

- [53] Laudise, R. A.; Ballman, A. A. Hydrothermal Synthesis of Sapphire. *J. Am. Chem. Soc.* **1958**, *80*, 2655–2657.
- [54] Robson, H.; Lillerud, K. P. *Verified Syntheses of Zeolitic Materials*; Elsevier, 2001.
- [55] Hu, B.; Wang, K.; Wu, L.; Yu, S.-H.; Antonietti, M.; Titirici, M.-M. Engineering Carbon Materials from the Hydrothermal Carbonization Process of Biomass. *Adv. Mater.* **2010**, *22*, 813–828.
- [56] Moreno, J. M. C.; Yoshimura, M. Hydrothermal processing of high-quality multiwall nanotubes from amorphous carbon. *J. Am. Chem. Soc.* **2001**, *123*, 741–742.
- [57] Takahashi, H.; Liu, L. H.; Yashiro, Y.; Ioku, K.; Bignall, G.; Yamasaki, N.; Kori, T. CO₂ reduction using hydrothermal method for the selective formation of organic compounds. *J. Mater. Sci.* **2006**, *41*, 1585–1589.
- [58] Hawthorne, D. G.; Hodgkin, J. H.; Jackson, M. B.; Loder, J. W.; Morton, T. C. Preparation and characterization of some new diaminobisimides. *High Perform. Polym.* **1994**, *6*, 287.
- [59] Dao, B.; Hodgkin, J.; Morton, T. C. Important factors controlling synthesis of imides in water. *High Perform. Polym.* **1999**, *11*, 205–218.
- [60] Zhong, Y. *et al.* Efficient Organic Solar Cells with Helical Perylene Diimide Electron Acceptors. *J. Am. Chem. Soc.* **2014**, *136*, 15215–15221.
- [61] Langhals, H. Cyclic carboxylic imide structures as structure elements of high stability. Novel developments in perylene dye chemistry. *Heterocycles* **1995**, *40*, 477–500.
- [62] Fraga-Dubreuil, J.; Çomak, G.; Taylor, A. W.; Poliakoff, M. Rapid and clean synthesis of phthalimide derivatives in high-temperature, high-pressure H₂O/EtOH mixtures. *Green Chem.* **2007**, *9*, 1067–1072.
- [63] Brunel, R.; Marestin, C.; Martin, V.; Marcier, R. Water-borne Polyimides via Microwave-assisted. *High Perform. Polym.* **2009**, *22*, 82–94.
- [64] Chiefari, J.; Dao, B.; Groth, A. M.; Hodgkin, J. Water as Solvent in Polyimide Synthesis: Thermoset and Thermoplastic Examples. *High Perform. Polym.* **2003**, *15*, 269–279.
- [65] Sengers, J. V.; Watson, J. T. R. Improved International Formulations for the Viscosity and Thermal Conductivity of Water Substance. *J. Phys. Chem. Ref. Data* **1986**, *15*, 1291–1314.
- [66] Uematsu, M.; Franck, E. U. Static Dielectric Constant of Water and Steam. *J. Phys. Chem. Ref. Data* **1980**, *9*, 1291–1306.
- [67] Marshall, W. L.; Franck, E. U. Ion Product of Water Substance, 0-1000 °C, 1-10000 Bars New International Formulation and Its Background. *J. Phys. Chem. Ref. Data* **1981**, *10*, 295–305.
- [68] Von Hippel, A. *Dielectric Materials and Applications*; Artech Haus Inc., 1995; p 456.
- [69] Yaghi, O. M.; O'Keeffe, M.; Ockwig, N. W.; Chae, H. K.; Eddaoudi, M.; Kim, J. Reticular synthesis and the design of new materials. *Nature* **2003**, *423*, 705–714.
- [70] Carothers, W. H. Diamine-dicarboxylic acid salts and process of preparing same. US 2130947. 1936.

- [71] Mandelkern, L. *Crystallization of Polymers*; Cambridge University Press, 2002; Vol. 6.
- [72] Demers, E.; Maris, T.; Wuest, J. D. Molecular Tectonics. Porous Hydrogen-Bonded Networks Built from Derivatives of 2,2',7,7'-Tetraphenyl-9,9'-spirobi[9H-fluorene]. *Cryst. Growth Des.* **2005**, *5*, 1227–1235.
- [73] Seo, J.; Han, H. Water sorption behaviour of polyimide thin films with various internal linkages in the dianhydride component. *Polym. Degrad. Stab.* **2002**, *77*, 477–482.
- [74] Ronova, I. A.; Bruma, M. Influence of conformational rigidity on membrane properties of polyimides. *Struct. Chem.* **2012**, *23*, 47–54.
- [75] Papaspyrides, C. D.; Vouyiouka, S. N. *Solid State Polymerization*; John Wiley & Sons, 2009; p 304.
- [76] Cote, A. P.; Benin, A. I.; Ockwig, N. W.; O'Keeffe, M.; Matzger, A. J.; Yaghi, O. M. Porous, Crystalline, Covalent Organic Frameworks. *Science (80-.)*. **2005**, *310*, 1166–1170.
- [77] El-Kaderi, H. M.; Hunt, J. R.; Mendoza-Cortés, J. L.; Côté, A. P.; Taylor, R. E.; O'Keeffe, M.; Yaghi, O. M. Designed synthesis of 3D covalent organic frameworks. *Science* **2007**, *316*, 268–72.
- [78] Akiya, N.; Savage, P. E. Roles of Water for Chemical Reactions in High-Temperature Water. *Chem. Rev.* **2002**, *102*, 2725–2750.
- [79] Clark, S. J.; Segall, M. D.; Pickard, C. J.; Hasnip, P. J.; Probert, M. J.; Refso, K.; Payne, M. C. First principles methods using CASTEP. *Z. Krist.* **2005**, *220*, 567–570.
- [80] Segall, M. D.; Lindan, P. J. D.; Probert, M. J.; Pickard, C. J.; Hasnip, P. J.; Clark, S. J.; Payne, M. C. First-principles simulation: ideas, illustrations and the CASTEP code. *J. Phys. Condens. Matter* **2002**, *14*, 2717–2744.
- [81] Coelho, A. Topas Academic Version 4.1. **2007**,
- [82] Wexler, A. Vapor Pressure Formulation for Water in Range 0 to 100 °C. A Revision. *J. Res. Natl. Bureau Stand. - A. Phys. Chem.* **1976**, *80A*, 775–785.
- [83] Hardy, B. ITS-90 Formulations for Vapor Pressure, Frostpoint Temperature, Dewpoint Temperature, and Enhancement Factors in the Range -100 to +100 C. Teddington, London, England, 1998.
- [84] Banwell, C. N.; McCash, E. M. *Fundamentals of Molecular Spectroscopy*, 4th ed.; McGraw-Hill College, 1994.
- [85] Lewis, D.; Mama, J.; Hawkes, J. A Review of Aspects of Oxidative Hair Dye Chemistry with Special Reference to N-Nitrosamine Formation. *Materials (Basel)*. **2013**, *6*, 517–534.